Detection of NADPH oxidase subunits NOX1 and NOX4 in lung adenocarcinoma A549 cells, and impact of NOX1 on Nrf2- and HIF-1-dependent gene regulation

Inaugural Dissertation
submitted to the
Faculty of Medicine
in partial fulfillment of the requirements
for the PhD-Degree
of the Faculties of Veterinary Medicine and Medicine
of the Justus Liebig University Giessen

by
Malec, Viktor
born in
Liberec, Czech Republic

Giessen 2010

From the Department of Internal Medicine II
Director: Prof. Dr. Werner Seeger
of the Faculty of Medicine of the Justus Liebig University Giessen

First Supervisor and Committee Member: PD Dr. Jörg Hänze
Second Supervisor and Committee Member: Prof. Dr. Thomas Kietzmann
Committee Members: Prof. Dr. Ernst Petzinger
Prof. Dr. Andre Menke

Date of Doctoral Defense: 30th March 2010

Table of content

I. Table of content

II. List of figures

II. Table of abbreviations

AA	amino acid	DGR	double glycine repeat
ACN	acetonitrile	DMSO	dimethylsulfoxide
AEC	anion exchange chromatography	dNTP	deoxyribose nucleotide triphosphate
AIR	autoinhibitory region	ddNTP	di-deoxyribose nucleotide triphosphate
Akt	corresponds to PKB (protein kinase B) (homologue of v-Akt)	DPI	diphenyleneiodonium chloride
Ang II	angiotensin 2	dsDNA	double stranded DNA
AP-1	activator protein-1	DTT	dithiothreitol
ARE	antioxidant response element	Duox	dual oxidase
ARNT	aryl hydro-carbon nuclear translocator	ECL	enhanced chemiluminescence
ASK1	apoptosis signal-regulating kinase 1	EDTA	ethylendinitrilo-N,N,N',N',-tetra-acetate
ATCC	American Type Culture Collection	EFP1	EF-hand binding protein 1
ATF-1	activating transcription factor 1	EGF	epidermal growth factor
bHLH	basic helix-loop-helix	ER	endoplasmic reticulum
BSA	bovine serum albumin	ERK	extracellular signal-regulated kinase
bp	base pair	ETC	electron transport chain
C	cytosol	FAD	flavin adenine dinucleotide
CaCo2	colorectal carcinoma (cells)	FCS	fetal calf serum
CBB	Coomassie Brilliant Blue	FIH	factor-inhibiting HIF-1
CBP	CREB-binding protein	FT	flow through
cDNA	complementary deoxyribonucleic acid	GATA6	GATA (nucleotide sequence), (GATA transcription factor 6)
Csk	cytoskeleton	GDP	guanosine-5'-diphosphate
C-TAD	C-terminal transactivation domain	gp91phox	glycoprotein-91kDa-phagocytic-oxidase
Cul	cullin	Gth	glutathione

GTP	guanosine-5'-triphosphate
H2	2 h of hypoxia
H6	6 h of hypoxia
H2R	H2 followed by 2 h of reoxygenation
HA	hemagglutinin
HIF-1	hypoxia inducible factor 1
HPLC	high performace liquid chromatography
HRE	hypoxia response element
HRP	horseradish peroxidase
HUVEC	human umbilical vein endothelial cells
IEF	isoeletric focusing
IH4	IH (2x2 h of hypoxia interupted with 2 h of rexygenation)
IH6	IH (3x2 h of hypoxia interupted with 2x2 h of rexygenation)
IH4R	IH (IH4 followed by 2 h of rexygenation)
IKK	IκB kinase (IκB is inhibitor of kappa B)
IP3	inosiotol triphosphate
IPG	immobilized pH gradient
JNK	c-jun N-terminal kinase
kb	kilo base
kDa	kilo Dalton
Keap1	Kelch-like ECH-associated protein 1
Km	Michaelis constant
LB	Luria Bertani
Luc	luciferase
mAb	monoclonal antibody
MAF	avian musculoaponeurotic fibrosarcoma (protooncogene)
MAPK	mitogen-activated protein kinase
MALDI-TOF	matrix assisted laser desorption/ionisation-time of flight
Me	membrane
MEK	MAPK/ERK kinase
mRNA	messenger RNA
MS	mass spectrometry
mTOR	mammalian target of rapamycin
M-MuLV	moloney murine leukemia virus
Mw	molecular weight
N	normoxia
NADPH	nicotinamide adenine dinucleotide phosphate
NF-κB	nuclear factor kappa-light-chain-enhancer of activated B cells
NIH3T3	3-day transfer, inoculum 3 x 105 cells
NOX	NADPH oxidase
NOX1v	NOX1variant
NOXA	NOX activator protein
NOXO	NOX organizer protein
NQO1	NADPH quinone-oxido-reductase
Nrf2	nuclear factor (erythroid-derived 2)-like 2
N-TAD	N-terminal transactivation domain
Nu	nuclei
NuIns	nuclear insoluble
NuSol	nuclear soluble
OD	optical density
ODDD	oxygen-dependent degradation domain
p	pellet
PAGE	polyacryl-amid gel electrophoresis
PAS	Per, ARNT, SIM
PB1	phox-Bem1
PBS	phosphate buffer saline
PCR	polymerase chain reaction
PDGF	platelet-derived growth factor
PGF2α	prostaglandin F2α
PGK	phosphoglycerate kinase
Phox	phagocyte oxidase
PHD	prolyl hydroxylase
PI3K	phosphatidylinositol 3-kinase
PKC	protein kinase C
Pl.Me.	plasma membrane
p"x"phox	protein "x kDa" phox (e.g.p67phox, p47phox)
PtdInsP	phosphatidylintositol phosphate
PVDF	polyvinylidene fluoride
pVHL	von Hippel-Lindau protein
PX	phox homology
Ref-1	redox factor 1
RhoA	Ras homolog gene family, member A

RhoGDI	RhoGDP-dissociation inhibitor
RNA	ribonucleic acid
RNase	ribonuclease
ROS	reactive oxygen species
Rpm	rotations per minute
RPC	reverse phase chromatography
RT	room temperature
RT-PCR	reverse transcription-PCR
s	supernatant
SDS	sodium dodecyl sulfate
SEM	standard error of the mean
SH3	Src homology 3
siRNA	small interfering RNA
SOC	super optimal broth with catabolite repression
STAT	signal transducers and activators of transcription
TAD	transactivation domain
TEMED	N',N',N',N'-Tetra methyl diamine
TFA	trifluoroacetic acid
T.Me.	total membrane
TPR	tetratricopeptide repeat
Trx	thioredoxin
TrxR	thioredoxin reductase
TSR	template suppression reagent
Tx-100	Triton X-100
UV	ultra violet
VEGF	vascular endothelial growth factor
VHL	von Hippel Lindau
VSMC	vascular smooth muscle cells
2D-GE	two dimensional gel electrophoresis

1. Introduction

1.1 NADPH oxidase

NADPH oxidases (nicotinamide adenine dinucleotide phosphate oxidase) are membrane bound enzyme complexes that have the primary function to generate superoxide anions. The enzyme was originally described in phagocytic cells of the immune system, particularly in neutrophils. This NADPH oxidase type is the best explored and consists of five subunits: gp91phox (glycoprotein-91kDa-phagocytic-oxidase) (newly termed NOX2), p22phox, p47phox (newly termed NOXO2), p67phox (newly termed NOXA2), p40phox and the GTPase Rac1. The gp91phox and p22phox subunits are membrane bound. Recently, different types of NADPH oxidases were identified in non-phagocytic cells, among them are endothelial cells, smooth muscle cells, fibroblasts and epithelial cells. In these types of NADPH oxidases, the NOX2 subunit is replaced by several homolog subunits named: NOX1, NOX3, NOX4 and NOX5 with molecular weights in the range of 63-68kDa [1]. These homologs share considerable similarities with NOX2 in amino acid sequence, conformation and structural domains. Other homologs with lower degree of similarity to NOX2 represent DUOX1 and DUOX2. DUOXs are proteins of about 160kDa containing additional transmembrane and calcium binding domains at the N-terminus [2], [3]. Also, homologs of p47phox (NOXO2) and p67phox (NOXA2) named NOXO1 and NOXA1 have been identified. These subunits are critical for a functional and active NOX1, NOX2 and NOX3 containing NADPH oxidases [4] [5] (Figure 1).

1.1.1 Functions of NADPH oxidases and NOX subunits

The primary function of NADPH oxidase is the generation of superoxide anions ($O_2^{\cdot -}$). $O_2^{\cdot -}$ formation is based on reduction of molecular oxygen (O_2) by one electron. There are specific domains in the NOX subunits that bind the cofactors $NADP^+$ and FAD and a hem iron that mediates the electron transfer to O_2 as terminal acceptor. The electron flow is according to an increasing redox potential of individual components, i.e. from $NAD(P)^+$ to FAD to hem iron to O_2 [6], [5]. Whereas the C-terminal part of NOX is important for binding of $NAD(P)^+$, FAD and further NADPH oxidase subunits, the N-

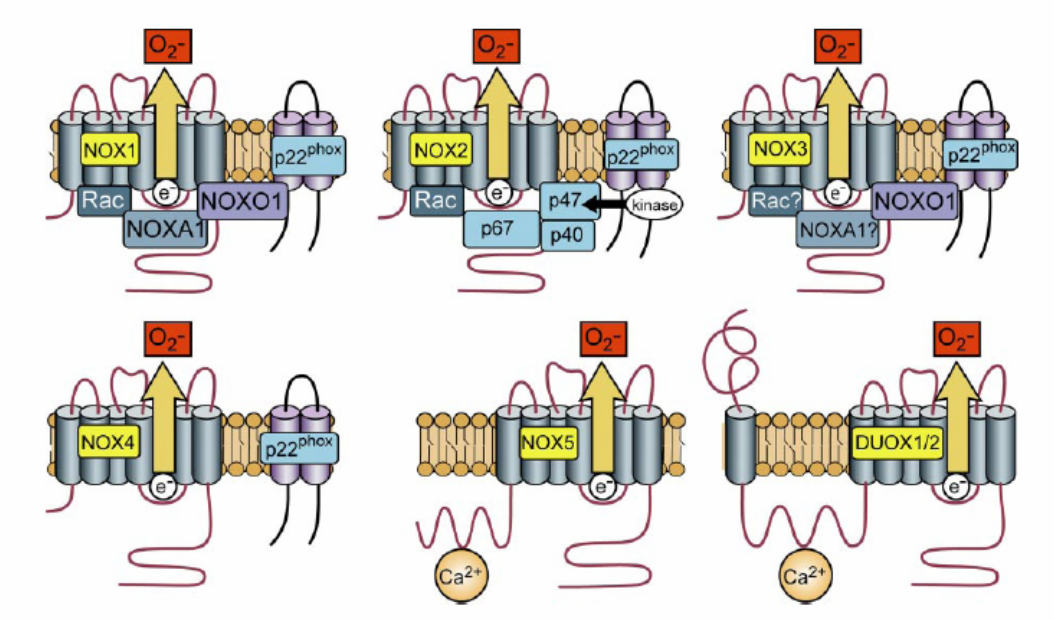

Figure 1: Activation and organization of NADPH oxidase subtypes
Despite of similarities in structure and enzymatic function, individual NOXs differ in their mechanism of activation. NOX1 activity requires p22phox, NOXO1 (or possibly p47phox in some cases) and NOXA1, and the small GTPase Rac. NOX2 requires p22phox, p47phox, p67phox, and Rac. p47phox phosphorylation is required for NOX2 activation. Although not absolutely required, p40phox also associates with this complex and may contribute to activation. NOX3 requires p22phox and NOXO1. The requirement for NOXA1 may be species dependent, and the requirement of Rac is still debated. NOX4 requires p22phox, but in reconstitute systems it is constitutively active without the requirement for other subunits. However, in native NOX4-expressing cells, activation, possibly including Rac, has been described. NOX5, DUOX1, and DUOX2 are activated by Ca^{2+} and do not appear to require other subunits. [5]

terminal part contains several histidine residues that are essential for the covalent binding of hem. Amino acids in the N-terminal part of the NOX protein form up to six hydrophobic alpha helices that have been suggested to pass cell membrane. Interestingly, the truncated C-terminal half of NOX displays a diaphorase activity [7], [8], i.e. the ability to reduce chromogenic electron acceptors, whereas the N-terminal half has proton conductance properties. The proton conductance is likely based on protonation and deprotonation of the flexible imidazole ring of histidines localized in the transmembrane domains of NOX. It may play a role in regulation of the intracellular pH [9], [10], [11].

Electron flow and superoxide generation are conditioned by the interaction of NOX with other NADPH oxidase subunits enabling binding of NADPH, FAD and the activation of NOX [4] [5]. The function and structure of individual NADPH oxidase subunits are described below (chapter 1.1.2) and schematically depicted (Figure 1 and 2).

1.1.2 Subunits of NADPH oxidases

1.1.2.1 NOX1 and NOX4

NOX1

NOX1 was the first described homolog of NOX2. NOX1 shares 60% amino acid sequence identity with NOX2 [5]. One alternative splice variant (NOX1v) lacking exon 11 has been identified. The exon 11 encodes amino acids predicted to participate in the binding of NADPH thereby the lack of this region diminishes the ability of NOX1v to generate ROS [12]. p22phox, NOXO1 (or p47phox) and NOXA1 (or p67phox) seem to be essential for the function of NADPH oxidase containing NOX1, i.e. NADPH oxidase 1 [4] [5] [13].

The predicted sizes of NOX1 and NOX1v are 65kDa and 59kDa respectively, however the commonly observed NOX1 bands in SDS-PAGE have 50-65 kDa [14], [15], [16], [17], [18], [19], [20]. Of note is that immuno-detection of NOX proteins is not well established and different antibodies differ in their immunoreactivity. Thus, also the subcellular localization of endogenous NOX1 is controversially described. Most of the studies with recombinant NOX1 protein show localization in the cell membranes, particularly in the plasma membrane [21], [22], [23], [24], [25]. Using immunofluorescence microscopy, also endogenous NOX1 protein displayed surface distribution along the cellular margins [26] where it was colocalized with caveolin-1 [18]. Also, subcellular fractionation detected NOX1 in fractions containing membranes [16], [27]. One recent study demonstrated colocalization of recombinant NOX1 with F-actin and cortactin in invadopodia of cancer cells [28]. On the other hand, other studies showed endogenous or overexpressed NOX1 protein also in the nuclei, cytosol [29], at endoplasmic reticulum (ER) [25] and even mitochondria [30].

NOX1 was found in many different cell- and tissue-types. Nevertheless, the highest expression level of NOX1 was detected in colon epithelium and in a cell line derived from colorectal carcinoma (CaCo2) [1], [31], [32], [33]. The NADPH oxidase 1 in intestinal epithelial cells may be an important component of mucosal host defense. In accordance with the high abundance of NOX1 in different cancer cell lines, it has been shown that overexpression of NOX1 in NIH3T3 cells led to increased mitotic rate, cell transformation and tumorigenicity [34], [32]. In particular, NOX1 derived ROS are involved in Ras dependent malignant transformation [35], [36]. The mechanism of transformation may involve NOX1-derived ROS triggering mutagenesis in oncogenes or tumor suppressor genes, and an action of NOX1-derived ROS as intracellular mediators in the regulation of proliferation [37], [35]. The relevant ROS targets related to growth and transformation may include p42/p44 mitogen activated protein kinase (MAPK) [38], [39], p38 MAPK [40], [41], p70S6kinase [42], signal transducers and activators of transcription (STAT) [43], vascular endothelial growth factor (VEGF) [44], [36], Akt1 (alias protein kinase B) [45] protein tyrosine phosphatase-1B [46], nuclear factor kappa-light-chain-enhancer of activated B cells (NF-κB) [47],[48], [49] and activator protein-1 (AP-1) [50], [34]. Also, this aspect is important in different cardiovascular diseases.

On the other hand, many signaling mediators have been shown to induce NOX1. NOX1 mediated ROS generation can be triggered by platelet-derived growth factor (PDGF), epidermal growth factor (EGF), prostaglandin $F_{2\alpha}$ ($PGF_{2\alpha}$) [51], [52], [53], [54], and by angiotensin II (Ang II) [55], [56]. The molecular mechanism of NOX1 activation by these factors includes signaling cascades leading to increased NOX1-mRNA expression or activation of NADPH oxidase subunits. Components of signaling cascades leading to an elevation of NOX1 expression may include different kinases that converge downstream in the activation of transcription factors such as GATA6 or activating transcription factor 1 (ATF-1) which are binding directly to the promoter regions of the NOX1 gene [52], [37]. Particularly in regard to malignant transformation, Ras dependent activation of NOX1 through the MEK/ERK pathway and GATA6 factor has been demonstrated [57].

NOX4

NOX4 is a 67kDa protein sharing 39% amino acid identity with NOX2 [58], [5]. Five splice variants of NOX4 resulting in different truncated forms have been identified at the mRNA level [59]. However, it is not clear whether they are also endogenously expressed at the protein level and thus also their functional role is not clear. Similarly to NOX1, the detection of NOX4 by antibodies is not well established. In many studies, in addition to the 67kDa protein band likely representing NOX4 full length, a putative band at 75-80kDa has been detected [60], [18], [61], [62], [63], [64]. Whether this band represents, for example, a posttranslational modification of NOX4 or other NOX4 splice variants is not known.

NOX4 is predominantly localized at the ER [21], [25] and in the nuclei [65], [18]. In addition, a colocalization of NOX4 with cytoskeleton and focal adhesions has been demonstrated [18], [64], [66]. p22phox appears to be the only subunit that is essential for the function of the NOX4 containing NADPH oxidase 4. Thus, the enzymatic activity of NADPH oxidase 4 mainly depends on the expression level of NOX4 and p22phox and probably does not need any further activation [67]. The type of ROS generated by NOX4 has been determined in some studies as H_2O_2, unlike NOX1 that is primarily producing $O_2^{\cdot-}$ [21]. NOX4 is functionally linked to senescence [58], proinflammatory responses, oxygen sensing [68], migration, differentiation [66], [69], proliferation [70], [71], [62] and apoptosis [72], [73]. This is in agreement with the association of NOX4 with cytoskeleton and focal adhesions, since both of these cellular compartments are involved in these processes. Mechanisms of NOX4 acting on cytoskeletal and focal adhesions may involve different structural changes of these proteins, e.g. phosphorylation, and/or direct regulation of relevant targets transcription by ROS [74], [66], [75], [62]. For example, ROS has been shown to induce the activity of $p125^{FAK}$ (non receptor protein tyrosine kinase) that in turn phosphorylates cytoskeleton associated proteins paxillin and p130cas [76]. Another study showed, that NOX4 in complex with Poldi2 protein ((DNA-directed), delta interacting protein 2) exerts an effect on focal adhesions turnover, stress fiber formation and VSCM migration by activation of RhoA protein (Rho GTPase family proteins regulate actin dynamic) [64].

1.1.2.2 p22phox, NOXO, NOXA, p40phox, Rac

p22phox

p22phox is a 22kDa basic, transmembrane protein that plays an important role during NOXs protein synthesis in the ER [77], [78] and it is essential for the function of NADPH oxidase since it mediates anchoring NOXs in the membrane and supports the interaction of NOX with the NOXO subunit [79],[80], [81], [82]. p22phox consists of two transmembrane domains at the N-terminal part and a proline rich region at the C-terminal part [79]. The proline rich region is critical for binding to the NOXO subunit . (Figure2)

NOXO

The NOX organizer (NOXO) is a 47kDa basic protein with a regulatory function of NADPH oxidase activity. It may translocate to the membrane upon phosphorylation [83] where it interacts with p22phox by a Scr homology 3 (SH3) domain [84], [80] and with the phospholipid membrane by a phox homology domain (PX) [23]. NOXO2 (originally named p47phox) and NOXO1, two known homologs of NOXO, appear to have similar functions in the activation of NOX2 and NOX1, respectively [33], [5]. However, they differ in specific properties, such as the ability of binding specific components of the membrane and the ability of autoregulation - NOXO2 contains autoinhibitory domains that is deactivated upon phosphorylation, whereas NOXO1 seems to be constitutively active [5]. A proline rich region of NOXO enables its interaction with NOXA. (Figure 2)

NOXA

The NOX activator (NOXA) contains several TPR (tetratricopeptide repeat) motifs at the N-terminus within the activation domain, a phox-Bem1 region in the central part and a SH3-homolog sequence at the C-terminus [5]. NOXA2 with a size of 67kDa (originally named p67phox) and its homolog NOXA1 with a size of 51kDa bind to NOX2 and NOX1, and mediate NOX interaction with the NOXO subunit. Similarly to NOXOs, also NOXA2 and NOXA1 differ in their structural properties - they only share 30% identity in the amino acid sequence [33]. Both NOXA2 and NOXA1 (similarly as NOXO2 and NOXO1) can substitute for each other, however the substitution has significant impact on NOX2 and NOX1 functions [85]. The TPR domain is important for Rac binding [86],

[87], the phox-Bem1 region for p40phox binding [85], the SH3 domain for NOXO interaction [88], [89], [80], and the activation domain is critical for the activation of NOXs [90]. (Figure 2)

p40phox

p40phox (40kDa) is a protein also containing PX region, a SH3 domain and in addition an octicosa peptide repeat. The PX domain interacts with components of the phospholipide membrane, the SH3 domain with NOXO and the octicosa peptide repeat with NOXA [91], [5]. p40phox can also be phosphorylated upon stimulation, such as oxidative stress, by PKCδ [92]. (Figure2)

Rac GTPase

Rac is a small (21kDa) G protein from the Rho family of GTPases. The N-terminal part of the protein binds GTP or GDP and displays a GTPase activity. The exchange of GDP for GTP leads to the activation of Rac and is prevented by the Rho GDP dissociation inhibitor (RhoGDI) that interacts with the C-terminal hydrophobic region of Rac in resting cells [93]. The function of Rac in the NADPH oxidase complex is likely to activate NOXA which occurs when Rac is released from RhoGDI and GTP is bound to Rac [94], [95], [24], [54]. (Figure 2)

1.1.2.3 Assembling and activation of NADPH oxidase subunits

The importance of the individual subunits, sequence and stimuli of activation of different subtypes of NADPH oxidase are partially explored. Most of the studies have been performed on the phagocytic NADPH oxidase (containing NOX2) which is the best described functional model of this enzyme (Figure 3). The model suggests that NOX2 and p22phox are constitutively expressed in the plasma membrane [13]. Upon activation, NOXO2 is phosphorylated and binds to p22phox [84], [83], which is a docking place for NOXO2 and NOXA2. Interestingly, NOXO1 unlike NOXO2 activation appears to be independent on phosphorylation. NOXA translocation to the membrane and its consequent interaction with NOXO seems to be dependent on the stimulation of NOXA by the Rac subunit which is likely changing the conformation of the NOXA activation domain [94], [95].

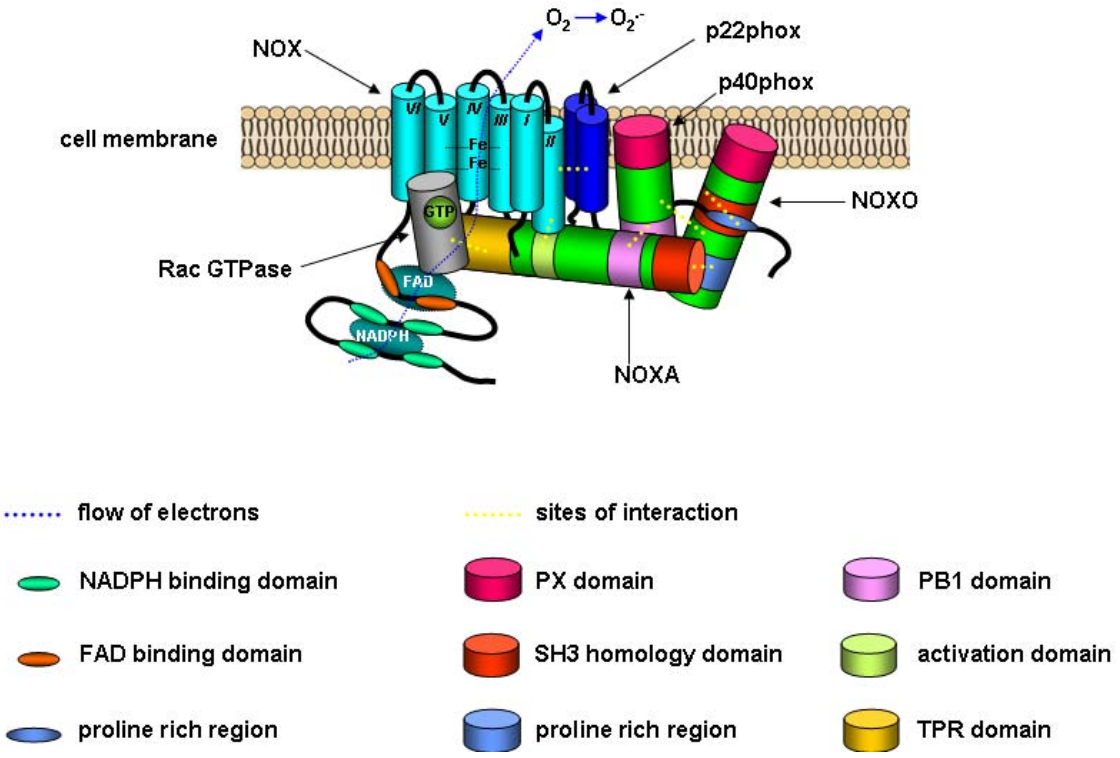

Figure 2: Proposed organization of NADPH oxidase subunits
NOX1, NOX2, NOX3, NOX4 and NOX5 contain six conserved transmembrane domains at the N-terminal part. The transmembrane domains III and V contain two histidine residues binding two hemes. The cytoplasmic C-terminal part of NOXs contains conserved domains binding FAD and NADPH. NOXs interact with the p22phox subunit a transmembrane protein linking further NADPH oxidase subunits to NOXs. NOXO (p47phox), NOXA (p67phox), p40phox are NADPH oxidase subunits containing specific domains critical for mutual interaction, association with the cell membranes and are important for NADPH oxidase function. Rac GTPases are involved in the regulation of NADPH oxidase complexes but they do not belong to NADPH oxidase subunits in the strict sense. Rac plays probably a role in the activation of NOXA. The importance of the individual subunits for the activation of different NOX subtypes is not fully explored (see Figure 1). Here depicted model is suggested to be relevant mainly for NOX1 and NOX2. All NOXs are though to be single electron transporters, passing electrons from NADPH to FAD to the first and to the second heme iron and finally to molecular oxygen.

When NOXA and NOXO are docked in the membrane, p40phox can interact with NOXA subunit. The role of p40phox in the NADPH oxidase complex is probably that it supports to anchor other subunits in the cell membrane [13], [96]. Proper assembling of all subunits consequently forms a specific tertiary structure of NADPH oxidase enabling effective ROS generation. An involvement of individual NADPH oxidase subtypes in different cellular signaling events is achieved not only through different patterns of their activation by cytosolic subunits but also by their cell and tissue type specific expression and particular subcellular localization.

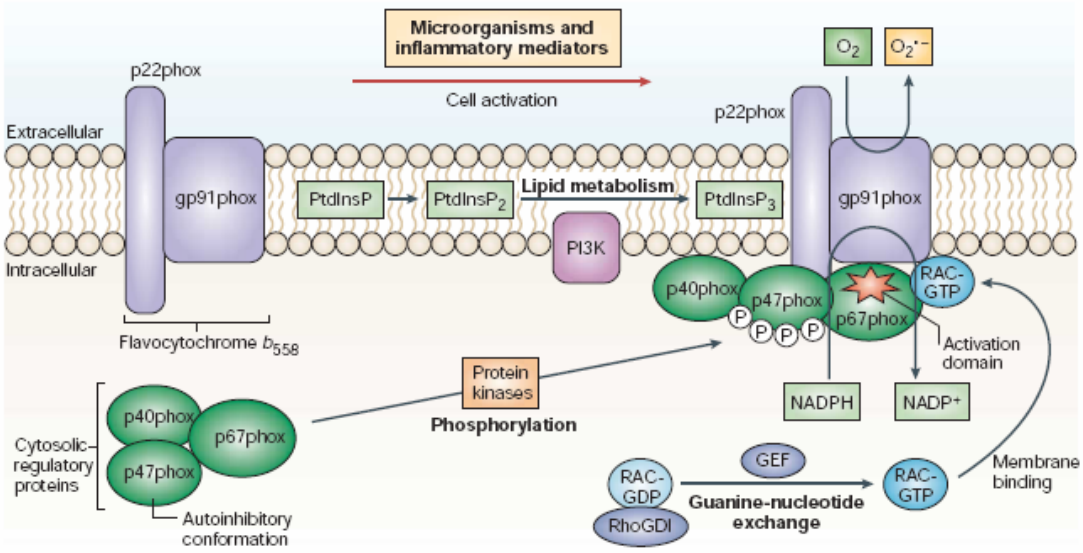

Figure 3: Activation of NADPH oxidase 2
Activation of the gp91phox (NOX2) system occurs by at least three signaling triggers that result in the assembly of the cytosolic regulatory proteins (p40phox, p47phox and p67phox) with flavocytochrome *b*558 (comprised of the membrane-associated catalytic subunit gp91phox plus p22phox). These triggers involve protein kinases, lipid-metabolizing enzymes and nucleotide-exchange proteins that activate the GTPase Rac. Protein kinases, including protein kinase C and Akt, catalyse many phosphorylations of the autoinhibitory region (AIR) of p47phox, releasing its binding to the bis-SRC-homology 3 (SH3) domain, allowing p47phox to bind to p22phox. This also relieves the inhibition of the Phox homology (PX) domain of p47phox, allowing binding to lipids. Because p47phox also binds to p67phox, it has been described as an organizer protein. Phosphatidylinositol 3-kinase (PI3K) and phospholipase D produce 3-phosphorylated phosphatidylintositols (PtdInsP) and phosphatidic acid, respectively, providing lipids to which the p47phox and p40phox PX domains bind. Rac is post-translationally modified with a carboxy-terminal hydrophobic geranyl-geranyl group. In Rac-GDP, this group is

masked by the inhibitory protein RhoGDP-dissociation inhibitor (RhoGDI), maintaining Rac in the cytosol. Activation of exchange factor(s) triggers GTP binding, resulting in conformational changes in Rac that promote dissociation from RhoGDI and membrane association through the geranyl-geranyl lipid. The conformational change also promotes Rac binding to the tetratricopeptide (TPR) region of p67phox, helping to assemble the active complex. [4]

1.2 Reactive oxygen species

1.2.1 Types of ROS, oxidative stress and antioxidants

Reactive oxygen species (ROS) include a number of chemically reactive molecules derived from oxygen. Some of them such as superoxide anion are free radicals, i.e. molecules with unpaired electrons in the atom valence shell, whereas others do not belong to the group of free radicals but they only exhibit high reactivity due to their strong oxidative properties. The major types of ROS in mammalian cells are: superoxide anion ($O_2^{\cdot -}$) a product of NADPH oxidases; hydrogen peroxide (H_2O_2) that can be generated either by conversion of $O_2^{\cdot -}$ or directly by some enzymes; peroxy radicals ($ROO^{\cdot}$), generated by reaction of lipid radicals with $O_2^{\cdot -}$; organic hydroperoxide (ROOH) a product of lipid peroxidation; hydroxyl radical $HO^{\cdot}$ a product of the Fenton reaction - the reaction of metals with H_2O_2; hypochlorous acid (HOCl) generated by myeloperoxidase [97], [98], [99].

ROS can readily react with many types of biomolecules leading to alterations of their structure or leading to the initiation of a chain reaction forming free radicals. In order to stop this chain reaction, a newly formed radical must either react with another free radical, eliminating the unpaired electrons or must react with a free radical scavenger. An imbalance between the production of ROS and the ability of the biological system to detoxify the reactive intermediates or to repair the resulting damage causes so called oxidative stress. Agents protecting cell from oxidative stress, i.e. antioxidants are either small molecules often with reducing effect (glutathione, ascorbic acid, polyphenols) or enzymes (thioredoxin, glutaredoxin, superoxide dismutase, catalase) [100], [99], [101]. The role of ROS in the organism is however much more complex. ROS are also generated as a natural product of the oxygen metabolism and they play an important role in the defense of organisms against pathogens and in cellular signaling [102].

1.2.2 Cellular sources of ROS

ROS may be generated by enzymatic reactions as a primary product or as side-product. ROS are produced as side-product within the mitochondrial electron transport chain [103], of xantin oxidase [104], of cytochrom P-450 [105], of lipooxygenase [106] and other enzymes in the ER [107] and of peroxisomes [108]. On the other hand, myeloperoxidase and NADPH oxidases are enzymes that have the primary function to produce ROS [100]. Both enzymes were originally discovered in the phagocytic cells of the immune system, paricularly in neutrophils. Later, also other non-phagocytic NADPH oxidase types have been described. These types of NADPH oxidases generate ROS that are important rather in cellular signaling than in defence against pathogens.

1.2.3 Mechanisms of ROS impact on cell signaling

An essential role of ROS in cellular signaling has been demonstrated in many studies. The concept of ROS signaling is based on oxidative modifications of proteins. This may work by at least two mechanisms. Either by alteration of the redox state of the glutathione (Gth) and the thioredoxin (Trx) systems that are the two most important cellular "redox buffers" or by direct oxidation of target proteins [102], [101]. The "reducing" environment of cells is accomplished by the "redox buffering" capacity of the Gth and Trx systems. Trx and Gth may regulate cell signaling by donating or accepting electrons [102]. An optimal ratio of reduced and oxidized Gth as electron donor-acceptor is critical for an effective enzymatic regulated protein folding [107], [109] that also significantly impacts cell signaling. Furthermore, both Gth and Trx were described to physically and functionally interact with different transcription factors. The ability of Gth and Trx to interact with various signaling molecules directly correlates with the ratio of their reduced and oxidized forms in the cell. For example, STAT3 [110], c-Jun [111], and IκB kinase (IKK-β) [112] are targets of glutathionylation and apoptosis signal-regulating kinase (ASK1) [113], redox factor 1 Ref-1 [114], [115] are bound by Trx [102]. Trx, in dependency on its redox state, also regulates the function of HIF-1α [116], NF-κB [117] and AP-1 [118], [119].

The mechanism of direct oxidation of signaling proteins by ROS may include [102], [97]: 1. oxidation of cysteine residues (e.g. p53 transcription factor oxidation [120], [121], [122], HIF-1α can be destabilized by oxidation of particular cysteine residues [123]), 2. formation of intra- or inter-molecular disulfide linkages (e.g. ASK1 homodimerization [124]), 3. H_2O_2-dependent formation of di-tyrosine (e.g. ROS participate in di-tyrosine formation of the amyloid β peptide in Alzheimer's diseases [125]), 4. oxidation of proteins by metal catalyzed reactions. For example, many enzymes contain metal ions in their active sites. The metal ion can consequently catalyze oxidation of these proteins by Fenton reaction, i.e. reaction of hydrogen peroxide with metal leading to generation of reactive hydroxyl radical [102], [126].

1.2.4 ROS, oxygen sensing and hypoxia inducible factor 1

1.2.4.1 HIF-1 is a target of oxygen sensors

Celluar oxygen sensing mechanisms exist that function in order to maintain cellular oxygenation under conditons of decreased partial oxygen pressure (pO_2) levels (i.e. hypoxia). At the level of gene regulation, oxygen sensor dependent signaling is mediated by the hypoxia inducible factor 1 (HIF-1) [127], [128]. HIF-1 was detected as the first transcription factor which was specifically induced by hypoxia [129], [130], [131], [132]. It was discovered during investigations of the molecular mechanism of erythropoietin induction, which induces erythropoiesis, and thus improves the oxygen-binding capacity of blood. In subsequent studies, it emerged that HIF-1 directly affects an increasing number of identified target genes which are involved in hypoxic adaptation processes and are activated by a common hypoxia responsive DNA binding element [133], [134], [135]. The HIF-1 complex is a heterodimer consisting of two structurally similar subunits: HIF-1α and HIF-1β (HIF-1β is ARNT, aryl hydro-carbon nuclear translocator) (Figure 4). Further HIF-1α homologs, termed HIF-2α [136] and HIF-3α [137], and homologs of ARNT, termed ARNT2 [138] and ARNT3 [139] have been identified and are all encoded by different genes. The α-subunit of HIF is the regulatory subunit, while the β-subunit is constitutively expressed. Heterodimerization of the α- and β-subunit is essential for

activation of HIF-dependent target genes. The HIF-1α is the relevant regulatory subunit for responses induced by hypoxia [140].

The N-terminal domain of HIF-1α is important for dimerization with HIF-1β and DNA binding. This domain contains a basic-helix-loop-helix and two PAS (Per, ARNT, SIM) motifs sharing homology with other transcription factors of this group. The C-terminal domain is the regulatory domain which contains an oxygen-dependent degradation domain (ODDD) and itself can be divided into a C-terminal transactivation domain (C-TAD) and N-terminal transactivation domain (N-TAD) [127].

1.2.4.2 Regulation of HIF by the oxygen sensors prolyl 4-hydroxylase and asparaginyl hydroxylase

Specific oxygen dependent enzymes exist that sense the induction of HIF-1. The regulation of HIF-1 activation occurs mainly at the level of protein stabilization via HIF prolyl 4-hydroxylases (PHD) which hydroxylate prolines at position 402 and 564 [141], [142]. If the proline-residues are hydroxylated as observed under normoxic conditions, *von Hippel Lindau* (VHL) protein binds to HIF-1α and targets it to proteasome for degradation, mediated by ubiquitination of HIF-1α by the E3 ubiquitin ligase [143]. Ubiquitination sites are three lysine residues at positions 532, 538 and 547 [144]. Thus, HIF-1α is rapidly degraded under normoxic conditions - a half-life time is in the ten-minute range [145]. Ubiquitination and degradation of HIF-1α do not occur under hypoxic conditions when these proline residues are non-hydroxylated [146] (Figure 4).

Additionally, hydroxylation of an asparagine residue at position 803 as observed under normoxic conditions by the asparaginyl hydroxylase FIH (factor inhibitory HIF) hinders the interaction of HIF-1α with the coactivators CBP/p300. On the other hand, the interaction of HIF-1α and CBP/p300 is enabled under hypoxic conditions, which promotes HIF-1 transactivation [147] (Figure 4).

In this regard, PHD and FIH enzymes appear to be the main cellular oxygen sensors since they regulate directly HIF-1α stability and activity. The oxygen sensing mechanism of HIF-1α hydroxylation by both PHD and FIH relies on the enzymatic reaction which requires O_2 as a substrate in addition to the cofactors α-ketoglutarate, Fe^{2+} and ascorbic

acid. The K_m values of PHD and FIH for oxygen are appropriate to sense the oxygen concentration in the physiologic relevant range [127], [128].

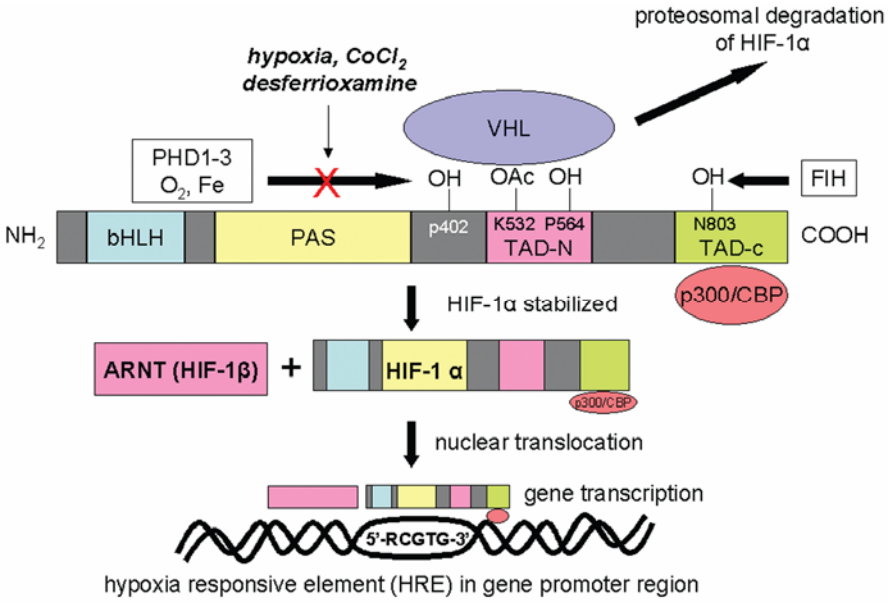

Figure 4: Regulation of HIF-1α in hypoxia
Hypoxic regulation of the hypoxia-inducible factor-1α (HIF-1α) transcription factor is primarily through inhibition of degradation. Under normoxic conditions, HIF-1α undergoes rapid proteosomal degradation once it forms a complex with *von Hippel–Lindau* tumor suppressor factor (VHL) and E3 ligase complex. This requires the hydroxylation of critical proline residues by a family of HIF-1α-specific prolyl hydroxylases (PHD-1,2,3), which requires O_2 and several cofactors, including iron. Under hypoxic conditions, or when iron is chelated or competitively inhibited, proline hydroxylation does not occur, thus stabilizing HIF-1α and allowing it to interact with the constitutively expressed HIF-1β (aryl hydrocarbon nuclear translocator; ARNT). The HIF-1 complex then translocates to the nucleus and activates genes with hypoxia-responsive elements in their promoters. bHLH, basic helix-loop-helix; CBP, cAMP response element binding protein; FIH, factor inhibiting HIF-1α; PAS, PER-ARNT-SIM; TAD, transactivation domain. [148]

1.2.4.3 Impact of reactive oxygen species on HIF regulation

Reactive oxygen species are important mediators of cellular signaling which affect HIF induction under normoxic and hypoxic conditions [149]. The possible ROS sources related to oxygen sensing include mitochondria and NAD(P)H oxidases (Figure 5).

ROS derived from the electron transport chain of mitochondria under hypoxic conditions have been demonstrated to increase stability of HIF-1α [150], [151]. This observation was further explored, and was related to mitochondria derived ROS-dependent activation of kinases p38α MAPK. Under hypoxic conditions, mitochondrial ROS stimulates p38α MAPK activity which likely phosphorylates HIF-1α at TAD, thereby enhancing the binding of the coactivator CBP to HIF-1α [152]. Another possibility is that ROS interfere with the regulation of PHD or FIH hydroxylases, by limiting the availability of free Fe^{2+} by oxidation of free Fe^{2+} to Fe^{3+}. Fe^{3+} generated during the hydroxylation reaction of PHD is reduced to Fe^{2+} by ascorbic acid which is a further potential target of ROS [153]. In contrast, hydroxyl radical generation from hydrogen peroxide by the Fenton reaction in the ER activates PHD, thereby destabilizing HIF-1α [154].

Interactions between HIF-1α and particular ROS derived from NADPH oxidase have also been described. However, both HIF-1α–inhibiting and HIF-1α–inducing effects of ROS derived from NADPH oxidases have been observed in different cellular contexts [155], [156], [157], [158].

The ROS-dependent induction of HIF-1α by Ang II-induced NADPH oxidase was mediated by enhanced cap-dependent translation of HIF-1α via activation of the phosphatidylinositol 3-kinase (PI3K)/Akt pathway [159], [160]. The study from Page et al. [160] further suggested that possible mechanism by which Ang II and ROS could increase the rate of HIF-1α translation involves activation of eukaryotic translation initiation factor 4F (eIF-4F) or the ribosomal S6 protein by the PI3K/p70S6K/mTOR pathway.

On the other hand, strong oxidative stress appears to have an inhibitory effect on HIF-1α. Huang et. al. showed that treatment of HeLa cells with 1mM H_2O_2 for 20min led to a rapid decrease of HIF-1α abundance [123].

Reactive oxygen species also affect the cellular redox systems, including thioredoxin, particularly cytoplasmic Trx1 [116]. Trx1 similarly as redox factor-1 (Ref-1) in reduced state stimulates HIF-1α activity by recruitment of cofactors CBP/p300 [161], [123]. In this context, the sulfhydryl groups of conserved cystein residues of HIF-1α (C^{800}) and of

HIF-2α (C^{844}) appear to be important. Additionally, protein stabilization of HIF-1α by Trx-1 has been suggested by inhibition of VHL and HIF-1α binding [162].

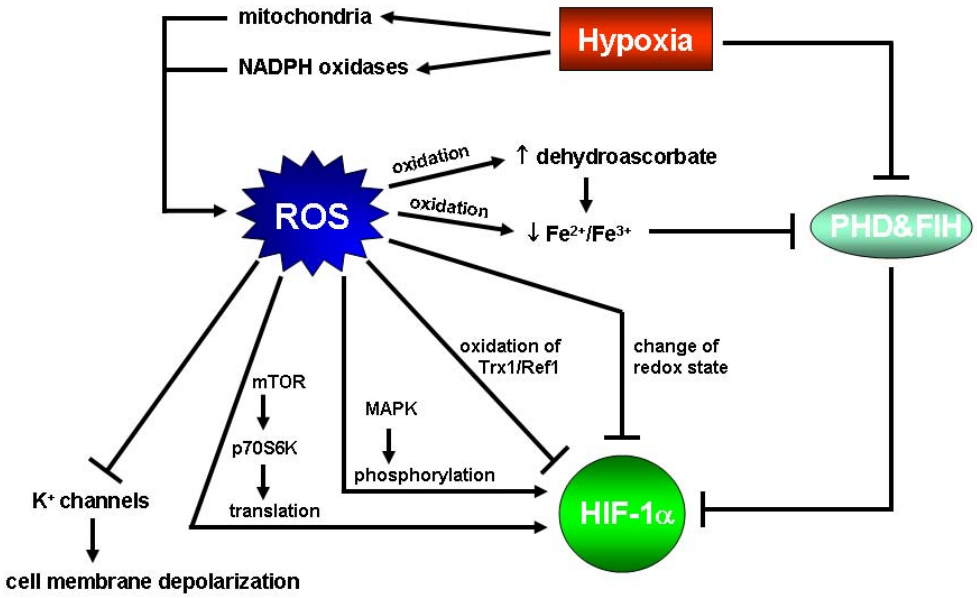

Figure 5: ROS in oxygen sensing
Hypoxia stimulates ROS generation by mitochondria or NADPH oxidases. ROS may regulate HIF-1α stability and activity directly by alteration of the HIF-1α redox state or indirectly. The indirect effect of ROS on HIF-1α is mediated by activation of mTOR dependent translation of HIF-1α, by activation of different kinases (e.g. MAPK) phosphorylating HIF-1α, by oxidation of Trx1 and Ref1 or other activators of HIF-1α and by effecting PHD/FIH activity. The regulation of PHD/FIH activity by ROS may depend on oxidation of cofactors, such as Fe^{2+} and ascorbate, important for the function of these enzymes. An HIF-independent mechanism of oxygen sensing is represented by ROS-mediated regulation of redox state sensitive K^+-channels leading to the depolarization of the cell membrane.

1.3 Nuclear factor (erythroid-derived 2)-like 2

1.3.1 Regulation of Nrf2 stability and activity

Nuclear factor (erythroid-derived 2)-like 2 (Nrf2), is a redox state-dependent transcription factor that is activated under different stress conditions, such as oxidative stress. Nrf2 induces the expression of enzymes that exert a cytoprotective role when cells are exposed to oxidative or electrophilic compounds (Figure 6). This adaptive response is

mainly regulated by an interaction between Keap1 (Kelch-like ECH-associated protein 1) and Nrf2, in which the exposure to reactive molecules is sensed by Keap1 [163], [164]. The interaction between Keap1 and Nrf2 is likely mediated by disulfide bridges and by non covalent bonds between specific structural domains of both proteins [165], [166] In the Keap1-Nrf2 complex, Keap1 serves as a bridge between Nrf2 and the subunit of Cullin 3-based E3-ubiquitin ligase holoenzyme [167], [166], [168], [164]. However, Keap1 negatively regulates Nrf2 not only by enhancing its rate of proteasomal degradation but also by altering its subcellular distribution. In fact, Nrf2-Keap1 heterodimer associates in cytosol with actin cytoskeleton under the "non-stress conditions" [169]. A disruption of Keap1-actin complex leads to translocation of Nrf2 into nucleus [165].

Nrf2 protein consists of six Neh (Nrf2-ECH homology) domains - each domain is characterized by specific physical-chemical properties based on amino acids sequence and on conformation. Neh2 domain structure is common among different species and it is responsible for binding Nrf2 to double glycine repeat (DGR) domain of Keap1, and consequently lysine residues inside of this domain are ubiquitinated by Cullin 3-based ligase [170]. Oxidative or electrophilic compounds alter the redox state of Keap1 cysteines and thus diminish Nrf2 binding and ubiquitination [166]. Another mechanism, partially independent on oxidative/electrophilic stimuli, leading to Nrf2 dissociation from Keap1 is based on the phosphorylation of particular serine residue(s) of Nrf2 [171]. For example, phosphorylation of Ser-40 by protein kinase C has been shown to stimulate Nrf2 release from Keap1 and consequently increase Nrf2 abundance in the nucleus [172].

1.3.2 Nrf2 target genes

Nrf2 posses redox insensitive nuclear signal sequences in the area of the leuciner zipper motif [173]. This sequence enables Nrf2 to translocate into the nucleus, where it binds with its leuciner zipper domain to a cis-acting enhancer called the antioxidant response element (ARE) located in the regulatory DNA region of its target genes. Once inside the nucleus, Nrf2 dimerises with small Maf proteins leading to binding Nrf2 to ARE of the target genes and their transcriptional induction [174], [175], [176]. Enhancement of Nrf2-mediated transcription has also been demonstrated by other proteins, in particular from

the Jun protein family (c-Jun, Jun-B, Jun-D) that can bind as a dimer with Nrf2 to the ARE sequences of the target genes [177].

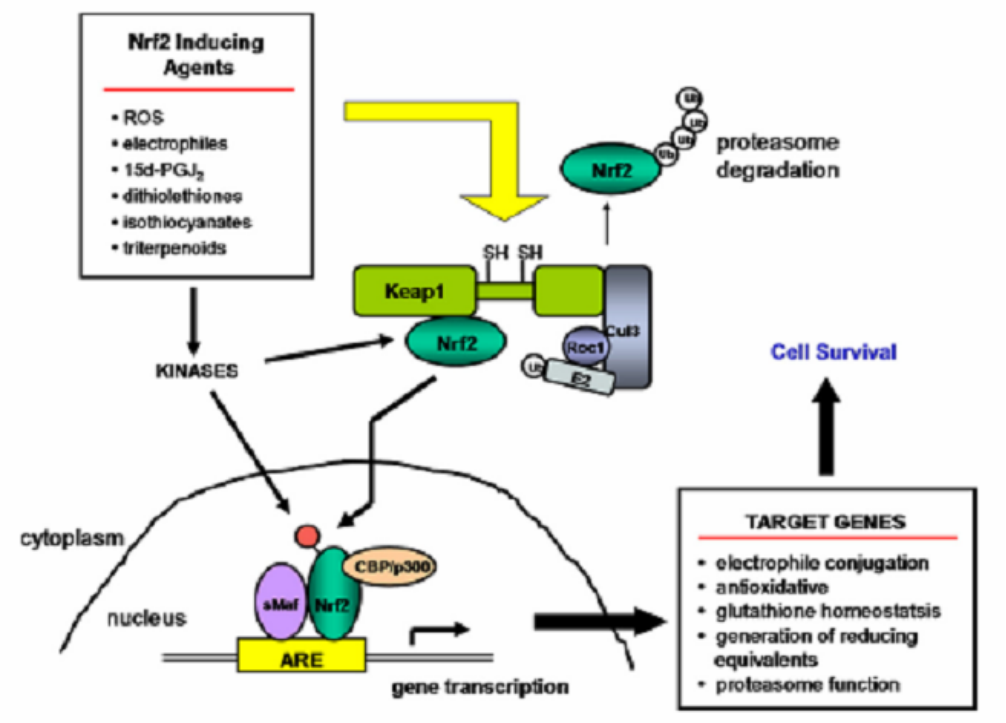

Figure 6: Mechanisms of Nrf2 activation
Reactive compounds such as ROS and electrophiles disrupt the interaction between Nrf2 and Keap1, likely by changing the redox state of specific cysteine residues. Keap1 in interaction with Nrf2 serves as a stress sensor which connects the Cullin 3-based E3-ubiquitin ligase with Nrf2. In non-stress conditions, the Nrf2-Keap1 complex is bound to the actin cytoskeleton and Nrf2 is targeted to rapid proteasome degradation. Disruption of Nrf2-Keap1 interaction by reactive molecules leads to translocation of Nrf2 into the nucleus, were it dimerizes with the small Maf protein and binds to the antioxidant responsive element (ARE) in the regulatory DNA sequence of target genes. In addition, Nrf2 activation is enhanced by phosphorylation of specific serine residues. Also, kinases responsible for Nrf2 phosphorylation may be activated by different reactive molecules. Similarly to HIF-1α, the transcriptional activity of Nrf2 is stimulated by the coactivators CBP or p300. Nrf2 enhances the transcription of genes that code enzymes important in metabolism of xenobiotics and in defense against oxidative stress. [164]

Nrf2 induces the expression of genes encoding cytoprotective enzymes. These are either enzymes that play an important role in metabolism of xenobiotics, such as glutathione-S-transferases, epoxide hydrolase, UDP-glucuronosyltransferase, aldehyde dehydrogenase, aldo-keto reductase or typical antioxidative enzymes, such as NADPH-quinone

oxidoreductase, glutathione reductase, peroxiredoxin, catalase, superoxide dismutase, glutathione peroxidase, thioredoxin and thioredoxin reductase [164]. Nrf2 is cytoprotective factor since it increases the resistance to chemically induced injuries and protects cells and organisms from various diseases. In this context, Nrf2 may prevent cancerogenesis by detoxification of cancerogenic agents [178], [179], [180], [181]. On the other hand, uncontrolled Nrf2 activation is a characteristic of some types of cancer cells [182]. Several cancer cell lines or primary tumor cell types display somatic mutations in the Nrf2 or Keap1 gene that are accompanied with non-efficient Nrf2 protein degradation due to diminished Nrf2-Keap1 interaction. For example, single amino acid mutation in the Neh2 region of Nrf2 have been detected in LK2 and EBC1 lung cancer cell lines [183]. A549 and H1395 lung cancer cell lines display single amino acid mutation in the first Kelch region (Kelch are structural motifs of the DGR domain) of Keap1 [184], [185]. Consequences of the insufficient Nrf2 degradation are aberrant elevation of the expression of cytoprotective enzymes that in turn attenuates apoptosis and leads to uncontrolled and disorganized cell growth that are typical hallmarks for malignant cells (Figure 7).

1.4 Thioredoxin system

1.4.1 Thioredoxin

Thioredoxin (Trx), a target gene of Nrf2 [186], [187], is a small (12kDa) ubiquitous protein that acts as oxidoreductase enzyme by facilitating the reduction of other proteins by cysteine thiol disulfide exchange. Trx and Trx-related proteins have an active center characterized by two cysteine residues (-Cys-Gly-Pro-Cys-) and a specific tertiary structure termed thioredoxin fold [188], [101]. The mechanism of protein reduction by Trx involves a transient mixed disulfide intermediate and fast thiol disulfide exchange in a hydrophobic environment. The reaction is reversible and thioredoxin may either break or form disulfides depending on the redox potential of its substrate. However, the very low redox potential of reduced Trx (Trx-(SH)2) usually ensures that Trx-(SH)2 is the major dithiol reductant in the cytosol [189], [101]. The human Trx may form a functionally inactive homodimer that is implicated to have a regulatory function. There are several isoforms of thioredoxins and thioredoxin related proteins [101]. The most

abundant isoform is Trx1 that is predominantly localized in the cytosol. Trx2 is another important thioredoxin isoform that contains a mitochondrial translocation signal and thus is mainly localized in mitochondria [190].

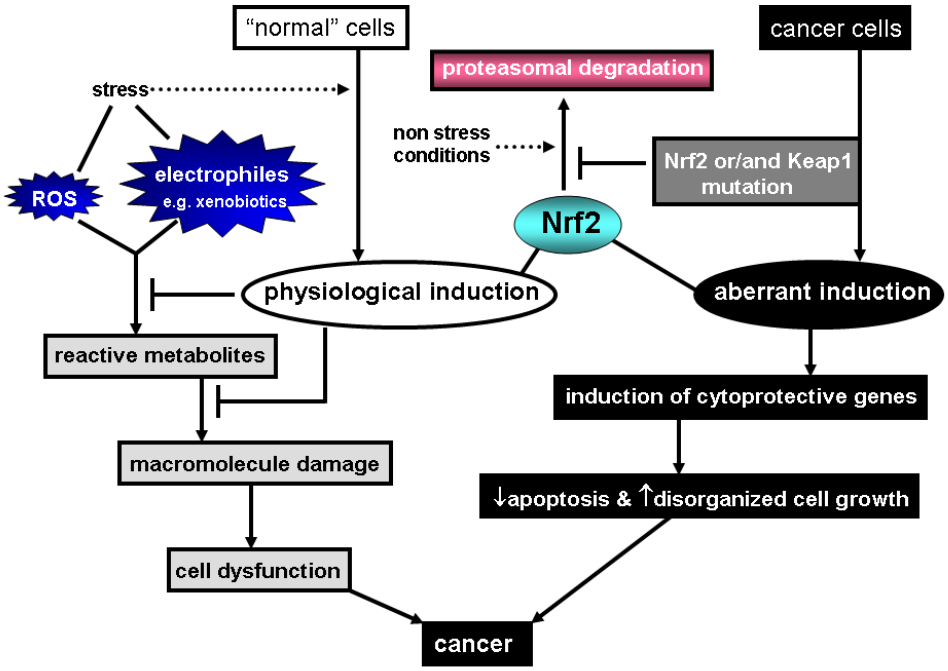

Figure 7: Dual role of Nrf2 in cancerogenesis
In "normal" cells, Nrf2 expression is increased upon stimulation (stress) by different reactive compounds such as ROS and electrophiles, whereas under "non-stress" conditions Nrf2 is rapidly degraded by the proteasome pathway. Nrf2 induction leads to enhanced expression of cytoprotective enzymes that play an important role in the metabolism of xenobiotics, ROS and in the elimination of their reactive metabolites. These effects are suggested to counteract carcinogenesis.
On the hand, some cancer cell types display an aberrant induction of Nrf2. This is caused by insufficient degradation of Nrf2 which is based on mutations of amino acids in Nrf2 or its interaction partner Keap1. The aberrant induction of Nrf2 strongly enhances expression of cytoprotective enzymes which leads to the weakening of apoptosis and to uncontrolled and disorganized cell growth that are characteristics of malignant transformation.

1.4.2 Thioredoxin reductase

The oxidoreductase function of thioredoxins is maintained by another oxidoreductase enzyme termed thioredoxin reductase (TrxR) [191]. TrxR enzymes are NADPH-

dependent homodimeric oxidoreductases reducing the active disulfide site in oxidized Trx. TrxR contains selenium in the form of selenocysteine that is incorporated in the amino acid chain during translation [192]. Selenocysteine is localized in the active site of TrxR and its oxidized form (selenenylsulfide) can be reduced to a selenolthiol only by the redox active dithiol of another TrxR in the dimer of this enzyme. Thus, the homodimeric form of TrxR is critical for its function [193]. There are several isoforms and splice variants of thioredoxin reductases, however they do not appear to have a high specifity for any particular type of thioredoxin. In general, a striking characteristic of mammalian TrxRs is the wide substrate specificity and the direct reduction of different protein disulfides, many low molecular weight disulfide compounds and non-disulfide compounds The wide substrate specificity can be explained by the unique and easily accessible Selene-containing redox active site [189], [101].

1.4.3 Function of the thioredoxin system

The thioredoxin system is the functional connection between Trx and TrxR. The thioredoxin 1 system is the most abundant system in mammalian cells. It consists of the cytosolic Trx1 and TrxR1. The function of the thioredoxin system, in particular the Trx1 system, is essential for many physiological processes. Together with the glutathione system, the Trx system is the most important “redox buffer” maintaining the intracellular environment in reduced state. Thioredoxins generally protect intracellular proteins from inactivation via oxidative formation of intra- or inter-molecular disulfides [101]. Furthermore, thioredoxins serve as electron carriers necessary for the catalytic cycles of biosynthetic enzymes, such as ribonucleotide reductases, methionine sulfoxide reductases and sulfate reductases [194], as well as enzymes important for protein folding, such as protein disulfide isomerases [195]. Thioredoxins also act through the regulation of the thiol redox state and direct binding to other molecules as signaling messengers. For instance, reduced Trx1 binds to ASK1 refelecting the redox-dependent regulation of apoptosis that is inhibited under conditions of reduced Trx when there is no oxidative stress [113],. Additionally, as described in chapter 1.2.3, Trx1 activates several transcription factors in a redox state-dependent manner among them are HIF-1α[116], AP-1 factor [118], [119] and NF-κB [117].

2. Aims of the work

Part I

NADPH oxidase 1 and NADPH oxidase 4 are enzymatic complexes that play an important role in cellular signaling by generation of ROS. The core subunits of NADPH oxidase 1 and 4 are NOX1 and NOX4, respectively. The expression, regulation and subcellular localization of NOX1 and NOX4 are not fully explored because of the lack of the availability of specific antibodies against these proteins. Thus, the aims in the first part of this study were:

1. To analyse immunoreactive proteins detected with different commercially available and custom made antibodies against NOX1 and NOX4, i.e. to select most suitable antibody for detection of NOX1 and NOX4 proteins.
2. To characterize the subcellular localization of NOX1 and NOX4 employing these antibodies.
3. To identify putative NOX1 and NOX4 proteins by different proteomic tools such as HPLC/2D-GE protein purification followed by MALDI-TOF MS analysis.
4. To design synthetic siRNAs for the efficient knock-down of NOX1 and NOX4 as a tool for testing the antibodies and for functional studying NOX1- and NOX4-dependent ROS generation.

Part II

The NOX1 containing NADPH oxidase is a significant source of ROS in human adenocarcinoma A549 cells. ROS are involved in the regulation of the transcription factors HIF-1 and Nrf2. A possible link between these transcription factors may represent the Nrf2 dependent target gene thioredoxin 1 (Trx1) that is known to induce HIF-1α. Both the regulation of HIF-1 and Nrf2 are affected by hypoxia, reoxygenation and intermittent hypoxia. These conditions are characterized by fluctuations of ROS levels, involving NADPH oxidases as relevant ROS sources in the regulation of HIF-1 and Nrf2. In particular, intermittent hypoxia may represent a situation where a cross-talk between HIF-1 and Nrf2 occurs. The specific aims of the second part of the work were:

1. To analyse the expression of NOX1 and the transcription factors HIF-1 and Nrf2, as well as its target Trx1 under different stages of continuous hypoxia, reoxygenation and intermittent hypoxia, in the human adenocarcinoma A549 cells.
2. To analyse possible cross-talk(s) between NOX1, Nrf2, Trx1 and HIF-1α.

3. Materials and Methods

3.1 Materials

3.1.1 Materials and instruments

Western blot and protein concentration measurement

Glasses for gels, combs, electrophoresis chambers, electroblotting chambers, power supplies, blotting paper (all from Bio-Rad, Hercules, CA, USA), polyvinylidene fluoride (PVDF) membrane (Millipore Corporation, Billerica, MA, USA), chemiluminiscence imager (Fluorchem^{TM} IS-8900) (Alpha Innotech, San Leandro, CA, USA), Immuno 96 MicroWell™ Plates (96 well plate) (Nunc, Roskilde, Denmark), spectrofluorometer (FL-600) (BioTek Instruments GmbH, Bad Friedrichshall, Germany)

Agarose gel electrophoresis

Gel chamber, traces, combs (Biometra GmbH, Goettingen, Germany)

HPLC

Nanonsep 10K/Microsep 3K (ultra-filters) (Pall life Sciences, Ann Arbor, MI, USA), QIAquick Spin Columns (DNA binding column) (Qiagen GmbH, Hilden, Germany), MonoQ (CV ≈ 1ml, column for AEC) (GE Healthcare, Amersham^{TM}, Buckinghamshire, UK), Symetry 300 (C8, column for RPC) (Waters, Milford, MA, USA), sample syringe of 2ml (Hamilton Company, Nevada, USA), HPLC system Agilent 1100 Series (Agilent Technologies, Santa Clara, CA, USA)

3.1.2 Chemical agents

Trifluoroacetic acid (TFA), MG132 (Z-Leu-Leu-Leu-al), diphenyleneiodonium chloride (DPI), protease inhibitor cocktail, Triton X-1000, bromophenol blue, glycerol, porcine skin gelatin, Tryptone, yeast extract (all from Sigma-Aldrich, St. Louis, MO, USA), agarose (broad range), Tris, NaCl, HEPES, dimethylsulfoxide (DMSO), Rotiphorese Gel 30, Roti-Block (all from Carl Roth GmbH, Karlsruhe, Germany), ethylenediaminetetraacetic acid (EDTA), HCl (36%), NaOH, sodium dodecyl sulphate (SDS), urea, methanol, acetonitrile (ACN), acetic acid (all from Merck KGaA, Darmstadt, Germany), prestained SDS-PAGE protein marker (PageRuler), DNA ladder

(NoLimits) (all from Fermentas Life Sciences, Burlington, Ontario, Canada), Enhanced Chemiluminiscence (ECL) plus (GE Healthcare, Amersham™, Buckinghamshire, UK), Coomassie® Brilliant Blue G 250 (powder for Coomassie Brilliant Blue), ethidium bromide (all from SERVA Electrophoresis GmbH, Heidelberg, Germany), Lipofectamin 2000 (Invitrogen, Carlsbad, CA, USA)

3.1.3 Buffers

Western blot

- 4x Laemmli sample buffer: 0.25 M Tris (pH adjusted with HCl to 6.8), 8% of SDS, 40% of glycerol, adjusted with dest. H_2O
- Collecting buffer: 0.625 M Tris (pH adjusted with HCl to 6.8)
- Separating buffer: 1.125 M Tris, 30% of sacharose, pH adjusted with HCl to 8.8
- 10x NET: 1.5 M NaCl, 50mM EDTA (pH adjusted with NaOH (25%) to 8), 0.5 M Tris (pH adjusted with HCl to 7.4), 0.5% of Tx-100
- Blocking buffer: 1x NET with 0.25% porcine skin gelatin
- Transfer buffer: 25 mM Tris, 192 mM glycine, 20% of methanol, 0.01% of SDS
- Coomassie Brilliant Blue (CBB): 0.1% of Coomassie® Brilliant Blue G 250, 50% of methanol, 10% of acetic acid, adjusted with dest. H_2O.
- CBB destaining buffer: 50% of methanol, 10% acetic acid, adjusted with dest. H_2O

HPLC

- AEC: buffer A: 20 mM Tris (pH adjusted with HCl to 8.8), buffer B: 1 M NaCl, 20 mM Tris (pH adjusted with HCl to 8.8)
- RPC: “buffer” A: H_2O, 0.1% TFA, “buffer” B: ACN, 0.07% TFA

DNA agarose gel electrophoresis

- 10x TAE buffer for agarose gels: 0.4 M Tris, 0.4 M acetic acid, 10 mM EDTA (pH adjusted with HCl to 8.0)
- Agarose gel (1%): 10% of 10x TAE, 1% of agarose, 0.5 µg/ml of ethidium bromide
- DNA Loading buffer: 0.01% of bromophenol blue, 40% of glycerol, 10% of 10x TAE buffer

3.1.4 Antibodies

HIF-1α (LS-B495, Lifespan Biosciences, WA, USA), HIF-1α (BD Biosciences, San Diego, CA, USA), Nrf2 (H-300), Trx1 (FL-105), MOX1 H-15, MOX1 H-75, NOX4 N-15, NOX4 H-300, PGK1/2 (E-20), Na^+/K^+-ATPase α (H-3), Lamin B (C-20), (all from Santa Cruz Biotechnology, Santa Cruz, CA, USA), NOX1jh, NOX4jh (both from laboratory of Dr.J.Hänze, University Giessen), NOX1ab55831, β-actin (AC-15) (both from Abcam, Cambridge, UK), NOX1wch (kind gift from Dr. W. Chamulitrat, University Heidelberg, Germany), mAb54.1 (kind gift from Prof.W.Kummer, University Giessen, The antibody was generated for laboratory of Dr.J.Burrit, Montana State University, Bozeman, USA.), monoclonal anti-HA (hem agglutinin) antibody (Clone HA-7) (Sigma-Aldrich, St. Louis, MO, USA), Cytokeratin (MNF16) (antibody reacts with cytokeratin 5, 6, 8, 17) (DakoCytomation, Denmark), secondary antibody (anti-rabbit, -goat, -mouse) conjugated to horseradish peroxidase (HRP) (Thermo Scientific, Pierce Biotechnology, Rockford, IL, USA)

3.1.5 Oligonucleotide sequences

Primer sets (+, forward; -, reverse) for PCRs

NOX1+: 5'-CTC TCT CCT GGA ATG GCA TC-3'

NOX1–: 5'-TGG AAA ACA TCC TCA CTG GC-3'

NOX4+: 5′-AAA CTT CTC TTC ACA ACTG TTC CTG-3′

NOX4-: 5′-TGG TAA GGA AAT ATT CTG AGA GCTG-3′

Trx1+: 5'-CAG ATC GAG AGC AAG ACT GCT TTT C-3'

Trx1-: 5'-CTT ATT GGC TCC AGA AAA TTC ACC C-3'

Nrf2+: 5'-TGC TTT CATA GCT GAG CCC AGT ATC-3'

Nrf2-: 5'-TCC ATA GCT GGA AGA TTC CAC TGAG-3'

HIF-1α+: 5'-AAA GGG TAA AGA ACA AAA CAC ACAG-3'

HIF-1α+: 5'-TAA AGG AAT TTC AAT ATT TGA TGGG-3'

β-actin+: 5'-TAT CCA GGC TGT GCT ATC CCT GTA C-3'

β-actin-: 5'-TTC ATG AGG TAG TCA GTC AGG TCC C-3'

Oligonucleotide sequences for cloning reporter gene plasmids

PGK-HRE:

Forward Nhe I: 5'-CTA GCG CGT CGT GCA GGA CGT GAC AAA TAG CGC GTC GTG CAG GAC GTG ACA AAT AGC GCG TCG TGC AGG ACG TGA CA AAT-3'

Reverse Xho I: 5'-TCG ACT TTG TCA CGT CCT GCA CGA CGC GCT ATT TGT CAC GTC CTG CAC GAC GCG CTA TTT GTC ACG TCC TGC ACG ACG CG-3'

NQO1-ARE:

Forward Nhe I: 5'-CTA GCA GTC ACA GTG ACT CAG CAG AAT CTG-3'

Reverse Xho I: 5'-TCG ACA GAT TCT GCT GAG TCA CTG TGA CTG-3'

3.1.6 siRNAs

siRNAs sequences (+, forward; -, reverse)

si-con+: 5'-UAG CGA CUA AAC ACA UCAA dTdT -3'

si-con-: 5'-UUG AUG UGU UUA GUC GCUA dTdT-3'

si-NOX1+: 5'-CCU GAG GGG CAC CUG CUCA dTdT-3'

si-NOX1-: 5'-UGA GCA GGU GCC CCU CAGG dtdT-3'

si-NOX4+: 5′-CCU CUU CUU UGU CUU CUAC dTdT-3′

si-NOX4-: 5′-GUA GAA GAC AAA GAA GAGG dTdT-3′

p22-phox+: 5'-CAU GAC CGC CGU GGU GAAG dTdT-3'

p22-phox-: 5'-CUU CAC CAC GGC GGU CAUG dTdT-3'

si-Nrf2+: 5'-GUA AGA AGC CAG AUG UUAA dTdT-3'

si-Nrf2-: 5'-UUA ACA UCU GGC UUC UUAC dTdT-3'

si-Trx1+: 5'-UGA UCA ACC CUU UCU UUCA dTdT-3'

si-Trx1-: 5'-UGA AAG AAA GGG UUG AUCA dTdT-3'

3.1.7 Plasmids

Plasmid isolation: Maxiprep Kit (MACHEREY-NAGEL GmbH, Düren, Germany)

Used plasmids: pcDNA3.1+ (Invitrogen, Carlsbad, CA, USA), pCMV-HA (Clontech, Mountain View, CA, USA), pIRES, pGL3-TK (both from Promega, Promega Corporation, Madison, WI, USA)

3.1.8 Cell culturing

3.1.8.1 Bacteria, mediums for bacteria culturing and transformation

Bacterial strains: *E.Coli* TOP10 bacterial strain from Invitrogen (Invitrogen, Carlsbad, CA, USA) was used for plasmid transformation. Genotype of the strain was "F- *mcr*A Δ(*mrr-hsd*RMS-*mcr*BC) φ80*lacZ*ΔM15 Δ*lac*X74 *rec*A1 *ara*D139 Δ(*araleu*) 7697 *gal*U *gal*K *rps*L (StrR) *end*A1 *nup*G".

Transformation medium: 2% of Tryptone, 0.5% of yeast extract, 10mM NaCl, 2.5mM KCl, 10 mM $MgCl_2$, 10 mM $MgSO_4$, 20 mM Glucose, pH = 7.3

Agar plates: 7.5g bactoagar, 500ml LB medium, 500µl ampicillin (stock 100µg/ml)

Luria Bertani (LB) medium: 1% of Tryptone, 0.5% of yeast extract, 10mM of NaCl, pH = 7.3

3.1.8.2 Mammalian cells and cell culturing mediums

A549

The human lung adenocarcinoma A549 cell line was obtained from the American Type Culture Collection (Manassas, VA, USA). Cells were cultured in D-MEM/F-12 medium (Gibco, Invitrogen, Carlsbad, CA,USA) supplemented with 10% fetal bovine serum (Greiner BioOne, Frickenhausen, Germany), non-essential amino acids (1mM), penicillin (1U/ml) with streptomycin (100µg/ml), L-glutamine (2mM), and vitamins (1×) (all supplements were from Gibco, Invitrogen, Carlsbad, CA,USA).

CaCo2

The colorectal carcinoma cell line (CaCo2) was obtained from the American Type Culture Collection (Manassas, VA, USA). Cells were cultured in DMEM medium (containing 4.5g/l glucose, L-glutamine, pyruvate) supplemented with 10% fetal bovine serum (Greiner BioOne, Frickenhausen, Germany), 25mM HEPES (Carl Roth GmbH, Karlsruhe, Germany), non-essential amino acids, (1mM), penicillin (1U/ml) with streptomycin (100µg/ml) (DMEM and supplements were from Gibco, Invitrogen, Carlsbad, CA, USA).

HUVEC

These endothelial cells, kindly provided by Dr. K. Mayer (University of Giessen Lung Center (UGLC), Justus-Liebig-University of Giessen, Giessen, Germany), were isolated from human umbilical veins (Human Umbilical Veins Endothelial Cells). Briefly, cells obtained from collagenase digestion were washed, pooled, centrifuged for 10 min at 210g, and resuspended in fresh medium. Before splitting, cells were grown for 2 to 3 days on T 75 culture flasks coated with gelatine in an atmosphere of 95% O_2 and 5% CO_2. For the experiments HUVECs from passage 2 and 3 were used. Cells were always cultured in Endothelial Cell Growth Medium (containing 10ml FCS, 2ml ECGS/H, 0.1ng EGF/ml, 0.1ng bFGF, 0.1µg Hydrocortison/ml in 500ml of medium) supplemented with Supplement Mix C-39215 (all from PromoCell GmbH, Heidelberg, Germany).

Cell culturing medium for transfection experiments

In all transfection experiments, OPTI-MEM (Gibco, Invitrogen, Carlsbad, CA, USA) was used instead of cell culture medium for transient incubation of cells with siRNA or plasmid.

3.2 Methods

3.2.1 Biochemical methods

3.2.1.1 Subcellular fractionation

A) Isolation of cytosol, nuclei, membranes and cytoskeleton

The cytosolic, nuclear, membrane and cytoskeleton fractions were isolated from cells according to the protocol of the *Complete Cell Fractionation Kit* (PromoKine, PromoCell GmbH, Heidelberg, Germany). One modification of the protocol was that DTT was not added to of the extraction buffers, since DTT would interfere with the assay used for protein concentration measurement. The isolated fractions were directly mixed with 4x Laemmli sample buffer in the ratio of 3:1 or dissolved in 1x Laemmli sample buffer.

B) Separation of Tx-100 soluble and insoluble fraction

Cells were washed with PBS, scraped in a PBS containing protease inhibitor cocktail, transferred to eppendorf tubes and on ice lysed by sonication (four times for five seconds). Subsequently, Tx-100 was added into the cell lysate with a final concentration of 1%. After incubation of the cell lystate in ice for 30 minutes, the samples were centrifuged for 15 min at 14000g. The pellet (Tx-100 insoluble fraction) was directly dissolved in 1x Laemmli sample buffer and the supernatant (Tx-100 soluble fraction) was mixed with 4x Laemmli sample buffer in a ratio of 3:1. In order to analyse the effect of Tx-100 on cell fractionation, a sample without treatment by Tx-100 was used as a negative control.

C) Isolation of plasma membrane

The cytosolic, total membrane (containing all membranes and also cytoskeleton) and plasma membrane fractions were isolated from cells according to the protocol of the *Membrane Protein Extraction Kit* (PromoKine, PromoCell GmbH, Heidelberg, Germany). The isolated fractions were directly mixed with 4x Laemmli sample buffer in a ratio of 3:1 or dissolved in 1x Laemmli sample buffer.

D) Isolation of nuclei

The cytoplasmic, nuclear soluble and nuclear insoluble fractions were isolated according to the protocol of the *Nuclear and Cytoplasmic Extraction Reagent* (Thermo Scientific, Pierce Biotechnology, Rockford, IL, USA). The isolated fractions were directly mixed with 4x Laemmli sample buffer in a ratio of 3:1 or dissolved in 1x Laemmli sample buffer.

E) Subcellular fraction of samples for HPLC

Since the composition of commercially available buffers used in the kits for subcellar fractionation was not known, the fractions could not be applied directly for HPLC. Also acetone precipitation of the proteins from the subcellular fractions was not suitable for further HPLC based analysis, because the acetone precipitate was difficult to dissolve in any buffer. Thus, self-made crude subcellular fractionation was performed as desribed:

Cells were scraped in 20mM Tris (pH was adjusted with HCl to 8.0) containing a protease inhibitor cocktail, homogenized on ice by a Dounce homogenizator and gradually centrifuged at 1050g, 14000g, 110000g. The 1050g pellet was called as nuclei enriched fraction, the 14000g pellet as cytoskeleton and mitochondria enriched fraction, the 110000g pellet as membrane enriched fraction and 110000g supernatant as cytosol enriched fraction. The fractions containing the highest amount of the protein of interest (checked by Western blot) was used for further HPLC purification.

3.2.1.2 Protein concentration measurement

The *BCA protein assay kit* (Thermo Scientific, Pierce Biotechnology, Rockford, IL, USA) was used for the measurement of the protein concentration. This method is based on peptide bonds mediated reduction of Cu^{2+} to Cu^{1+} that interacts with bicinchoninic acid (BCA) generating a purple-colored product and it is useful for the measurement of protein concentrations in buffers containing various chemical agents including SDS and Tx-100. Thus, samples dissolved in 1x Laemmli sample buffer and buffer containing 1% of Tx-100 were directly applicable for the protein concentration measurement. Preparation of standards (differently diluted bovine serum albumin), incubation conditions, spectrophotometric measurement and calculation of protein concentration were performed according to the company's protocol. The absorbance of the purple color product was measured on a 96 well plate at 492nm with a spectrofluorometer (FL-600). As background, values of absorbance of relevant buffer(s) were used.

3.2.1.3 Western blot

After protein concentration determination, samples were mixed with β-mercaptoethanol (final concentration of 2.5%) and trace amount of bromophenol blue (final concentration of ca. 0.01%) and stored at -80°C. Immediately before loading onto the gel, samples were heated at 85°C for 5min and mixed. The gel electrophoresis, i.e. sodium dodecyl sulfate-polyacrylamide gel electrophoresis (SDS-PAGE), was performed with self-made 8% or 10% or 12% polyacrylamid gel at constant voltage of approx. 100-120V. The run of the gel was controlled by separation of prestained molecular weight marker.

Proteins in the gel were transferred to a PVDF membrane by semi-dry electroblotting. The PVDF membrane was wetted with methanol and then placed onto the gel. Two layers of with transfer buffer soaked 3mm blotting papers were placed on and under the membrane-gel sandwich in the electroblotting chamber. The electroblotting was performed at a constant current of approx. 2mA/cm^2 for 90min.

After transfer of proteins, the PVDF membrane was blocked with 1x NET buffer containing 0.25% of porcine skin gelatin for 1 hour. The the PVDF membrane was incubated with the primary antibody diluted in the same buffer containing gelatin overnight at 4°C. The second day, the PVDF membrane was washed with 1x NET buffer three times for 10 minutes and subsequently incubated with the appropriate secondary antibody conjugated to HRP for 2 hours. The membrane was then again washed with 1x NET buffer three times for 10 min. Immunoreactive bands were visualized on the membrane by addition of the ECLplus reaction mixture employing a chemiluminiscence imager (Fluorchem^{TM} IS-8900).

3.2.1.4 HPCL protein purification

After subcellular fractionation, pellets (1050g or 14000g or 110000g) containing protein of interest were dissolved in chromatographic buffer A containing 6M urea and passed through a DNA binding column and placed on ice. If the supernatant (110000g) was used, it was mixed with urea to a final concentration of 6M and again passed through the DNA binding column and placed on ice. Samples containing urea were mixed with chromatographic buffer A in a ratio of 1:5 and immediately used for AEC.

A) Anion exchange chromatography

The anion exchange chromatography (AEC) was performed with a strong anion exchange chromatography column (MonoQ, column volume of 1ml) applying a Tris-HCl based buffer system and a NaCl gradient based elution with a buffer flow rate of 1ml per 1min. After sample injection into the sample loop, the column was equilibrated until the initial peak representing unbound material (i.e. flow-through (FT) decreased to base line level. Then, the gradient for the elution of proteins from the column by buffer B (0-100% of buffer B) was started and the individual fractions were collected per minute (1 minute ≈1

fraction) for approx. 30 min. Proteins eluted from the column were detected at 280 and 220nm.

An aliquot (usually 10-20%) from each fraction including the FT was precipitated by acetone (final concentration of 80%), solubilized in 1x Laemmli sample buffer and analysed by Western blot.

B) Reverse phase chromatography

Reverse phase chromatography (RPC) was performed with a silica based C8 column (Symetry300) applying "buffers" (solutions) containing trace amount of TFA (max. 0.1%) and an ACN gradient based elution with a buffer flow rate of 1ml per 1min. Relevant fractions from AEC were acidified by TFA to a final concentration of 0.1% and injected into the sample loop. The column was equilibrated until the initial peak representing FT decreased to base line. Then, the gradient for the elution of proteins from the column by "buffer" B (10-80% of "buffer" B) was started and individual fractions were collected per minute (1 minute ≈ 1 fraction) for approx. 60 min. Proteins eluted from the column were detected at 280 and 220nm.

Fractions were evaporated in a vacuum centrifuge, dissolved in 1x Laemmli sample buffer and used for Western blot analysis.

3.2.1.5 2D gel electrophoresis

Samples were precipitated by acetone (final concentration of 80%), dried and analyzed by 2D-gel electrophoresis (2D-GE) (Department of proteomics).

Briefly, 400µg of protein sample was dissolved in rehydration buffer and loaded onto an immobilized pH gradient (IPG) gel strip (pH range 3-10, 11 cm). After isoelectric focusing (IEF) the IPG gel strip was incubated with the equilibration stock solution, alkylated by iodoacetamide and loaded onto the top of a 12% SDS-polyacryl-amid gel. Protein separation efficiency according to the molecular weigh was checked by the same prestained molecular weight marker as for 1D SDS-PAGE (section 3.2.1.3). Proteins from the gel were transferred onto a PVDF membrane that was subsequently blocked by 1x NET buffer with 0.25% porcine skin gelatin for at least 1 hour. The subsequent

procedures of incubation with antibodies and immunodetection were performed in the same way as described for Western blot (section 3.2.1.3).

3.2.1.6 MALDI-TOF MS

The polyacryal-amid gel from SDS-PAGE was stained with Coomassie Brilliant Blue (CBB) and slices of the gel containing proteins of interest were analyzed by MALDI-TOF MS (matrix assisted laser desorption/ionisation-time of flight mass spectrometry) analysis (Department of Proteomics). Alternatively, immunoreactive bands detected on the PVDF membrane were labeled and excised from the membrane for further MALDI-TOF MS analysis. If proteins transferred onto the PVDF membrane were subjected to MS analysis, the membrane was blocked with the non-protein containing polymeric solution Roti-Block instead of porcine skin gelatin. For CBB staining, the SDS-polyacryal-amid gel was firstly incubated with gentle shaking for 1 hour in CBB solution and then destained until the protein bands were visible. In parallel with CBB staining of the gel, the same sample was usually used for Western blot analysis by the relevant antibody to show the presence of protein of interest in the gel. In order to make sure that the appropriate protein would be cut from the gel for further analysis, the whole area near to the expected size of the protein was cut in small gel slices and subjected to MALDI-TOF MS.

Briefly, gel slices were rinsed by ultrapure water and, by a solution of $(NH_4)HCO_3$/ACN (1:1) and by 100% ACN. Subsequently, trypsin digestion at 37°C was performed overnight. Peptides were extracted by 1% TFA containing octyl-glucopyranoside. Aliquots of peptide digests were mixed with a solution of 2,5-dihydrobenzoic acid, ACN/H_3PO_4 on a stainless steel target (Bruker Daltonik, Bremer, Germany) using a dried-droplet method. Peptide mass fingerprints (PMF) of tryptic digests were obtained by MALDI-TOF-MS using an Ultraflex TOF/TOF mass spectrometer (Bruker Daltonik). Peptide mass standards (Bruker Daltonik) were used for external calibration of the mass spectra. Mass spectra were acquired in a reflector mode using FlexControl 2.4 Software (Bruker Daltonik), and analysed by the FlexAnalysis software 3.0. The SwissPprot database employing the MASCOT 2.0 program was used for search of peptide masses to

identify the proteins. The versions used were SwissProt 48.8 or MSDB. The taxonomic category was "homo sapiens (human)" since human cells were analyzed. In addition to PMF, other main search parameters were set as follows: enzyme specifity: trypsin, fixed modification: carabamidometylation of cysteine, variable modification: oxidation of methionine, mass values: monoisotopic, protein mass: unrestricted peptide, peptide mass tolerance: +/-100 ppm, peptide charge state: 1+, max. missed cleavage: 1. Protein matches were assessed on the basis of the number of peptides matched to target protein. The intensity of these peptides was expressed as percentage of all submitted peptides, and MOWSE (molecular weight search) score greater than 60 ($p<0.05$) for MS data were regarded positive for protein identifications. The score threshold to achieve $p<0.05$ was set by Mascot algorithm and was based on the size of the database used in the search. Only proteins with the score higher than 60 and highest number of matching peptides in each Mascot search were accepted as successful indications.

3.2.1.7 Reactive oxygen species measurement

Total cellular reactive oxygen species (ROS) were measured as concentration of H_2O_2 by *Amplex Red Hydrogen Peroxide/Peroxidase Assay* (Invitrogen, Carlsbad, CA, USA). This method is based on the reaction of Amplex Red with H_2O_2 in the presence of HRP (included in kit) generating a red product (resorufin) that can be quantified by fluorescence measurement. Nanomolar concentrations of H_2O_2 in solutions can be sensitively measured using this kit.

Cells on a six-well plate were washed with the kit reaction buffer, scraped into dark eppendorf tubes and briefly sonicated on ice (three times four seconds). An equal amount of sample and reaction mixture (prepared according to the product protocol) were mixed together on a 96 well plate and incubated protected from light for at least 30min at room temperature. Then, the fluorescence was measured at 595nm after excitation at 530nm using a spectrofluorometer (FL-600). Values of fluorescence were normalized to µg of protein in each sample.

3.2.1.8 Luciferase activity

The activity of luciferase in cells transfected with ARE- and HRE-reporter plasmids was measured as relative light units (RLU) with the Luciferase Assay System according to the manufacturer's protocol (Promega Corporation, Madison, WI, USA). In brief, cells were lysed with passive lysis buffer (100µl per well, 48 well plate), shaken for 15 min at room temperature, and frozen at -80°C. After thawing and measurement of the protein concentration, the components of the Luciferase Assay System were added to the aliquot of the sample on a 96 well plate, and the chemiluminescence was measured using a spectrofluorometer (FL-600). The values of RLU were normalized to µg of protein in each sample.

3.2.2 Molecular biological methods

3.2.2.1 Transformation of bacteria and isolation of plasmid

Transformation of competent cells: For transformation of competent cells, i.e. *E.coli* TOP10, was performed with the heat shock method. The plasmid was gently mixed with one aliquot of the competent cells and incubated on ice for 30 min. Then the mixture was heated at 42°C for 1 min followed by immediate cooling on ice. Thereafter, the bacterial cells were cultured in 100µl SOC medium at 37°C for 1 hour. The transformed bacterial cells were spread over an ampicillin containing agar dish and incubated overnight at 37°C. The successfully transformed cells formed colonies on the agar plates.

Plasmid isolation: Plasmids isolation was performed with Maxiprep Kit (MACHEREY-NAGEL GmbH, Düren, Germany). The colonies of transformed *E.Coli* TOP10 cells were picked and cultured in 200ml LB medium and grown up to a density of about 10^9 cells per ml. The cells were pelleted by centrifugation at 5800g for 30 min. Subsequently, the pellet was used for the isolation of plasmid-DNA according to the Maxiprep Kit protocol.

3.2.2.2 RNA isolation, reverse transcription and real-time PCR

Cells were washed with PBS and scraped in extraction buffer (peqGOLD TriFast, Peqlab Biotechnology GmbH, Erlangen, Germany). RNA isolation was performed in accordance

with the manufacturer's instruction. To eliminate potential DNA contamination, RNA (1µg) was mixed with H_2O and 1µl of DNAse (1U/µl) to a final volume of 20µl and incubated for 30 min at 37°C and 7 min at 75°C. After cooling on ice, the following components were added to each sample: 8µl of M-MuLV reaction buffer (5x), 4µl of deoxynucleotide triphosphate mixture (10mM of each nucleotide), 2µl of random hexamer primer (100µM), 2µl of H_2O, 2µl of RiboLock RNAse inhibitor (40U/µl), 2µl of ReverseAid M-MuLV reverse transcriptase (20U/µl) (all from Fermentas Life Sciences, Burlington, Ontario, Canada). After 60 min at 39°C, the reverse transcriptase was inactivated by heating the mixture at 96°C for 2 min. As a negative control, reverse transcriptase was omitted from the reactions. The cDNA was used as a template in the real-time PCR reactions using the primer pairs listed in section 2.1.5. The real-time PCR was performed using the ABI Prism 7300 Detection System (Applied Biosystems, Lincoln Centre Drive Foster City, CA, USA) with SYBR-Green as fluorescent dye, enabling real-time detection of PCR products. The real-time PCR mixture was prepared according to the manufacturer's protocol (Platinum SYBR Green qPCR SuperMix-UDG, Invitrogen, Carlsbad, CA, USA). Cycling conditions were 50°C for 2 min, 95°C for 10 min, followed by 45 cycles of 94°C for 10 s, 55°C for 20 s, 72°C for 30 s. For quantification, the target gene was normalized to β-actin mRNA, using the standard equation for real-time PCR analysis: $T_0/R_0=k2^{CT,R-CT,T}$ with T_0 representing the initial number of target gene mRNA copies, R_0 representing the initial number of standard gene mRNA copies, CT,R is the threshold cycle of reference (β-actin) and CT,T threshold cycle of target gene. The values of the control groups were normalized to 1.

3.2.2.3 DNA agarose gel electrophoresis

The DNA samples were mixed with loading buffer and loaded onto a 1% agarose gel. The electrophoresis was performed for around 1 hour with 5 V/cm. The negatively charged DNA migrated from the cathode (-) to the anode (+). To visualize DNA, the gel was treated with ethidium bromide that intercalates into the DNA double strands forming a fluorescent complex by excitation with UV light. DNA bands were detected by chemiluminiscence imager (Fluorchem™ IS-8900). The size of DNA fragments was determined by comparison with a DNA size marker.

3.2.2.4 RNA interference by synthetic siRNA

Selective inhibition of target gene was performed using specific siRNAs. As a control, a siRNA sequence (si-con) was employed that does not target any gene in the human genome and has been tested by micro-array analysis (Dharmacon Inc., Chicago, IL, USA). The forward (+) and reverse (-) strands of the siRNAs were synthesized commercially (Biomers.net GmbH, Ulm, Germany). Forward (+) and reverse (-) strands were annealed at a final concentration of 40mM each by incubation at 95^{o}C for 1 min and at 37^{o}C for 1 hour in annealing buffer (20mM K-acetate, 0.4mM Mg-acetate 6mM HEPES, pH=7.4).

3.2.2.5 Plasmids

The full length NOX1 or NOX4 cDNA was ligated into the pCMV-HA plasmid. NOX1 was tagged with HA at its N- or C-terminus and NOX4 at its C-terminus and their integrity was confirmed by sequencing. The Trx1 cDNA was ligated into pIRES vector. The Trx1 plasmid was kindly provided by Prof. Brüne (Frankfurt/Main) and it was described previously [196]. The pGL3-TK plasmid with the thymidine kinase minimal promoter was used to construct the HRE- and ARE-reporter plasmids as described [197]; [198]. The forward and reverse oligonucleotides of the HRE from the phosphoglycerate kinase (PGK) gene and the forward and reverse oligonucleotides from the NADPH quinone-oxido-reductase (NQO1) gene were employed for plasmid construction. The oligonucleotide sequences for the production of the relevant PCR products are given in section 2.1.6.

3.2.3 Cell biological methods

3.2.3.1 Cell culturing under different oxygenation conditions

Cells were incubated at 37^{o}C in a water-saturated atmosphere containing 5% CO_2 in air (normoxic conditions). A hypoxic environment was prepared in a chamber equilibrated with a water-saturated gas mixture of 1% O_2, 5% CO_2 at 37^{o}C (Innova CO-48, New Brunswick Scientific, Edison, NJ, USA). For culturing of cells in the different normoxic and hypoxic exposure intervals, cells were transferred between these two chambers.

When switching from normoxic to hypoxic conditions, the equilibration time to reach 1% O_2 within the cell supernatant was determined as about 1 hour, and *vice verse*, within minutes.

3.2.3.2 Cell transfection by siRNA and plasmid

Transfection of cells with siRNA and plasmid was performed by Lipofectamine 2000 according to the company's protocol. The final concentration of siRNA was 100nM and the amount of plasmid used for transfection was approx. 2µg per 150000 cells. After transfection, cells were incubated with OPTI-MEM for six hours, then the OPTI-MEM was replaced by cell culture medium. Cells were grown for 48 hours after siRNA transfection and for 24 hours after plasmid transfection.

4. Results

4.1 Detection of NOX1 and NOX4 proteins, and analysis of NOX1- and NOX4-dependent ROS generation

4.1.1 Expression of NOX1 and NOX4 mRNA in A549 cells

Firstly, the presence of NOX1 and NOX4 mRNA in A549 cells was demonstrated using specific primers applied in RT-PCR (Figure 8A, B, upper panels). Secondly, the same set of primers was used for quantification of mRNA by real-time RT-PCR (Figure 8A, B, lower panels). Expression of NOX1 mRNA in A549 was compared to NOX1 expression in CaCo2 cells employed as a cell line with high abundance of NOX1. NOX4 mRNA expression in A549 cells was compared to NOX4 expression in HUVEC employed as a cells with high abundance of NOX4. In both cases, the number of mRNAs copies in A549 cells was normalized to 1. As expected, the quantification of mRNA by real-time RT-PCR revealed a significantly higher level of NOX1 mRNA in CaCo2 cells when compared to A549, and significantly higher NOX4 mRNA level in HUVEC in comparison to A549.

Finally, based on these results, we also compared ΔCt values from real-time RT-PCR of NOX1 and NOX4 in A549 cells (Figure 8C). The comparison showed significantly higher expression of NOX1 mRNA than NOX4 in A549 cells.

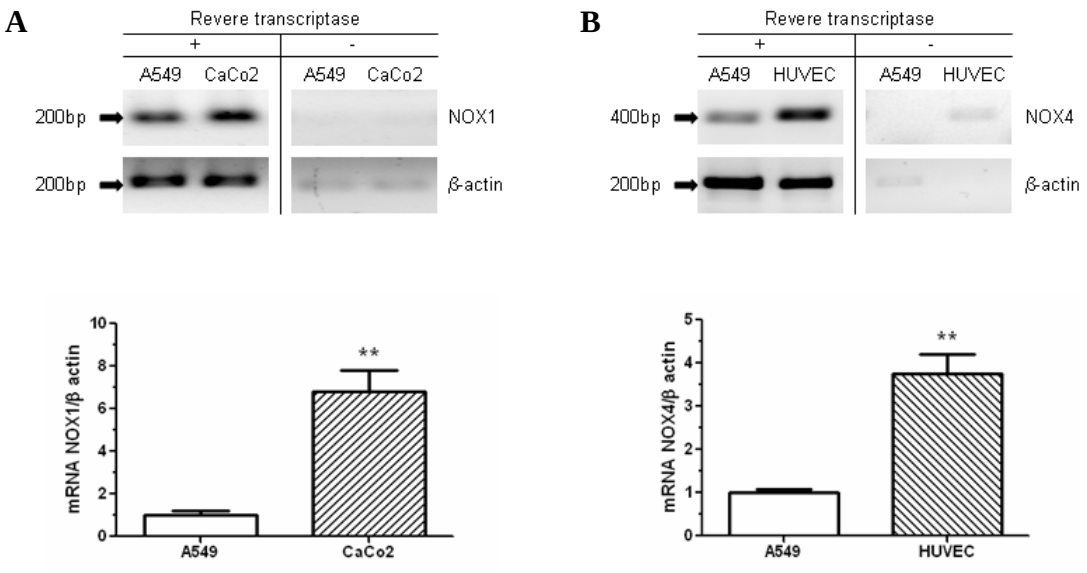

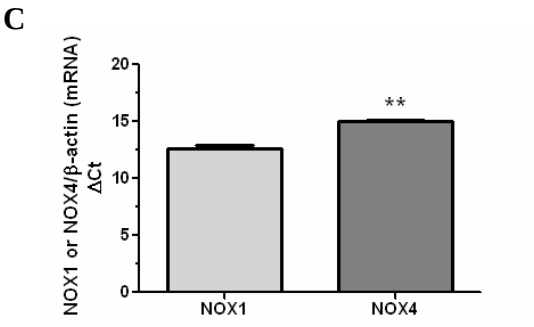

Figure 8: Expression of NOX1 and NOX4 mRNA in A549 cells
A) Upper panel: Ethidium bromide stained agarose gel electrophoresis of RT-PCR analysis of NOX1 mRNA expression in A549 and CaCo2 cells. cDNA made from total RNA in the presence (+) or absence (-) of reverse transcriptase. Lower panel: Quantification of NOX1 mRNA levels by real-time RT-PCR in A549 and CaCo2 cells (** $p<0.01$, n=3, unpaired t-test). **B)** Upper panel: Ethidium bromide stained agarose gel electrophoresis of RT-PCR analysis of NOX4 mRNA expression in A549 cells and HUVEC. cDNA made from total RNA in the presence (+) or absence (-) of reverse transcriptase. Lower panel: Quantification of NOX4 mRNA levels by real-time RT-PCR in A549 cells and HUVEC (** $p<0.01$, n=3, unpaired t-test). **C)** Comparison of ΔCt values from real-time RT-PCR of NOX1 and NOX4 mRNAs in A549 cells (** $p<0.01$, n=4, unpaired t-test). In all experiments, β-actin was used as reference gene.

4.1.2 Schema of binding sites of different NOX1 and NOX4 antibodies to NOX1 and NOX4 proteins

The immunodetection of NOX1 and NOX4 proteins is a common problem since different antibodies display different patterns of immunoreactive protein bands in Western blot. Based on this fact, one of the aims of our work was to characterize and select the most suitable antibodies for NOX1 and NOX4 proteins detection. We used several commercially available and custom made antibodies targeted to different epitopes of NOX1 and NOX4 proteins. The schematic structure of NOX1 and NOX4 proteins with the binding sites of the different antibodies are depicted on Figures 9A and B.

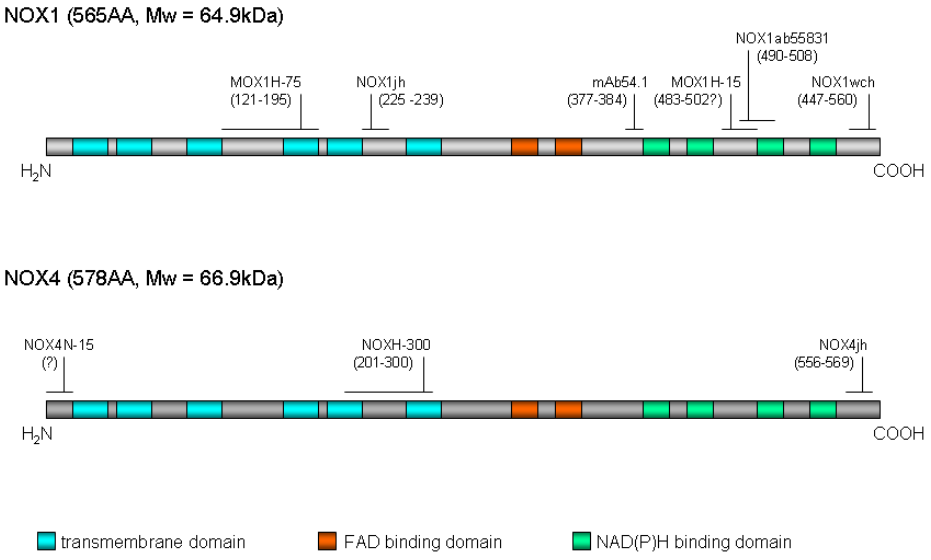

Figure 9: Binding sites of NOX1 and NOX4 antibodies
NOX1 and NOX4 antibodies binding sites, molecular weights, N- and C-terminus, length and characteristic domains of NOX1 and NOX4 proteins are depicted.

4.1.3 Detection of putative NOX1 and NOX4 proteins by different antibodies in total cell lysates

4.1.3.1 NOX1 antibodies (A549 versus CaCo2)

Initially, western blot analyses of total cell lysates from A549 and CaCo2 cells were performed. For detection, five different NOX1 polyclonal antibodies were used. In addition, the mAb54.1 monoclonal antibody detecting primary NOX2 was applied since this antibody has been described to be able to recognize a fragment of NOX1 recombinant protein [199]. 50ug of protein was loaded per well and β-actin was used as a loading control (Figure 10A).

The NOX1jh antibody produced by a custom service detected a band at 95kDa that was more strongly abundant in A549 than in CaCo2 cells. MOX1 H-75 detected the strongest bands at 45kDa and 50kDa. Both these proteins were present at a higher level in A549 than in CaCo2 cells. MOX1 H-15 did not show any band. NOX1ab55831 showed bands at 38kDa, 60kDa and 80kDa. The 60kDa band was pronounced in A549 cells whereas the 80kDa band in CaCo2 cells. NOX1wch detected two bands - the first at 55kDa and the

second at 65kDa. Both bands were more strongly abundant in CaCo2 than in A549 cells. mAb54.1 displayed a strong band at 55kDa with similar intensity in A549 and CaCo2 cells.

4.1.3.2 NOX4 antibodies (A549 versus HUVEC)

At least three different polyclonal antibodies were used for detection of NOX4 in total cell lysate of A549 cells and HUVEC. Again, 50ug of protein was loaded per each well and β-actin was used as loading control (Figure 10B).

The NOX4jh antibody (produced by a custom service) detected bands at 42kDa, 62kDa and at 67kDa in A549 cells and at 40kDa, 42kDa, 50kDa, 67kDa, 80kDa and 98kDa in HUVEC. The predicted size of NOX4 is 67kDa. The band of 67kDa was detected in both cell types but it was more strongly abundant in HUVEC than in A549 cells. On the other hand, proteins at 62kDa and 42kDa were very weakly expessed in HUVEC and strongly expressed in A549 cells. Bands at 40kDa, 50kDa, 80kDa and 98kDa were only present in HUVEC and not in A549. NOX4 H-300 and NOX4 N-15 did not detect any bands.

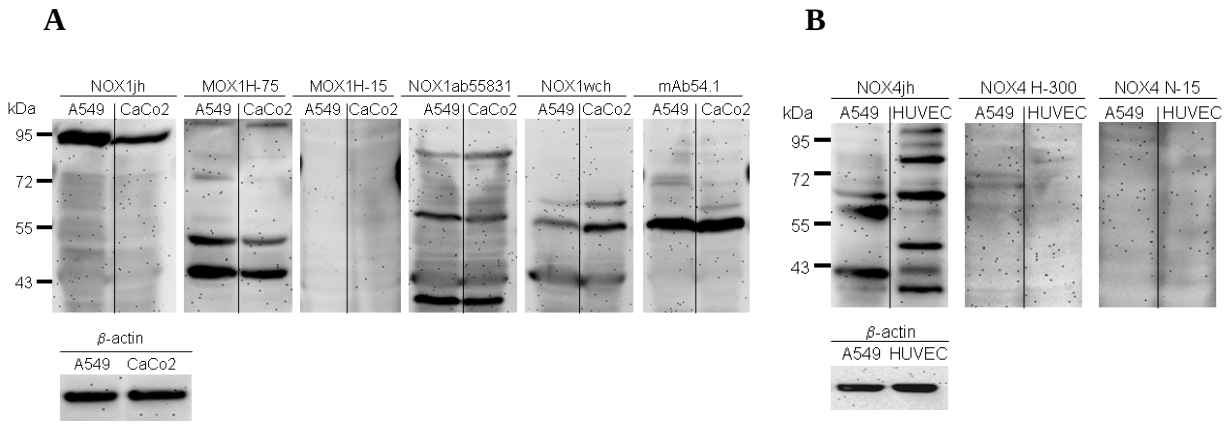

Figure 10: Detection of putative NOX1 and NOX4 proteins in total cell lysates employing different NOX1 and NOX4 antibodies
Western blot analysis of total cell lysates from **A)** A549 and CaCo2 cells employing different NOX1 antibodies, and from **B)** A549 cells and HUVEC employing different NOX4 antibodies. 50µg of protein were loaded per well and β-actin was used as loading control.

4.1.4 Detection of putative NOX1 and NOX4 proteins, p22phox and NOXO1 in cell compartments

4.1.4.1 NOX1 in cytosol, membrane, nuclei and cytoskeleton

NOX1 has been described as a 50-65kDa protein anchored in the plasma membrane. Thus in the next step, we were interested in the subcellular localization of proteins reacting with different NOX1 antibodies. Since the antibodies were not suitable for immunocyto-staining, we performed subcellular fractionation. Cytosolic, membrane, nuclear and cytoskeleton fractions were separated using the *Complete Cell Fraction Kit*. The purity of crude fractions was evaluated by relevant cellular markers (Figure 11D). Again, five NOX1 antibodies and mAb54.1 were used to detect potential NOX1 proteins (Figure 11A).

NOX1jh detected a band at 95kDa localized most strongly in the cytosol and less strongly in the membrane and nuclei of A549 cells. In CaCo2 cells, this band was expressed almost equally in cytosol, membrane and nuclei. In both A549 and CaCo2 cells, MOX1 H-75 detected bands at 43kDa in the membrane and nuclei, a very weak 50kDa band and, a 55kDa band in the nuclei and two bands between 72 and 95kDa also in the nuclei. MOX1 H-15 visualized bands at 67kDa, 80kDa and 97kDa in the nuclei, both in A549 and CaCo2 cells beside weak 60kDa and 45kDa bands in the cytosol of A549 cells. NOX1ab55831 interacted with a protein band at 60kDa mainly in the cytosol. This band was stronger in A549 than in CaCo2 cells. Additional bands at 40kDa and 90kDa both in A549 and CaCo2 cells were detected. NOX1wch displayed strong band at 55kDa and a weaker band at 65kDa, both bands were localized predominantly in the cytoskeleton and at a lower level in the nuclei. An additional weak 67kDa band was present in the cytoskeleton fraction of CaCo2 cells. The 55kDa and 65kDa bands were slightly more abundant in CaCo2 than in A549 cells. Other strong immunoreactive proteins were detected with the NOX1wch antibody at the position of 43kDa in all fractions. Interestingly, this antibody also detected a band at 97kDa (more strongly in CaCo2 than in A549 cells) in nuclei that seemed to be in common with the band detected by MOX1 H-15 in the same fraction. mAb54.1 detected a band at 55kDa in the cytosol, membrane, and nuclei both in A549 and in CaCo2 cells, a 70kDa band in the membrane of A549 and

a 60kDa band in the cytosol of CaCo2 cells. Additionally, several weak bands were present in CaCo2 cells in the range of 60-72kDa in the membrane, nuclei and cytosol.

4.1.4.2 NOX4 in cytosol, membrane, nuclei and cytoskeleton

Subcellular fractionation was also performed for the detection of NOX4 proteins (Figure 11B).

NOX4jh detected a strong band at 62kDa predominantly in the cytosol and a 67kDa band predominantly in the cytoskeleton of A549 cells. The band of 62kDa was almost not present in HUVEC and the band of 67kDa was most strongly present in nuclei and weakly in the cytoskeleton of HUVEC. Additional bands at 80kDa observed only in the cytosol and at 50kDa in the cytosol and cytoskeleton were detected in HUVEC. NOX4 H-300 reacted with a band of 65kDa that was highly abundant in the cytosol and weakly in the membrane of A549 cells. Additional weak bands at 67kDa in the membrane and at 72kDa in the cytosol of A549 cells also reacted with this antibody. In HUVEC, the NOX4 H-300 only detected a very weak band at 72kDa in the cytosol. NOX4 N-15 did not detect any band.

4.1.4.3 p22phox and NOXO1 in cytosol, membrane, nuclei and cytoskeleton

p22phox and NOXO1 have been described as essential components of the functional NADPH oxidase complex containing NOX1. Thus, in the context to the previous experiments demonstrating different localizations of potential NOX1 proteins, we were interested, in which fractions these two subunits would be localized. Both in A549 and CaCo2 cells, p22phox was most highly abundant in the membrane, less in nuclei and a very low abundance was observed in the cytoskeleton. In the cytosolic fraction, p22phox was almost undetectable. Interestingly, NOXO1 was almost entirely present in the cytoskeleton fraction of A549 and CaCo2 cells (Figure 11C).

In order to evaluate the purity of the subcellular fractions, different cellular compartment markers were applied. PGK1/2 was used as a typical cytosolic protein, Na^+/K^+-ATPase α as a (plasma) membrane protein, cytokeratin (types 5, 6, 8, 17) as a cytoskeleton proteins and lamin B as a nuclear and cytoskeleton protein. As displayed in Figure 11D, the

subcellular fractionation showed only small cross-contamination by the appropriate markers. In this regard, interesting observations were that these types of cytokeratin were not detectable in HUVEC and that lamin B was mainly localized in the cytoskeleton of A549 and CaCo2 cells, but in nuclei and cytoskeleton of HUVEC. Lamin B is a component of nuclear intermediate filaments that are known to be difficult to dissolve in many weak detergents, including likely those employed for the cell lysis in our study. Therefore, this observation may be explained by differences of the solubility of lamin B complexes that may be altered between different cell types.

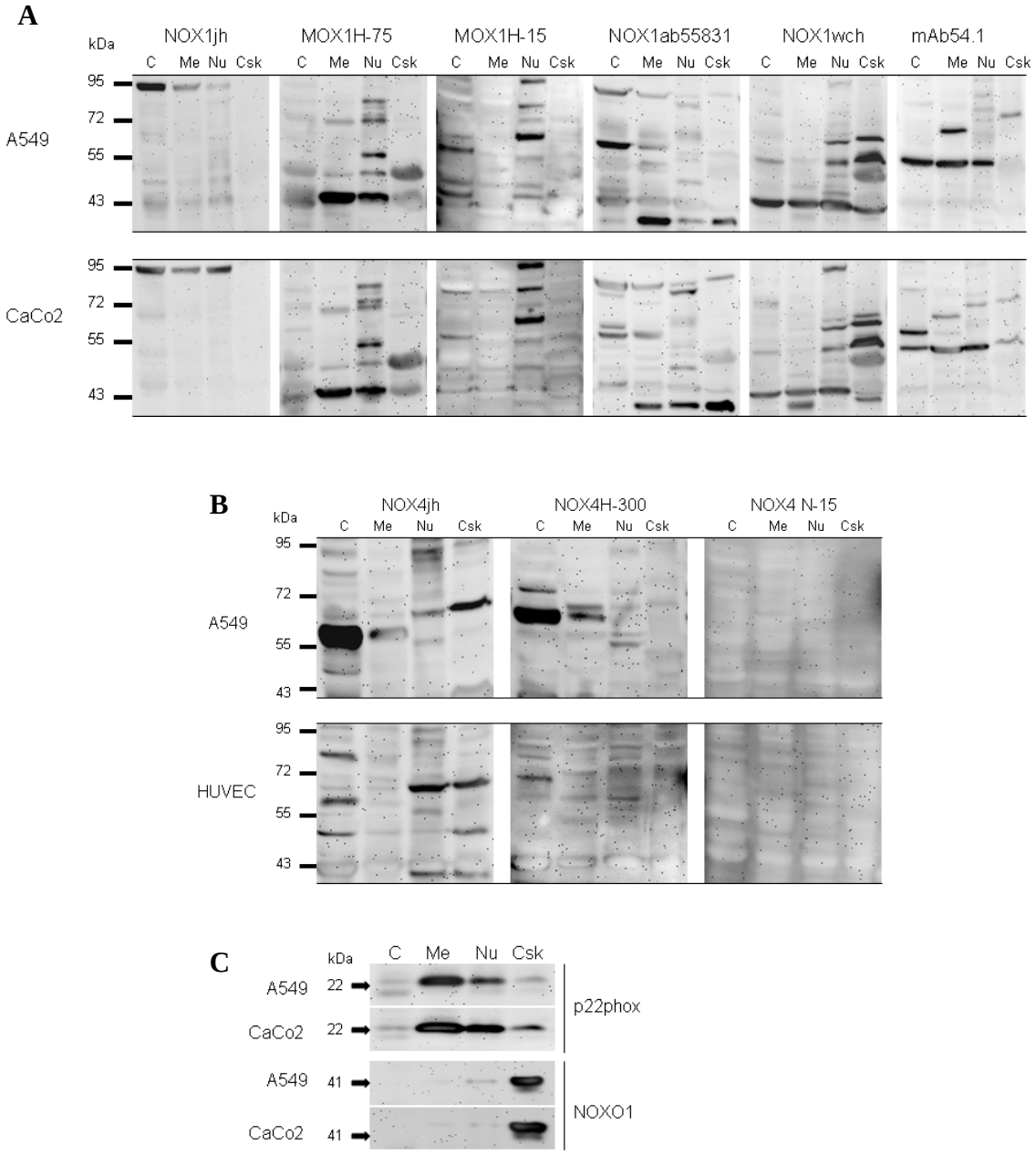

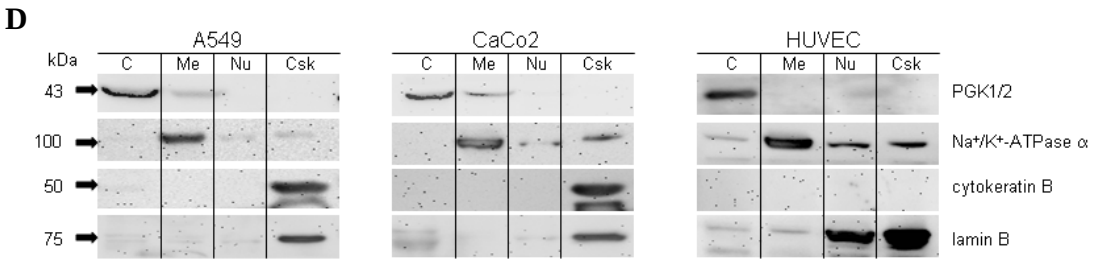

Figure 11: Detection of putative NOX1 and NOX4 proteins, p22phox and NOXO1 in different cell compartments
Western blot analysis of subcellular fractions (cytosol (C), membrane (Me), nuclei (Nu) and cytoskeleton (Csk) from **A)** A549 and CaCo2 cells using different NOX1 antibodies, **B)** A549 cells and HUVEC using different NOX4 antibodies, **C)** A549 and CaCo2 cells using p22phox and NOXO1 antibodies, **D)** A549, CaCo2 cells and HUVEC using antibodies against different subcellular markers (PGK1/2 - cytosol marker, Na^+/K^+-ATPase α – membrane marker, cytokeratin – cytoskeleton marker, lamin B – cytoskeleton and nucleus marker). In experiments A, B, C 50µg of protein and in D 20µg of protein were loaded per well.

4.1.5 Detection of putative NOX1 and NOX4 proteins, p22phox and NOXO1 in Tx-100 soluble and insoluble fraction

Non-ionic detergents such as Triton X-100 (Tx-100) are commonly used for permeabilization of cell membranes. Another technical approach employing Tx-100 is centrifugal separation of the Tx-100 soluble fraction containing cytosolic, organelle and membrane proteins and of the Tx-100 insoluble fraction containing cytoskeleton and cytoskeleton associated proteins. Since the previous experiment applying the *Complete Cell Fractionation Kit* showed that some of NOX1 and NOX4 immunoreactive proteins were localized in the cytoskeleton fraction, we wanted to know whether the use of Tx-100 would confirm these results.

4.1.5.1 NOX1 in Tx-100 soluble and insoluble fraction

The NOX1jh antibody detected a band at 95kDa that was localized both in the 14000g pellet (p) and in the supernatant (s) in samples not treated with Tx-100. In contrast, in samples treated with Tx-100 this protein was localized predominantly in the 14000g supernatant representing the Tx-100 soluble fraction. This phenomenon was observed

both in A549 and CaCo2 cells. The MOX1 H-75 immunoreactive band at 43kDa was mainly localized in the supernatant after 14000g centrifugation both in samples with and without Tx-100. Additionally, several weak bands occurred in the 14000g pellets, both in A549 and CaCo2 cells. MOX1 H-15 did not detect any band. NOX1ab55831 displayed a band at 60kDa in A549 but not in CaCo2 cells. This band was present in the 14000g supernatant regardless of treatment by Tx-100. NOX1wch detected bands at 55kDa and 65kDa that were always enriched in the 14000g pellet. After treatment of the samples with Tx-100, the abundance of the 55kDa band in the Tx-100 soluble fraction of CaCo2 was increased (Figure 12A).

4.1.5.2 NOX4 in Tx-100 soluble and insoluble fraction

The NOX4jh antibody detected bands at 62kDa and 67kDa in A549 cells. The 62kDa band was mainly present in the 14000g supernatant and the 67kDa band in the 14000g pellet both in samples with and without Tx-100. In HUVEC, bands at 50kDa, 67kDa and 80kDa were detected. Without addition of Tx-100, the 80kDa band was present in the 14000g supernatant whereas the 50kDa and 67kDa bands were strongly present in the pellet and weakly in the supernatant. Treatment of samples with Tx-100 slightly increased the presence of 50kDa and 67kDa proteins in the 14000g supernatant. NOX4 H-300 detected only a pronounced band in HUVEC at the position of 42kDa in the 14000g supernatant. NOX4 N-15 did not detect any band (Figure 12B).

4.1.5.3 p22phox and NOXO1 in Tx-100 soluble and insoluble fraction

p22phox was present at a similar level in the 14000g supernatant and the pellet in samples not treated with Tx-100. After treatment of the cell lysates with Tx-100, p22phox was much stronger abundant in the 14000g supernatant (Figure 12C). This was a typical observation both for A549 and CaCo2 cells.

NOXO1 was localized in the 14000g pellet, but after adding Tx-100 it was partially transferred to the Tx-100 soluble fraction in A549 cells and completely transferred to this fraction in CaCo2 cells (Figure 12C). Interestingly, the NOXO1 antibody showed a

double band in A549 cells but a single band in CaCo2 cells. The double band may represent different splice variants or phosphorylation states of NOXO1.

The effects of Tx-100 on the solubility of membrane and cytoskeleton associated proteins, were evaluated with the different subcellular compartments markers (Figure 12D). PGK1/2 used as the cytosolic marker was always present in the 14000g supernatant without regard to Tx-100 treatment. Similarly, the intermediate filament component cytokeratin was always present in the 14000g pellet. On the other hand, the plasma membrane marker Na^+/K^+-ATPse α was present both in the 14000g pellet and in the supernatant of samples containing no Tx-100. However, addition of Tx-100 caused a transfer of this membrane protein to the Tx-100 soluble fraction indicating that Tx-100 effectively solubilized membrane proteins. As observed previously, the particular types of cytokeratins were not detectable in HUVEC.

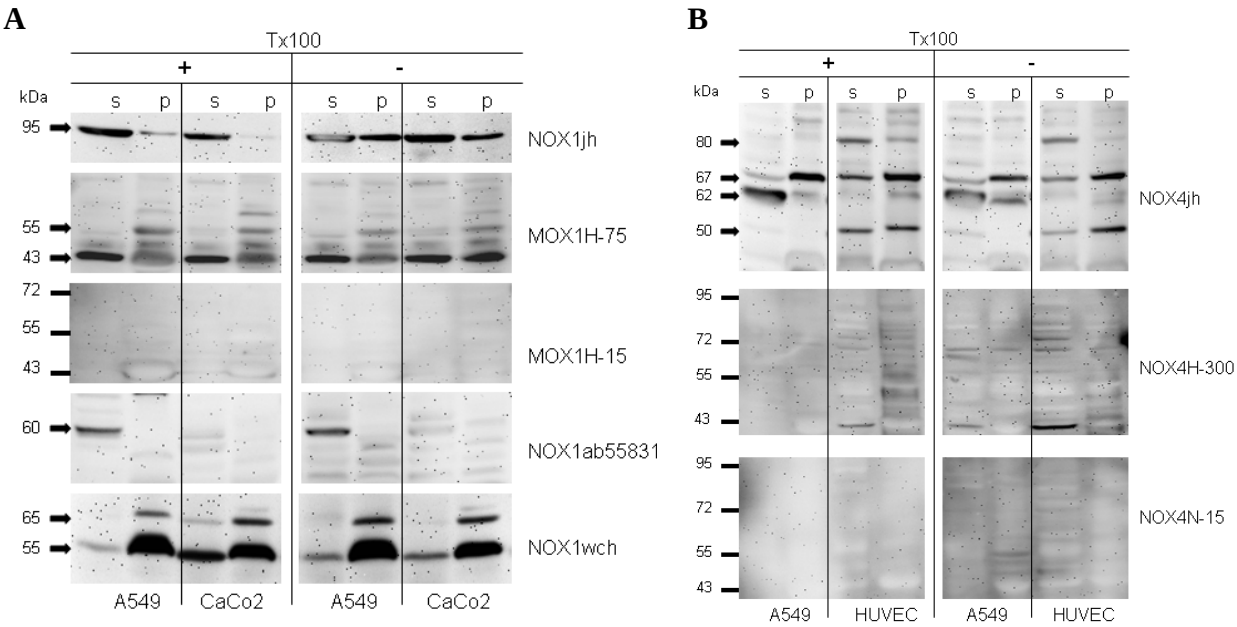

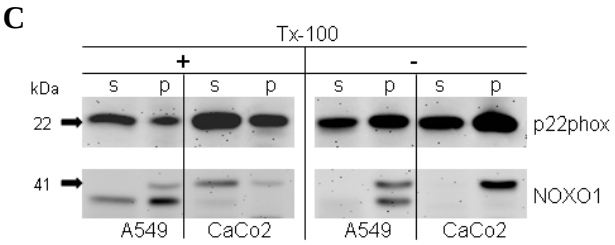

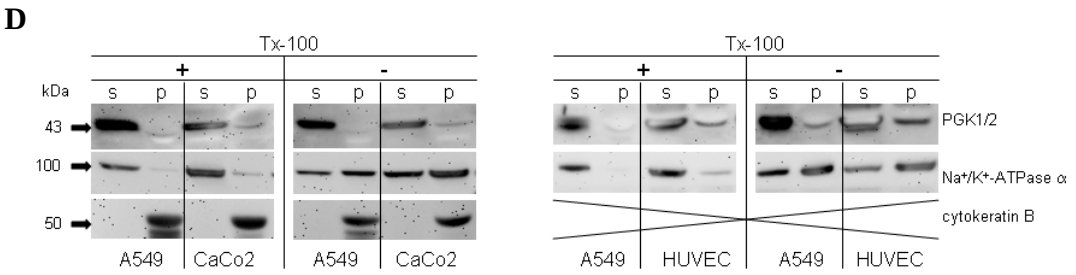

Figure 12: Detection of putative NOX1 and NOX4 proteins, p22phox and NOXO1 in Tx-100 soluble and insoluble fractions
Western blot analysis of cell lysates fractionated by centrifugation after treatment with Tx-100 (+) or without treatment (-) from **A)** A549 and CaCo2 cells employing different NOX1 antibodies, **B)** A549 cells and HUVEC employing different NOX4 antibodies, **C)** A549 and CaCo2 cells employing p22phox and NOXO1 antibodies, **D)** A549, CaCo2 cells and HUVEC employing antibodies against different subcellular markers. In A, B, C experiments 50μg of protein and in D 20μg of protein per well were loaded.

4.1.6 Detection of putative NOX1, NOX4 proteins and p22phox in the plasma membrane of A549 cells

Both NOX1 and NOX4 have been suggested to be plasma membrane proteins. However, our results applying different NOX1 and NOX4 antibodies for the analysis of subcellular fractions did not confirm the membrane localization of these proteins. In order to ensure that the potential NOX1 and NOX4 proteins were not localized in the plasma membrane, we performed Western blot analysis of proteins from high purity plasma membrane fraction. Accurate and selective plasma membrane isolation was achieved by using a commercially available *Membrane Isolation Kit*. Western blots were performed with the NOX1 and NOX4 antibodies that appeared to have the best immunoreactive properties.
NOX1jh detected a band at 95kDa that was present in all fractions. NOX1ab55831 detected bands at 60kDa in the cytosol, at 95kDa predominantly localized in the cytosol and at 43kDa present in all fractions. NOX1wch detected 55kDa and 65kDa bands in the total membrane fraction containing however also cytoskeleton proteins and a 43kDa band in all fractions. NOX4jh detected a 67kDa band localized mainly in the total membrane fraction and a 62kDa band localized in the cytosolic fraction. In addition, a weak 80kDa band was detected in the plasma membrane fraction (Figure 13A).

Interestingly, p22phox was most strongly abundant in the total membrane fraction and very weakly in the plasma membrane fraction. There was no p22phox signal in the cytosolic fraction (Figure 13B).

For evaluation of the separation processes, the markers of the cytosol (PGK1/2), cytoskeleton (cytokeratin) and plasma membrane (Na^+/K^+-ATPse α) were used. Indeed, as demonstrated at Figure 13C, PGK1/2 was mainly present in the cytosol, cytokeratin in the total membrane fraction containing also cytoskeletal proteins, and Na^+/K^+-ATPse α was most strongly abundant in the plasma membrane fraction and less in total membrane fraction.

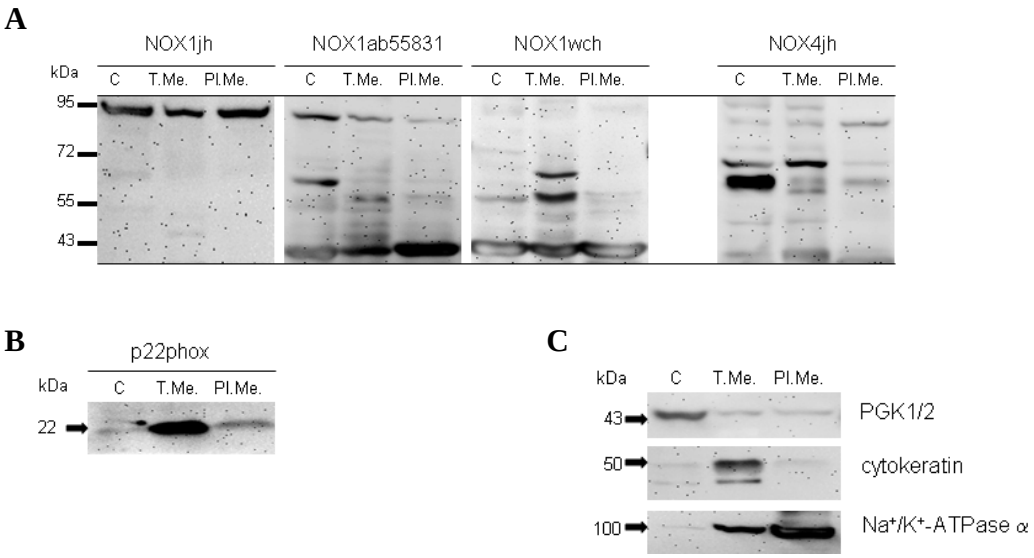

Figure 13: Detection of putative NOX1, NOX4 proteins and p22phox in plasma membrane of A549 cells

Western blot analysis of cytosolic (C), total membrane (T.Me.) and plasma membrane (Pl.Me.) fractions from A549 cells employing **A)** NOX1 and NOX4 antibodies, **B)** p22phox antibody, **C)** antibodies against different subcellular markers. In A, B experiments 50μg of protein and in C 20μg of protein per well were loaded.

4.1.7 Knock-down of NOX1 and NOX4 in A549 cells by siRNA

In parallel with applying different antibodies and subcellular fractionation, knock-down of NOX1 and NOX4 by siRNA was used as another approach for identification of NOX1 and NOX4 proteins. We have designed several siRNAs targeting different sequences of

NOX1 and NOX4 genes. Subsequently, we selected the most effective siRNAs based on NOX1- and NOX4-mRNA quantification by real-time RT-PCR (Figure 14A, B upper panels). Transfection of A549 cells by these siRNAs and subsequent incubation for 48 hours considerably decreased the mRNA levels of NOX1 and NOX4. Next, we tested the effect of siRNA treatment on immunoreactive NOX1 and NOX4 antibodies proteins. Si-NOX1 decreased the level of the 55kDa and 65kDa bands detected by NOX1wch. Bands detected by NOX1jh and NOX1ab55831 were not decreased (Figure 14A, lower panels) employing the si-NOX1. Si-NOX4 effectively down-regulated a band at 67kDa but not at 62kDa (Figure 14B, lower panels).

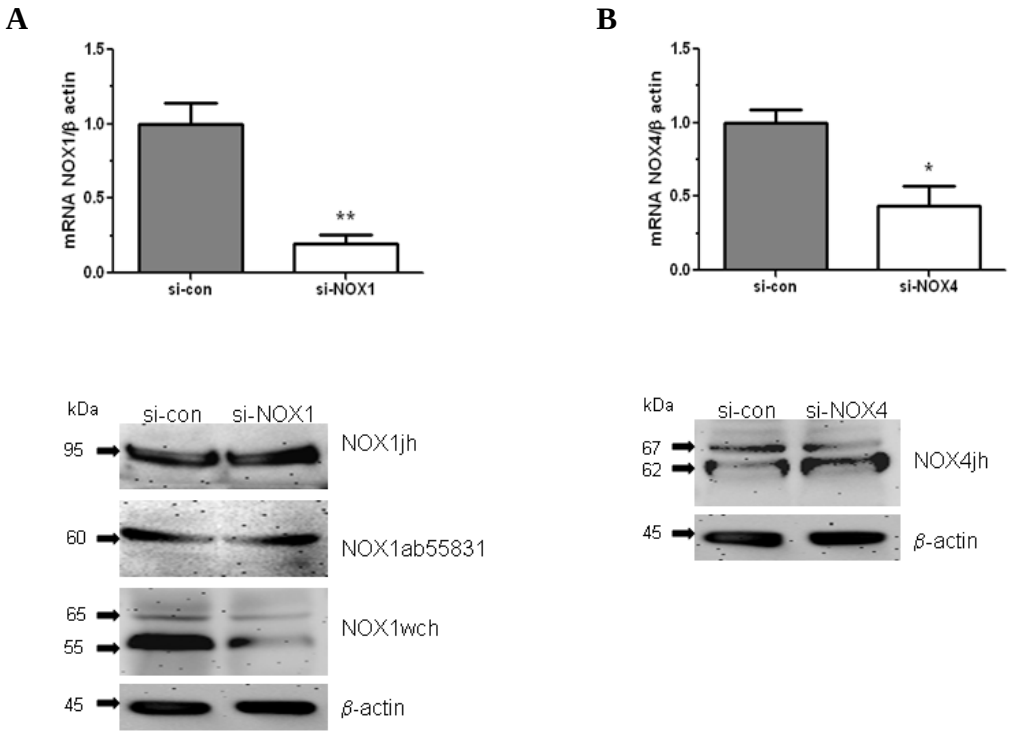

Figure 14: Knock-down of NOX1 and NOX4 in A549 cells by siRNA
A) Upper panel: Quantification of NOX1 mRNA level by real-time RT-PCR in A549 cells transfected with si-con or si-NOX1 (** $p<0.01$, n=3, unpaired t-test). β-actin was used as reference gene. Lower panel: Western blot analysis of total cell lysates from A549 cells transfected with si-con or si-NOX1 employing different NOX1 antibodies. β-actin was used as a loading control. **B)** Upper panel: Quantification of NOX4 mRNA level by real-time RT-PCR in A549 cells transfected with si-con or si-NOX4 (* $p<0.05$, n=3, unpaired t-test). β-actin was used as reference gene. Lower panel: Western blot analysis of total cell lysate from A549 cells transfected with si-con or si-NOX4 employing NOX4jh antibody. β-actin was used as loading control. For all Western blot analyses, 50µg of protein were loaded per well.

4.1.8 Interaction of NOX1wch and NOX4jh antibodies with recombinant NOX1 and NOX4 proteins

Using the siRNA approach in the previous experiments, NOX1wch and NOX4jh were determined as the most suitable antibodies for the detection of endogenous NOX1 and NOX4 protein in A549 cells. Both NOX1 and NOX4 were present in the Tx-100 insoluble fraction, representing likely mainly cytoskeleton and cytoskeleton associated proteins. Based on these results, we further investigated whether firstly, NOX1wch and NOX4jh are also able to recognize recombinant NOX1 and NOX4 proteins and, secondly, whether recombinant NOX1 and NOX4 would also be localized in the Tx-100 insoluble fraction.

A549 cells were transiently transfected with HA-tagged NOX1- and HA-tagged NOX4-encoding plasmids (NOX1-HA, NOX4-HA). 24 hours after transfection, cells were lysed in Tx-100 containig buffer and Tx-100 soluble and insoluble fractions were separated and subjected to Western blot.

NOX1wch detected bands at 55kDa and 65kDa in the Tx-100 insoluble fraction of NOX1-HA transfected and non-transfected cells. In addition, a band at 46kDa appeared only in transfected cells (Figure 15A). When using a monoclonal HA antibody for analysis of these samples, bands at 55kDa and 46kDa in the Tx-100 insoluble fraction of NOX1-HA transfected cells and no band in non-transfected cells were detected (Figure 15A). The 46kDa protein band that was detected both with NOX1wch and HA-antibody may be a proteolytic cleavage product of highly expressed NOX1-HA.

NOX4jh detected several weak bands in the range of 62kDa and a strong band at 40kDa in the Tx-100 insoluble fraction, only in NOX4-HA transfected cells, but not in non-transfected cells. The endogenous 62kDa and 67kDa bands detected with NOX4jh were common for transfected and non-transfected cells (Figure 15B). The HA-antibody visualized a strong double band in the range of 62kDa and a weak band at 40kDa in the Tx-100 insoluble fraction of transfected but not in non-transfected cells (Figure 15B). Using the same antibodies, proteins from total cell lysate of A549 cells transfected with a plasmid encoding NOX4E-HA (a truncated NOX4 splice variant) were analysed by

Western blot. Both NOX4jh and HA antibodies displayed strong immunoreactivity with NOX4E-HA (Figure 15B, right panel).

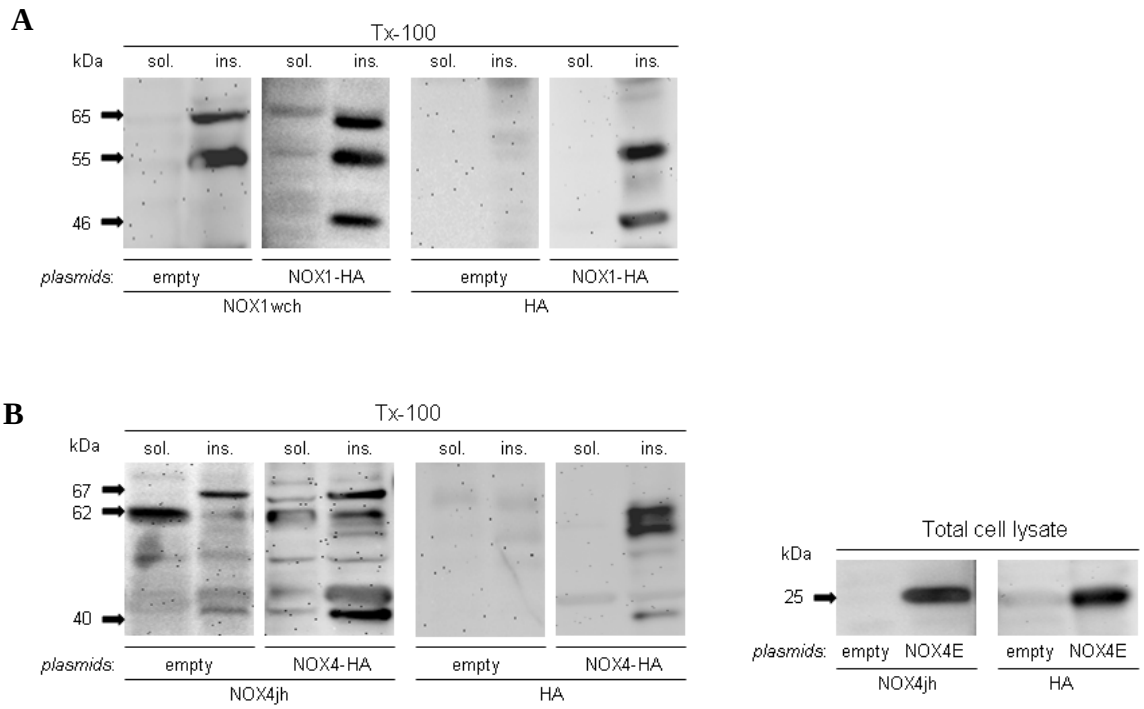

Figure 15: Interaction of NOX1wch and NOX4jh antibodies with recombinant NOX1 and NOX4 proteins
A) Western blot analysis of Tx-100 soluble and insoluble fractions from A549 cells transfected with empty plasmid or with NOX1-HA plasmid employing NOX1wch- or HA-antibody. **B)** Left panel: Western blot analysis of Tx-100 soluble and insoluble fractions from A549 cells transfected with empty plasmid or with tagged NOX4-HA plasmid employing NOX4jh- or HA-antibody. Right panel: Western blot analysis of total cell lysate from A549 cells transfected with empty plasmid or with NOX4E-HA plasmid employing NOX4jh- or HA-antibody. In all experiments, 30µg of protein were loaded per well.

4.1.9 Localization of NOX1, NOX4, p22phox and NOXO1 in cell nuclei

The experiment applying siRNA for inhibition of NOX1 and NOX4 revealed NOX1wch and NOX4jh as most suitable antibodies for the detection of these proteins. Both NOX1 and NOX4 proteins were demonstrated to be associated with the cytoskeleton. The cytoskeleton is also part of the nuclei. Furthermore, NOX4 and other NOXs have been detected in nuclei of several cell types. Thus, in the next step, we were interested whether

NOX1 and NOX4 are localized in the nuclei of A549 and CaCo2 cells or HUVEC. For isolation of high purity nuclear fraction we used *Nuclear and Cytoplasmic Extraction Reagents* kit.

NOX1wch detected bands at 55kDa and 65kDa that both were more abundant in CaCo2 in comparison to A549 cells. In CaCo2 cells, both bands were strongly localized in the nuclear insoluble fraction containing cytoskeletal proteins and weakly in nuclear soluble fraction containing soluble proteins from the nuclear lumen and nuclear membrane. In contrast, the 55kDa protein in A549 cells was present only in the nuclear soluble fraction whereas the 65kDa band was predominantly present in the nuclear insoluble fraction (Figure 16A).

NOX4jh visualized a strong band at 62kDa mainly localized in the cytosolic fraction (containing also membrane proteins) and a 67kDa band mainly localized in the nuclear insoluble fraction of A549 cells. The same antibody showed a strong band at 67kDa both in the nuclear soluble and the insoluble fraction and at 50kDa and 40kDa in the nuclear insoluble fraction of HUVEC (Figure 16B).

p22phox was present strongly in the cytosolic fraction, in the nuclear soluble fraction and weakly in the nuclear insoluble fraction of A549 and CaCo2. NOXO1 was present only in the nuclear insoluble fraction of both these cell types (Figure 16C).

Lamin B is a typical nuclear protein, thus we used it as nuclear marker. Lamin B is also part of intermediate filaments. In accordance with this, lamin B was present strongly both in the nuclear soluble and insoluble fractions but not in the cytosolic fraction (Figure 16A, B).

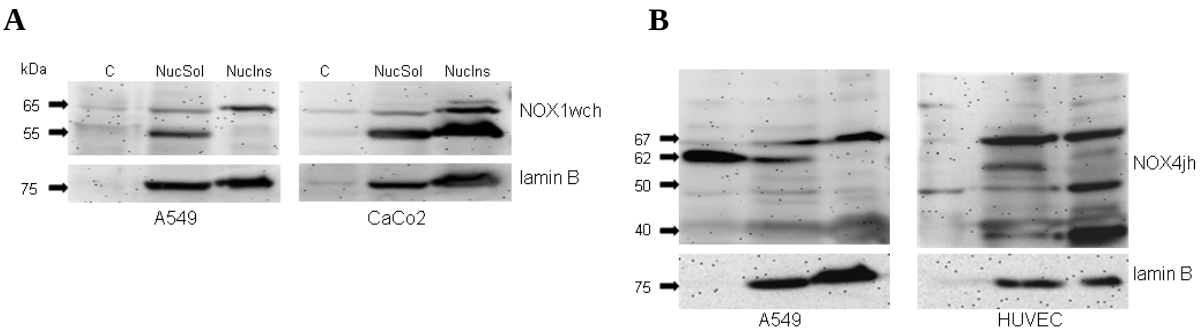

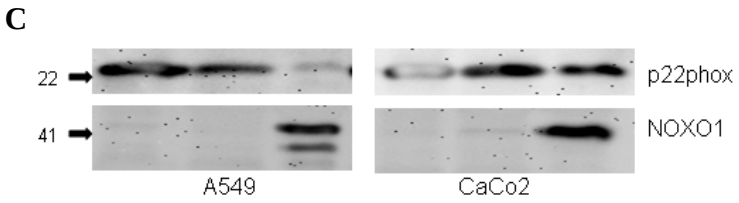

Figure 16: Localization of NOX1, NOX4, p22phox and NOXO1 in cell nuclei
Western blot analysis of cytosolic (C), nuclear soluble (NuSol) and nuclear insoluble (NuIns) fractions from **A)** A549 and CaCo2 cells employing NOX1wch and lamin B antibodies, **B)** A549 cells and HUVEC employing NOX4jh and lamin B antibodies, **C)** A549 and CaCo2 cells employing p22phox and NOXO1 antibodies. In all experiments, 40μg of protein were loaded per well.

4.1.10 Regulation of NOX1 and NOX4 stability by p22phox

One of the important roles of p22phox is stabilization of NOX proteins during their synthesis in the ER. In fact, p22phox is suggested to form a heterodimer with NOX proteins and thereby protecting NOX from proteasomal degradation. Based on this observation, we were interested whether p22phox inhibition would influence the stability of NOX1 and NOX4. We did not observe any effect of p22phox inhibition on the endogenous NOX1 and NOX4 protein levels (Figure 17A). Furthermore, we overexpressed recombinant NOX1-HA and NOX4-HA in cells treated with si-p22phox (24h prior to transfection with plasmid). p22phox inhibition led to a strong decrease of the abundance of recombinant NOX1 and NOX4 proteins (Figure 17B). To test whether the effect of p22phox knock-down on NOX1 and NOX4 proteins was mediated by proteosomal degradation, we treated cells by MG132, a proteasomal inhibitor. Indeed, MG132 treatment partially canceled the down-regulatory effect of si-p22phox on recombinant NOX1 and NOX4 proteins (Figure 17C).

Furthermore, we also investigated the effect of the inhibition of NOX1 and NOX4 on the p22phox protein expression. Interestingly, whereas knock-down of NOX1 decreased the level of endogenous p22phox, knock-down of NOX4 showed no strong effect on the p22phox protein level (Figure 17D, upper panels). The inhibition of p22phox by siRNA was also validated (Figure 17D, lower panel).

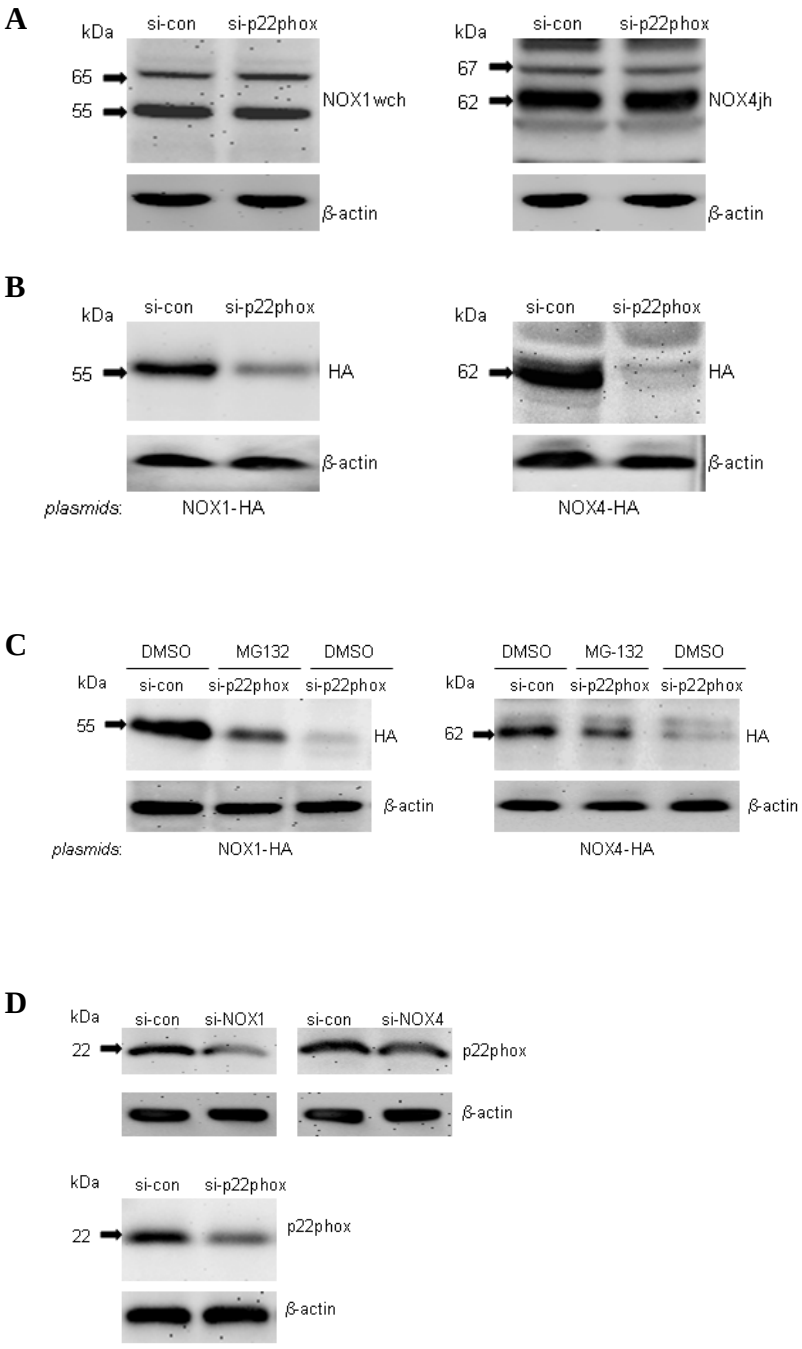

Figure 17: Regulation of NOX1 and NOX4 stability by p22phox
A) Western blot analysis of total cell lysates from A549 cells transfected with si-con or si-p22phox employing NOX1wch and NOX4jh antibodies. **B)** Western blot analysis of total cell lysates from A549 cells transfected with si-con or si-p22phox and NOX1-HA or NOX4-HA plasmid employing HA antibody. **C)** Western blot analysis of total cell lysates from A549 cells transfected with si-con or si-p22phox and with NOX1-HA or NOX4-HA plasmid and treated by solvent (DMSO) or MG132 employing HA antibody.

D) Upper panel: Western blot analysis of total cell lysates from A549 cells transfected with si-con or si-NOX1 or si-NOX4 employing p22phox antibody. Lower panel: Western blot analysis of total cell lysate from A549 cells transfected with si-con or si-p22phox employing p22phox antibody. In all experiments, 40μg of protein were loaded per well and detection of β-actin was performed to control protein loading.

4.1.11 Purification of putative NOX1 and NOX4 proteins

In parallel with the developing of effective siRNAs to knock-down NOX1 and NOX4 proteins employed for the evaluation of the different antibodies, we also attempted to purify some of the potential NOX1 and NOX4 proteins. NOX1wch that subsequently turned out to be the most suitable antibody for the detection of NOX1, visualized strong band at 55kDa and weak band at 65kDa (both in A549 and in CaCo2 cells). Similarly, NOX4jh detected bands at 67kDa and 62kDa in A549 cells, and in addition a strong band at 50kDa and previously described 80kDa band in HUVEC. However, the theoretically predicted size of NOX1 is 65kDa and of NOX4 67kDa. In addition, several splice variants of NOX4 and NOX1 have been found at the mRNA level. In the context of all these observations and facts, we aimed at the identification of some putative NOX1 and NOX4 immunoreactive proteins.

4.1.11.1 Strategy of purification

Since subcellular fractionation and subsequent cutting of relevant bands areas directly from polyacryl-amid gel or PVDF membrane appeared not to suitable for the detection of low abundant proteins by MALDI-TOF MS or N-terminal sequencing, we attempted to perform gradual protein purification to get high amount and purity of potential NOX1 and NOX4 proteins. The purification procedure consisted of several steps, primary based on HPLC protein purification as depicted on Figure 18. After each purification step an aliquot of the purified fractions was used for Western blot analysis. The fraction containing the protein(s) of interest, was submitted to a further step of purification. Techniques like 2D gel electrophoresis (2D-GE) and MALDI-TOF MS (including preparation of samples for MS) were performed in cooperation with experienced staff at the Department of proteomics, Institute of Biochemistry, Giessen (Laboratory of Dr. G. Lochnit).

Finally, MALDI-TOF MS analysis of the purified putative NOX1 and NOX4 protein bands did not identify any protein as NOX-related protein. However, this does not exclude that some of these bands may represent NOX1 or NOX4 proteins. The most critical factors of the performed purification processes are discussed in chapter 5.1.4.

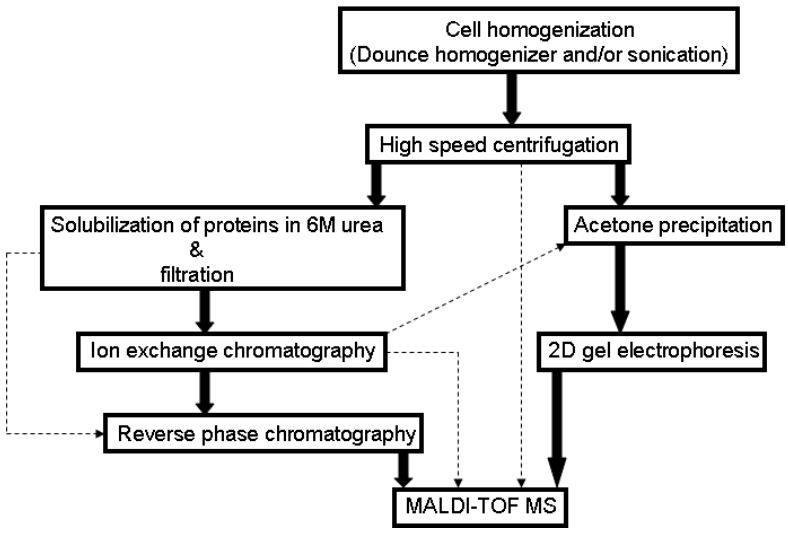

Figure 18: Schema of purification strategy for the identification of putative NOX1 and NOX4 proteins
Main purification steps are labeled by thick arrows and alternative ways of purification are labeled by thin, dashed arrows

4.1.11.2 Homogenization and fractionation

A549 cells were homogenized and fractionated by gradual centrifugation according to the protocol described in the Method section.

MOX1H-15 and NOX1wch were used for the detection of NOX1 in A549 cells because, firstly, these antibodies were reacting with protein bands near to the predicted size of NOX1 and, secondly, both antibodies were described previously as relevant for NOX1 detection [21], [200], [201], [18], [29], [14]. MOX1H-15 detected bands at 60kDa and 45kDa in 110000g supernatant, whereas NOX1wch detected bands at 55kDa in 1050g and 14000g pellet, 65kDa in 14000g pellet and 45kDa in 110000g supernatant and in 1050g, 14000g pellet (Figure 19, left panels). NOX4jh was used for detection of NOX4

proteins in HUVEC (Figure 19, right panels). This antibody detected bands at 62kDa and 67kDa in 1050g fraction, and 62kDa and 80kDa bands in 110000g supernatant. In addition, mAb54.1 and p22phox antibodies were used for analysis of these fractions (Figure 19, right panels). mAb54.1 detected a band at 50kDa in all fractions, at 70kDa a double band in all fractions except 110000g supernatant, and a very weak band at 90kDa in the 1050g pellet fraction. The p22phox antibody detected a band at 22kDa most strongly in 1050g and less in 14000g and 110000g pellets. In the 110000g supernatant, there was no p22phox immunoreactive band.

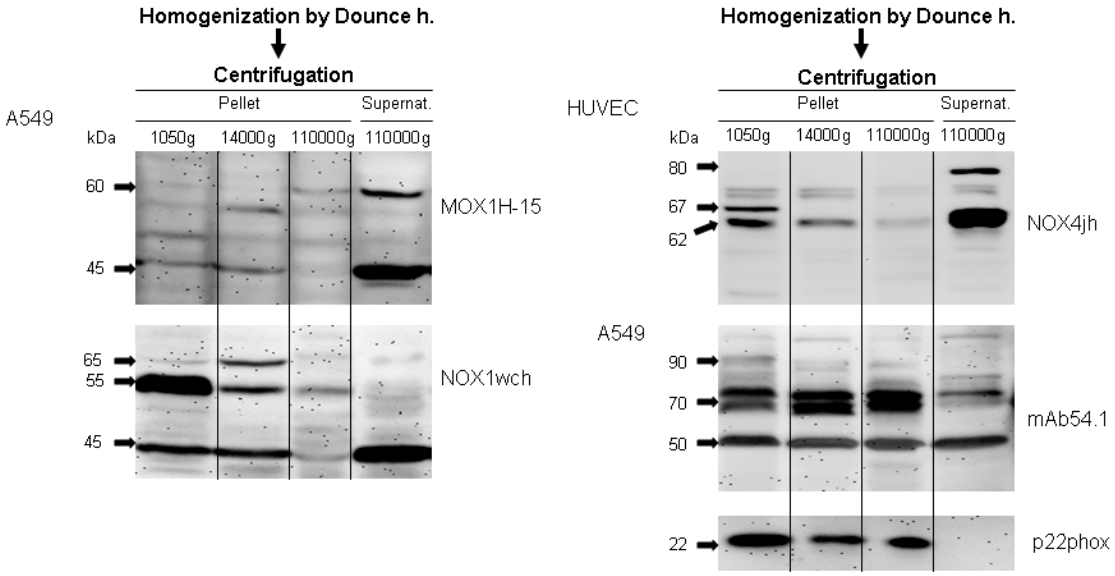

Figure 19: Homogenization and fractionation of A549 cells and HUVEC
Western blot analysis of lysates from A549 cells or HUVEC after mechanic homogenization (using Dounce homogenizer) and centrifugal fractionation employing NOX1 (MOX1 H-15, NOX1wch) (left panels), NOX4jh, mAb54.1 and p22phox (right panels) antibodies. In all experiments, 40µg of protein per well were loaded.

4.1.11.3 Chromatographic or 2D gel electrophoretic protein purification for MALDI-TOF MS

After homogenization and centrifugal separation, the relevant fractions were dissolved or diluted in the appropriate buffer and used for further purification (Figures 20A-H).

A1) The 110000g supernatant (from A549) containing 60kDa and 45kDa MOX1H-15 immunoreactive bands was subjected to anion exchange chromatography (AEC). The fractions were analysed by Western blot. A 60kDa band was detected in the fractions 15 and 16, and a 45kDa band was present mainly in the fraction 16. The fractions 15 and 16 were pooled together and further analysed by reverse phase chromatography (RPC). RPC fractions were submitted to Western blot. A 60kDa band was present in the fractions 36 and 37, and a 45kDa band was predominantly in fraction 43. The selected fractions (36,37 and 43) were again loaded on gel that was stained by Coomassie blue. The bands visible at the corresponding molecular weight were cut for MALDI-TOF MS analysis. The 60kDa band was identified as pyruvate kinase isozymes M1/M2 and the 45kDa as β-actin.

Figure 20A-H: Purification of proteins by chromatography or 2D gel electrophoresis for further analysis by MALDI-TOF MS

A1

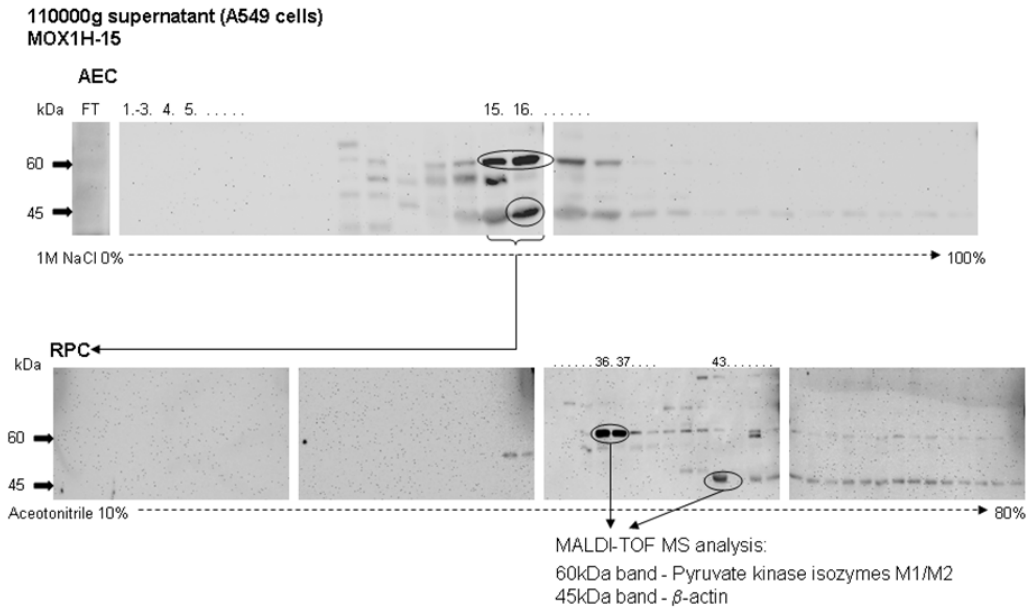

Figure 20A1: The supernatant from A549 cells after centrifugation at 110000g subjected to HPLC purification: Upper panel: Western blot analysis of different fractions and the flow-through (FT) from anion exchange chromatography (AEC) employing MOX1 H-15 antibody. The bands of interest, numbers of individual fractions and the gradient of NaCl are presented. Lower panel: Western blot analysis of fractions 15 and 16 from AEC subjected to reverse phase chromatography (RPC) employing MOX1 H-15 antibody for detection. Bands of interest, numbers of individual fractions and the acetonitrile (ACN)

gradient are labeled. 60kDa and 45kDa proteins from the positive fractions (36, 37 and 43) were subsequently analysed by MALDI-TOF MS.

A2) Each HPLC purification run was recorded in a chromatogram. Figure 20A2 is representing an example of the chromatograms, here particularly related to the purification of MOX1 H-15 immunoreactive proteins (60kDa and 45kDa). The upper panel is showing a chromatogram from AEC of the 110000g supernatant of A549 cells. The NaCl gradient, the buffer system, the column and the detection wavelength are given. The fractions were collected each minute. The lower panel is showing a RPC chromatogram of the fractions 15 and 16 from the AEC. The acetonitrile (ACN) gradient, the buffer system, column and the detection wavelength are given. The fractions were collected each minute (1fraction ≈ 1minute). Proteins of 60kDa and 45kDa from the RPC fraction 36, 37 and 43 were selected for MALDI-TOF MS analysis.

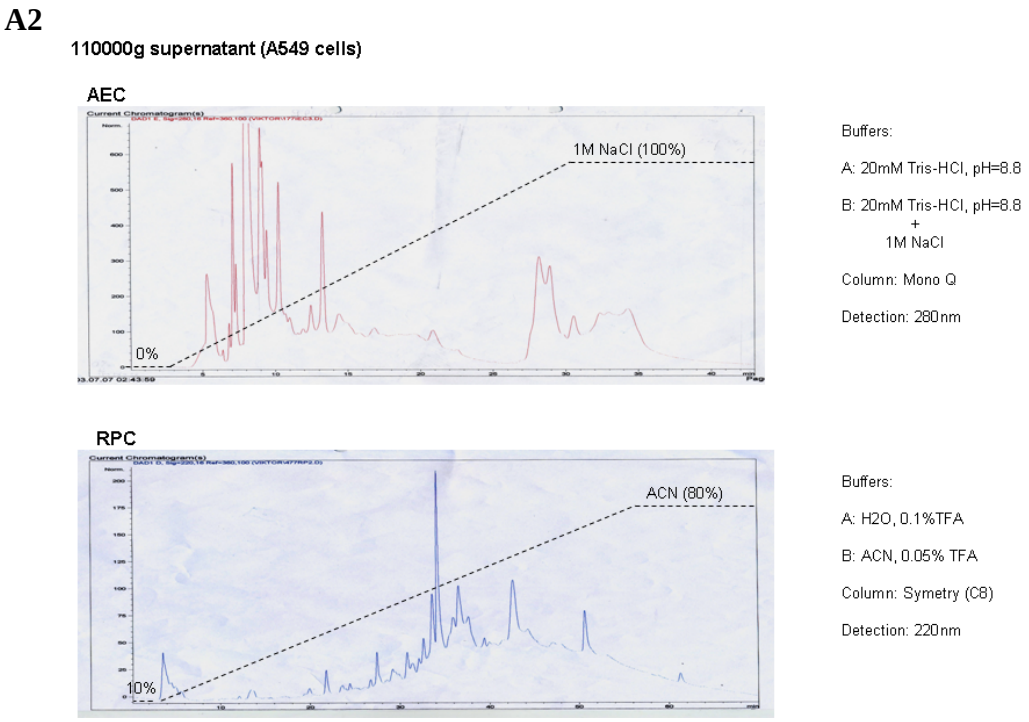

Figure 20A2: AEC and RPC chromatograms from purification of MOX1 H-15 antibody immunoreactive proteins contained in the 110000g supernatant from A549 cells: Upper panel: AEC chromatogram. The NaCl gradient is represented by a dashed line in the chromatogram. Lower panel: RPC chromatogram. The ACN gradient is represented by a dashed line in the chromatogram. The buffer system, names of the columns and wavelengths for the detection of proteins in the eluates are described.

B) The 1050g and 14000g pellets (from A549cells) containing potential NOX1 bands at 55kDa and 65kDa were dissolved in 6M urea, pooled together, filtered (DNA binding filter), mixed with AEC buffer A (1:5) and used for AEC. Both 55kDa and 65kDa NOX1wch immunoreactive bands were present in the flow-through (FT). Because of technical problems with RPC, the proteins in the AEC FT were precipited by acetone and directly used for 2D-GE. However, NOX1wch did not detected any prominent dots in the range of the molecular weight between 55kDa and 72kDa on the PVDF transferred from 2D gel.

B

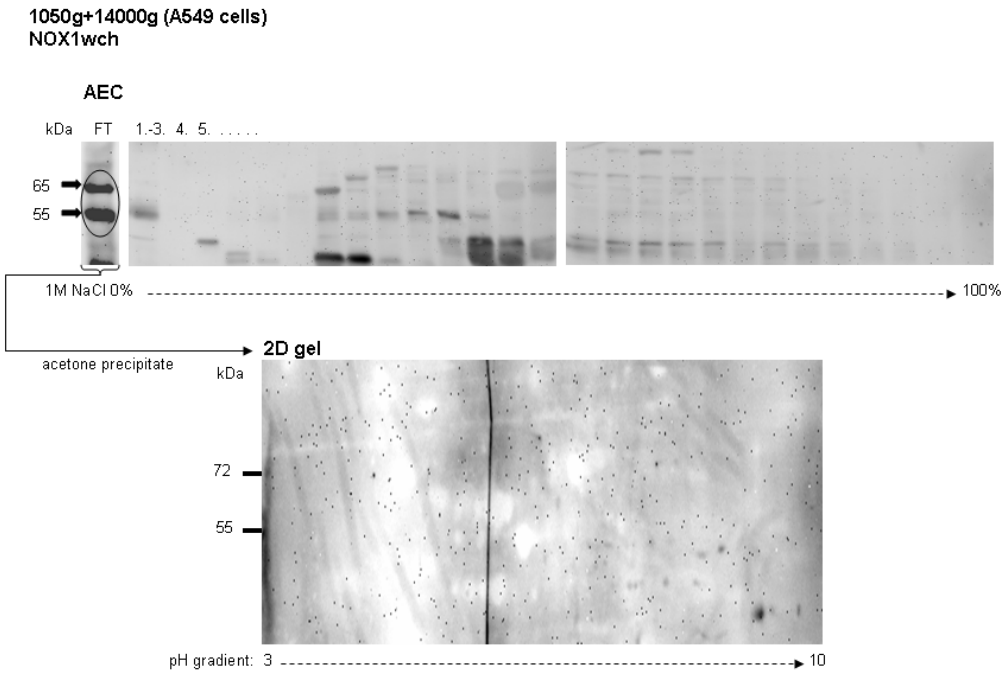

Figure 20B: 1050g and 14000g pellets (pooled together) from A549 cells subjected to AEC and 2D gel electrophoresis (2D-GE): Upper panel: Western blot analysis of fractions including the FT from AEC employing the NOX1wch antibody. Bands of interest, numbers of individual fractions and the NaCl gradient are labeled. Lower panel: Acetone precipitated proteins in FT were separated by 2D-GE, transferred to a PVDF membrane that subsequently was incubated with NOX1wch antibody. The pH gradient of the strip for isoelectric focusing (IEF) and the molecular weights are labeled.

C) The 1050g pellet (from HUVEC) containing 67kDa and 62kDa NOX4 bands was dissolved in 6M urea, filtered (DNA binding filter), mixed with AEC buffer A (1:5) and

applied in AEC. NOX4jh detected bands at 69kDa and 66kDa in the FT, and a 62kDa protein most strongly present in fractions 13 and 14. The proteins in the FT were precipited by acetone and used for 2D-GE. In the range between 55kDa and 72kDa no strong dots on the corresponding PVDF membrane could be detected by NOX4jh.

C

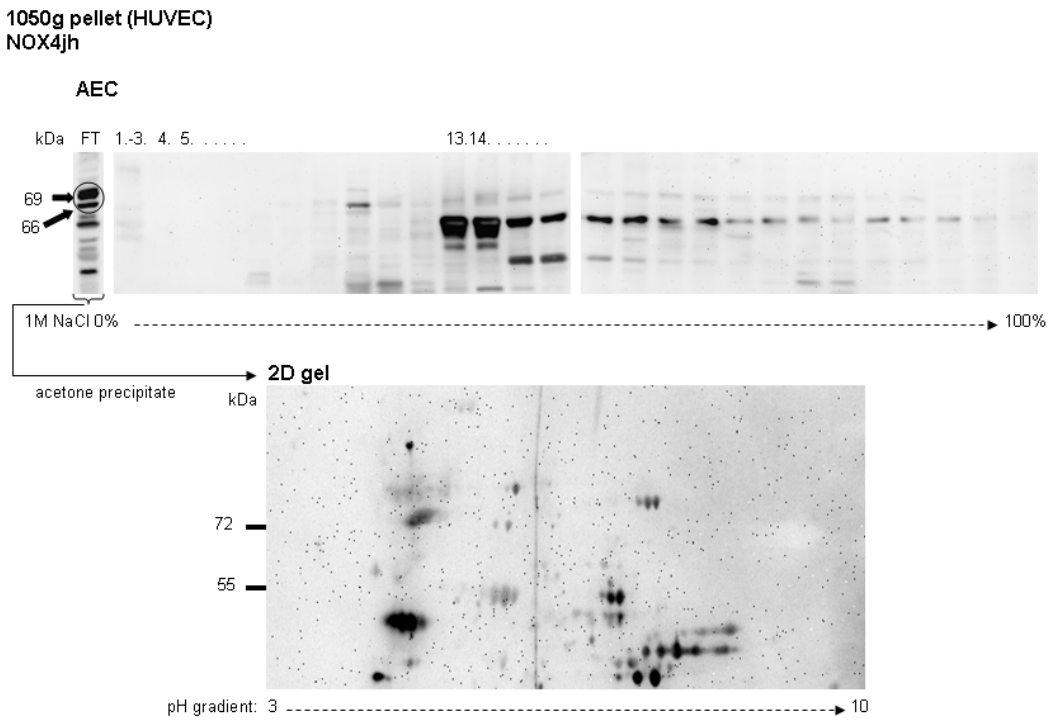

Figure 20C: The 1050g pellet from HUVEC subjected to AEC and 2D-GE: Upper panel: Western blot analysis of fractions including the FT from AEC employing the NOX4jh antibody. Bands of interest, numbers of individual fractions and the NaCl gradient are labeled. Lower panel: Acetone precipitated proteins in FT were separated by 2D-gel electrophoresis, transferred to a PVDF membrane that subsequently was incubated with NOX4jh antibody. The pH gradient of the strip for IEF and the molecular weights are labeled.

D) The 110000g supernatant (from HUVEC) containing a NOX4jh immunoreactive band at 80kDa was subjected to AEC. The 80kDa NOX4jh reactive band was present most strongly in fractions 20 and 21. These fractions were pooled together and applied for RPC. The band at 80kDa appeared in none of the RPC fractions. Thus the same AEC

fractions were also used for 2D gel electrophoresis. However, in the range of 72-95kDa not any strong dots were detected by NOX4jh.

D

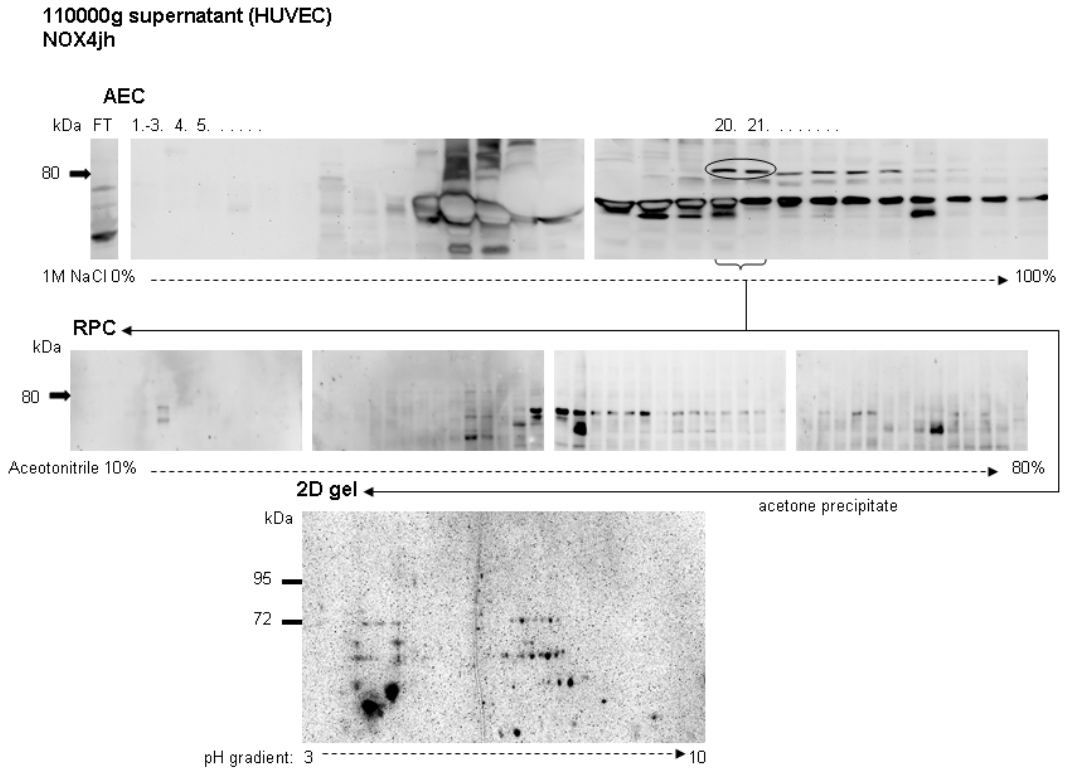

Figure 20D: The 110000g supernatant from HUVEC subjected to AEC and RPC or 2D-GE: Upper panel: Western blot analysis of fractions including the FT from AEC employing NOX4jh antibody. The bands of interest, numbers of individual fractions and NaCl gradient are labeled. Middle panel: Western blot analysis of the AEC fractions 20 and 21 that were subjected to RPC. The ACN gradient in RPC is labeled. Lower panel: Acetone precipitated proteins in fractions 20 and 21 were separated by 2D-GE, transferred to a PVDF membrane that subsequently was incubated with NOX4jh antibody. The pH gradient of the strip for IEF and the molecular weights are labeled.

E) The 1050g pellet from A549 cells containing a strong 70kDa and a weak 90kDa band immunoreacting with mAb54.1 was dissolved in 6M urea, filtered (DNA binding filter), mixed with AEC buffer A (1:5) and applied for AEC. The 70kDa band was in the FT and the 90kDa band was strongly present in fractions 14 and 15.

E

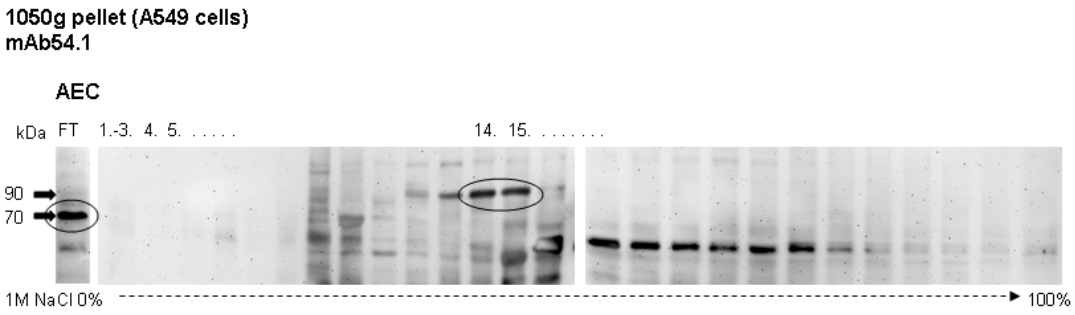

Figure 20E: The 1050g pellet from A549 cells subjected to AEC: Fractions including the FT from AEC were analysed by Western blot employing the mAb54.1 antibody. Bands of interest, numbers of individual fractions and the NaCl gradient are labeled.

F) The 1050g pellet from A549 cells also contained the p22phox immunoreactive band. When this fraction was analysed by AEC, the p22phox band appeared in the FT. The FT was subsequently concentrated by ultrafiltration and used for preparative SDS-PAGE. Different protein amounts (25µg, 50µg, 75µg) were loaded on the gel. The p22phox antibody immunoreactive band was labeled on PVDF and cut for MALDI-TOF MS analysis. 50µg of protein was not sufficient for detection of any protein by MALDI-TOF, thus 75µg was used in the second round of analysis. A protein at 22kDa was surprisingly not identified as p22phox but as tetraubiquitin.

F

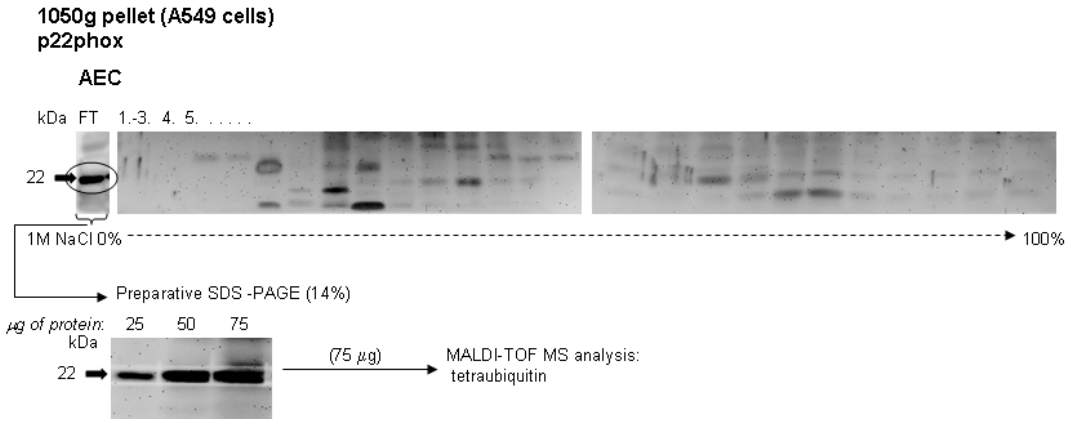

Figure 20F: The 1050g pellet from A549 cells subjected to AEC and preparative SDS-PAGE: Upper panel: Western blot analysis of fractions including the FT from AEC employing the p22phox antibody. Bands of interest, numbers of individual fractions and the NaCl gradient are labeled. Lower panel: Western blot analysis of acetone precipitated

proteins in FT employing the p22phox antibody. The amounts of proteins loaded per well are given. The p22phox-positive band (75µg of total protein) was subsequently analysed by MALDI-TOF MS.

G) We also tried to analyse fractions from A549 cells after centrifugation of 1050g directly by RPC without preceding AEC. The 1050g pellet was dissolved in 6M urea, filtered by DNA binding filter, mixed with RPC buffer A (1:5) and applied in RPC. mAb54.1 detected a strong band at 70kDa in fractions 36, 37, 38, 39, and weak band at 90kDa in fractions 35, 36 and 37. The fractions 36 and 37 were pooled together and loaded onto a preparative SDS-PAGE. In order to avoid cutting of non-matching bands from the gel, the whole area between 60-100kDa was cut into small pieces of gel slices that were subsequently submitted to MALDI-TOF MS analysis. However, none of the bands was identified as NOX2 or any other NOX protein. Examples of the identified proteins are given in the figure.

G

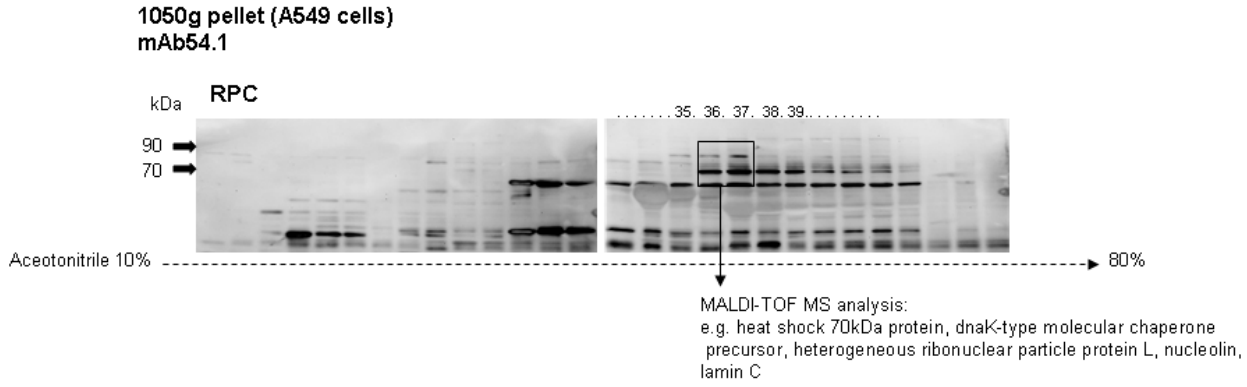

Figure 20G: The 1050g pellet from A549 cells subjected to RPC: Western blot analysis of selected fractions from RPC employing m54.1 antibody. The whole gel area with bands of interest was subjected to MALDI-TOF MS analysis. The area containing the bands of interest, the numbers of individual fractions and the ACN gradient are labeled. Examples of indentified proteins are given.

H) The nuclear insoluble fraction of CaCo2 cells was isolated by *Nuclear and Cytoplasmic Extraction Reagents* kit. As we observed previously, this fraction from CaCo2 contained 55kDa and 65kDa bands detected by NOX1wch. After acetone precipitation a part of the fraction (about 10%) was again used for SDS-PAGE and the

second part was used for 2D-GE. NOX1wch detected a strong band at 55kDa and a weak band at 65kDa on the PVDF membrane from the SDS-PAGE. However, no dot in the range of 55-72kDa could be detected on the PVDF from the 2D-GE.

H

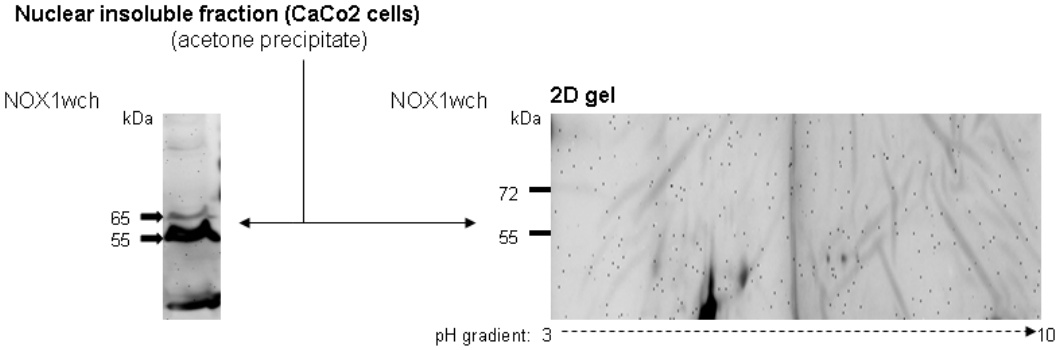

Figure 20H: Left panel: Western blot analysis of acetone precipitated proteins in the nuclear insoluble fraction from CaCo2 cells employing NOX1wch antibody. Right panel: The acetone precipitated proteins in the nuclear insoluble fraction were separated by 2D-GE, transferred to a PVDF membrane that subsequently was incubated with NOX1wch antibody. The pH gradient of the strip for IEF and the molecular weights are labeled.

4.1.12 Effect of NOX1 and NOX4 knock-down on ROS generation in A549 cells

The primary function of NADPH oxidase 1 and 4 is ROS generation. We could show that NOX1-mRNA is expressed in A549 at a higher level than NOX4-mRNA. Thus our further question was, whether NOX1 in A549 cells contributes with a higher extent to ROS generation than NOX4. Since the measurement of superoxide anion is problematic and superoxide anion is rapidly transformed to hydrogen peroxide, the intracellular ROS were measured as concentration of hydrogen peroxide in total cell lysate by *Amplex Red Hydrogen Peroxide/Peroxidase Assay Kit*. Whereas inhibition of NOX1 by siRNA led to a significant decrease of ROS levels (decrease more than 20%), NOX4 inhibition was not accompanied by any significant decrease in ROS concentration (Figure 21).

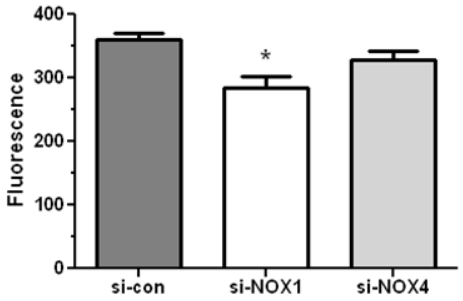

Figure 21: Effect of NOX1 and NOX4 knock-down by siRNAs on the ROS generation in A549 cells
Measurement of H_2O_2 concentrations in total cell lysates from A549 cells transfected with si-con or si-NOX1 or si-NOX4. The H_2O_2 concentrations were determined by the *Amplex Red Hyrogen Peroxide/Peroxidase Assay Kit* using excitation/emission wave lengths of 540nm/595nm for detection of fluorescence. The fluorescence values were always normalized to µg of protein. Significant differences compared to si-con (* $p<0.05$, n=5, unpaired t-test).

4.1.13 Expression of NOX1 and NOX4 under normoxic and hypoxic conditions

Expression of NADPH oxidase subunits can be influenced by different stimuli, including the oxygen concentration. Here, we studied the regulation of NOX1 and NOX4 expression under different hypoxic conditions. A549 were subjected to hypoxia of 2 hours (H2), hypoxia of 4 hours (H4), hypoxia of 6 hours (H6), hypoxia of 12 hours (H12), hypoxia of 24 hours (H24) and hypoxia of three times 2 hours interrupted by 2 hours of normoxia (intermittent hypoxia, IH6).

Real-time RT-PCR revealed significant induction of NOX1 mRNA expression in H24 and IH6, and no significant changes in H2, H4, H6, H12 groups when compared to normoxia (N) (Figure 22A, upper panel). A similar pattern of NOX1 protein expression was demonstrated by Western blot analysis of total cell lysate from A549 where NOX1 was detected as a strong band at 55kDa and a weak band at 65kDa that was most strongly increased in H24 and IH6, followed by H12, H6, H4, H2 and N groups (Figure 22A, lower panel). On the other hand, NOX4 mRNA expression in A549 did not show any significant changes in any of groups subjected to hypoxia when compared to N (Figure 22B, upper panel). Interestingly NOX4 protein represented by a band at 67kDa appeared to be even slightly down-regulated in long term (H24) and intermittent (IH6) hypoxia in comparison to N (Figure 22B, lower panel).

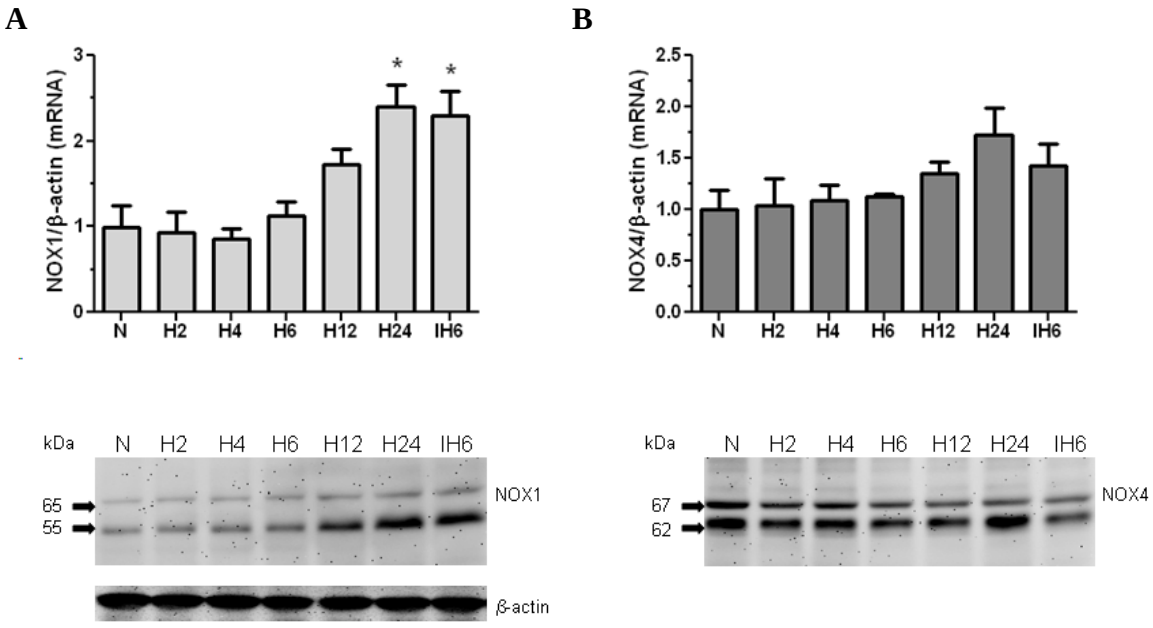

Figure 22: Expression of NOX1 and NOX4 under normoxic and hypoxic conditions
A) Upper panel: Quantification of NOX1 mRNA levels in A549 cells subjected to normoxic and different hypoxic conditions (for description see Results section) by real-time RT-PCR. β-actin was used as reference gene. Significant differences compared to N (* $p<0.05$, n=3, unpaired t-test). Lower panel: Western blot analysis of total cell lysates from A549 cells subjected to normoxic and different hypoxic conditions employing NOX1wch antibody. **B)** Upper panel: Quantification of NOX4 mRNA levels in A549 cells subjected to normoxic and different hypoxic conditions by real-time RT-PCR. β-actin was used as reference gene. Significant differences compared to N (* $p<0.05$, n=3, unpaired t-test). Lower panel: Western blot analysis of total cell lysates from A549 cells subjected to normoxic and different hypoxic conditions employing the NOX4jh antibody. For Western blots analysis (A, B), 50µg of protein was loaded per well and β-actin was used as loading control.

4.1.14 NOX1-derived ROS generation under normoxic and hypoxic conditions

The previous experiments demonstrated that NOX1 mRNA and protein expression were increased after continuous long term hypoxia (H24) and intermittent hypoxia (IH6) (Figure 22A). Thus, the further aim was to explore whether the increased NOX1 expression would correlate with altered ROS levels in the different hypoxic conditions. Total cellular ROS were measured as concentration of hydrogen peroxide by Amplex Red.

Indeed, continuous long term hypoxia (H24) and intermittent hypoxia (H6) displayed strong increases of ROS levels. However, also the H12 and H6 groups displayed significantly higher levels of ROS in comparison to N (Figure 23A), in spite of the fact that NOX1 mRNA was not significantly increased under these conditions. In the next step, we investigated the contribution of NOX1 to the ROS generation (Figure 23B). A549 cells were transfected by si-NOX1 for 24 hours prior to hypoxia treatments. Interestingly, measurement of ROS concentration revealed the strongest dependency of ROS on NOX1 in IH6 and H24, that was weaker in the other hypoxic conditions. In particular, a decrease of ROS concentration after treatment of cells by si-NOX1 was about of 45% in IH6, 37% in H24, 27% H12 and 20% in the other groups. Only in the H4 group, the ROS level was not decreased significantly after treatment of cells by si-NOX1.

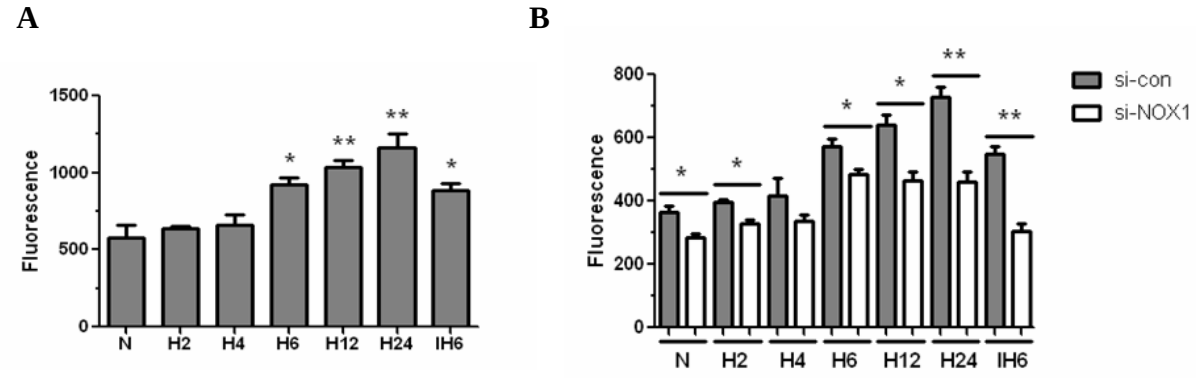

Figure 23: Total ROS and NOX1-derived ROS levels under normoxic and hypoxic conditions
A) H_2O_2 levels in total cell lysates from A549 cells subjected to normoxic and different hypoxic conditions. Significant differences compared to N (* $p<0.05$, ** $p<0.01$, n=4, unpaired t-test). **B)** H_2O_2 levels in total cell lysates from A549 cells transfected with si-con or si-NOX1 and subsequently subjected to normoxic and different hypoxic conditions. Significant differences compared to N (* $p<0.05$, ** $p<0.01$, n=3, unpaired t-test).

4.2 Cross-talk between NOX1 and redox state-dependent transcription factors Nrf2 and HIF-1 in intermittent hypoxia

NADPH oxidase 1 is a significant source of ROS in A549 cells. In our work, we could show that NOX1, a core subunit of NADPH oxidase 1, was induced under the conditions

of continuous long term and intermittent hypoxia (Figure 22A). The increase of NOX1 abundance was accompanied by elevated ROS level (Figure 23A, B). ROS have impact on the activity of several transcription factors including HIF-1 and Nrf2. HIF-1 is primarily induced in hypoxia whereas Nrf2 is induced in response to oxidative stress. In this context, an important observation was that whereas HIF-1α was stimulated both in continuous long term and intermittent hypoxia, Nrf2 was induced only in intermittent but not in continuous long term hypoxia (see below, Figure 24A). Additionally, an experiment under the same conditions applying si-Nrf2 for the inhibition of Nrf2, demonstrated that HIF-1α induction observed in IH6 was dependent on Nrf2 whereas induction of HIF-1α in H24 not (see below, Figure 24B). Nevertheless, both transcription factors displayed a strong dependency on NOX1 (Doctoral thesis, Shu Li, 2007). Nrf2 is a transcription factor regulating the expression of antioxidative enzymes, such as thioredoxin 1 (Trx1), which is a well known inductor of HIF-1α. Interestingly, Nrf2 and its targets have been described to be up-regulated in the reoxygenation stage after hypoxia [202],[203].

Based on these observations, our further aims were:

1. To perform detailed analyses of the expression of NOX1, HIF-1α, Nrf2 and Trx1 under different conditions of oxygenation, particularly in the different stages of intermittent hypoxia.
2. To analyse possible cross-talk(s) between NOX1 and the transcription factors HIF-1 and Nrf2 in intermittent hypoxia, since under these conditions both factors as well as NOX1-derived ROS were induced.

According to one of our hypothesis, ROS and Trx1 were considered as major mediators to link NOX1, Nrf2 and HIF-1α under the performed conditions of intermittent hypoxia

4.2.1 Regulation of HIF-1α and Nrf2 under continuous long term and intermittent hypoxia

Previous experiments showed that NOX1 and NOX1-derived ROS were most strongly increased in IH6 and H24 (Figure 22A, 23B). Since both HIF-1α and Nrf2 are known to be regulated by ROS, we firstly analysed the protein expression of these factors in

continuous long term (H24) and intermittent hypoxia (IH6), and secondly the impact of Nrf2 knock-down by siRNA on HIF-1α.

Whereas HIF-1α was increased both in IH6 and H24, Nrf2 displayed an elevation only in IH6 (Figure 24A). Interestingly, the extent of HIF-1α up-regulation after IH6 and after H24 was comparable in spite of the big difference in exposure time to hypoxia (24hours in H24 versus three times 2 hours in IH6), indicating the relevance of possible additional mechanisms of HIF-1α stimulation under the conditions of intermittent hypoxia. In the second experiment, knock-down of Nrf2 caused significantly stronger down-regulation of HIF-1α in IH6 than in H24 (Figure 24B), suggesting a regulatory dependence of these two transcription factors.

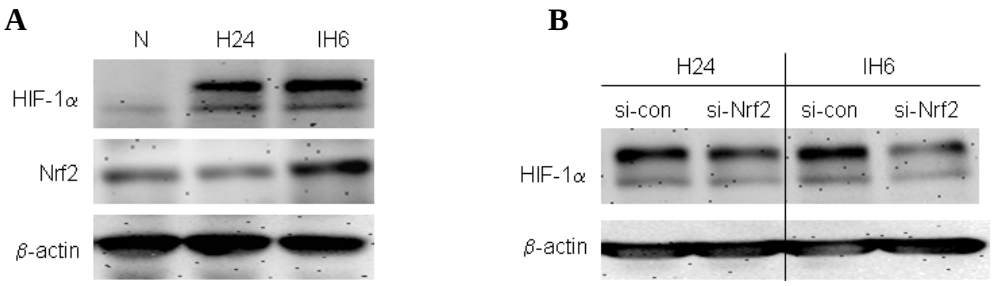

Figure 24: Regulation of HIF-1α and Nrf2 under continuous long term and intermittent hypoxias
A) HIF-1α and Nrf2 Western blot analyses of total cell lysates from A549 cells subjected to normoxia (N), continuous long term hypoxia (H24) and intermittent hypoxia (IH6). **B)** HIF-1α Western blot analysis of total cell lysates from A549 cells transfected with si-con or si-Nrf2 and subsequently subjected to H24 and IH6. 40µg of protein was loaded per well and β-actin was used as loading control.

4.2.2 Regulation of HIF-1α, Nrf2, Trx1 and NOX1 expression in A549 cells treated by different alternating hypoxic and normoxic intervals

Since NOX1, HIF-1α as well as Nrf2 were strongly induced under the conditions of intermittent hypoxia (IH6) (Figure 22A, 24A), we were further interested how the individual stages of IH6 influence the expression of these components. Additionally, in these experiments, analysis of the Nrf2 target gene Trx1 was included.

For this purpose, A549 cells were incubated in different sequences of normoxic and hypoxic intervals (Figure 25A) as follows: Normoxia (N), hypoxia for 2 hours (H2), hypoxia for 2 hours followed by reoxygenation for 2 hours (H2R), intermittent hypoxia for twice 2 hours interrupted by 2 hours of normoxia (IH4), intermittent hypoxia IH4 followed by 2 hours of reoxygenation (IH4R), intermittent hypoxia for three-times 2 hours interrupted twice by 2 hours of normoxia (IH6) and hypoxia for 6 hours (H6). HIF-1α was most strongly induced in IH6 and H6, induced to a lesser degree in IH4 and H2, whereas in N, H2R and IH4R, the HIF-1α signal was barely detectable (Figure 25B). HIF-1α was usually detected as a double-band by Western blot, most likely reflecting different phosphorylation states, as described previously [204]. Expression of both Nrf2 and Trx1 was up-regulated in IH4R and IH6 (Figure 25B). Nrf2 was detected as a 110 kDa band described previously [202, 205]. Expression of the NADPH oxidase subunit NOX1 was enhanced in IH4, IH4R and IH6 when compared to N (Figure 25B). NOX1 was detected as a band at 55kDa. The 65kDa band that we observed previously was barely detectable in the total cell lysate of A549 cells and therefore it could not be considered for Western blot evaluation. The identity of Nrf2 and NOX1 protein bands were further supported by specific inhibition with siRNA as described above and below. Employing real-time RT-PCR, we could determine increased expression of Trx1 mRNA in IH4R, IH6 and of NOX1 mRNA in IH4, IH4R and IH6 (Figure 25C) which is consistent with the increased protein abundance of Trx1 and NOX1. Expression of HIF-1α mRNA and Nrf2 mRNA was not affected (data not shown), revealing that the different oxygenation conditions affect these factors directly at the protein expression level.

A

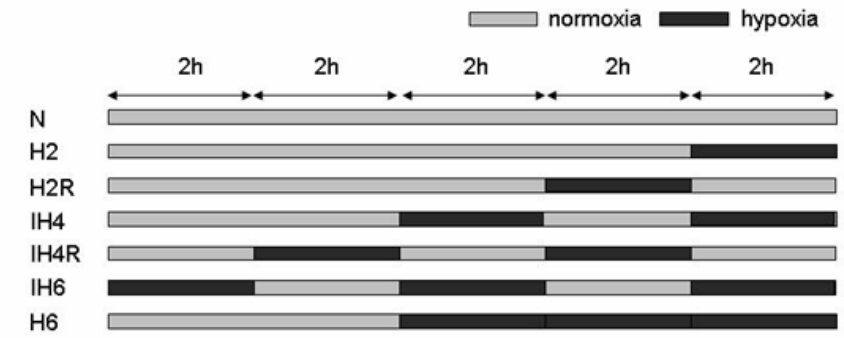

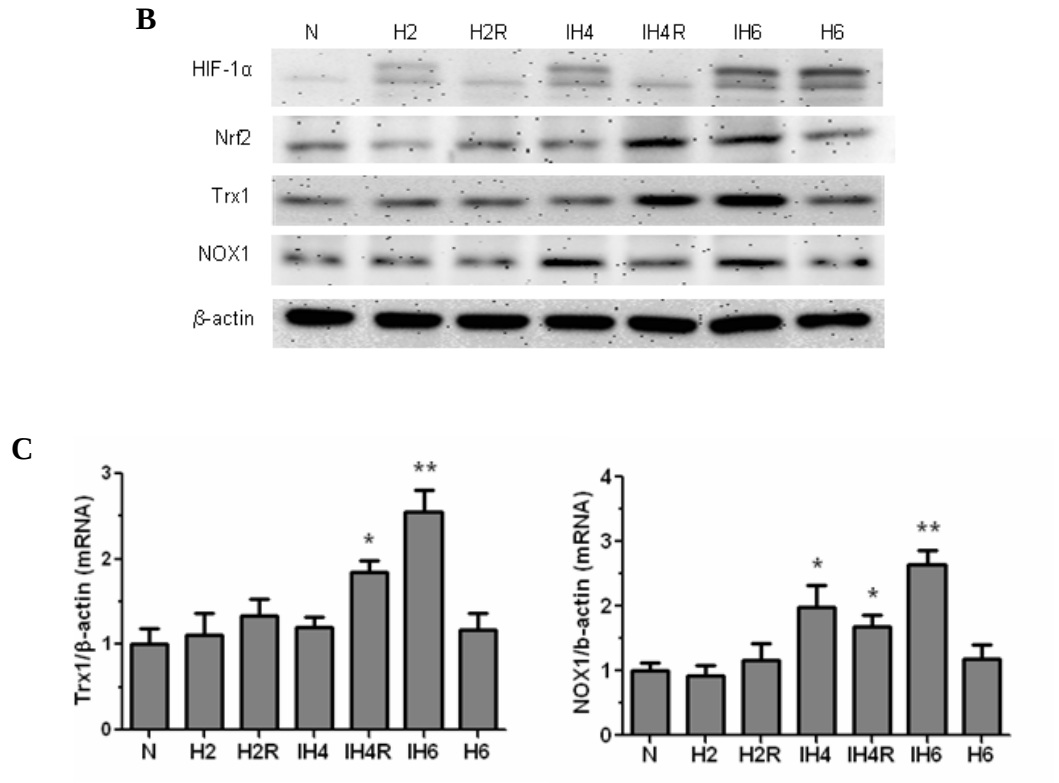

Figure 25: Regulation of HIF-1α, Nrf2, Trx1 and NOX1 expression in A549 cells treated by different alternating hypoxic and normoxic intervals
A) Scheme of the intervals under which the cells were cultured (for description see Results section). **B)** Western blot of HIF-1α, Nrf2, Trx1, NOX1 and β-actin (used as loading control). **C)** Quantification of Trx1 and NOX1 mRNA levels by real-time RT-PCR. Significant differences compared to N (* $p<0.05$, ** $p<0.01$, n=3, unpaired t-test).

4.2.3 Reactive oxygen species in A549 cells treated by different alternating hypoxic and normoxic intervals

The previous experiments showed increased expression of NOX1 mRNA and protein in different stages of IH6 (Figure 25B, C). Thus, we further tested whether theses changes in NOX1 expression would be reflected by alterations of ROS levels under the given oxygenation conditions.

Levels of ROS were most significantly elevated in H6 and IH6 followed by IH4 and IH4R when compared to normoxia (Figure 26A). In order to analyze the contribution of NOX1 to the alterations of ROS generation observed in different oxygenation conditions, we performed inhibition of NOX1 by siRNA in comparison to a random siRNA

employed as a control. The validation of the inhibition of NOX1 by si-NOX1 at the protein and mRNA level was shown at Figure 14A. The most significant dampening of ROS generation was observed in cells treated with si-NOX1 compared to si-con in the IH6 group (by approximately 45 %), less dramatic effects on ROS generation by si-NOX1 treatment were noticed in N, H2R, IH4 and IH4R, whereas the effects of H2 and H6 did not reach significance (Figure 26B). This indicates that NOX1 is important for ROS generation in conditions of intermittent hypoxia, while less relevant under conditions of stable oxygen levels.

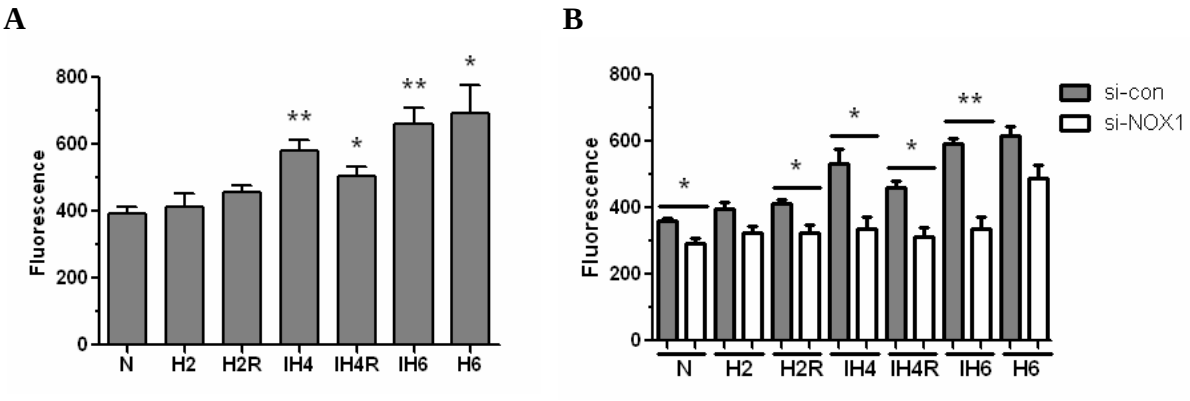

Figure 26: Total ROS and NOX1-derived ROS levels in A549 cells treated by different alternating hypoxic and normoxic intervals
A) H_2O_2 levels in naïve cells (* $p<0.05$, ** $p<0.01$, n=3, unpaired t-test). **B)** H_2O_2 levels after inhibition of NOX1 by si-NOX1 compared to si-con (* $p<0.05$, ** $p<0.01$, n=3, unpaired t-test).

4.2.4 Regulation of Nrf2 by NOX1

Next, we characterized the relevance of NOX1 generated ROS for cell signaling with regard to Nrf2 activation. This experiment was based on non published data of our group demonstrating that NOX1 inhibition decreased the Nrf2 transcription activity measured by ARE reporter gene assay (Doctoral thesis, Shu Li, 2007). Also we could show that inhibition of NOX1 by si-NOX1 or DPI (a NADPH oxidase inhibitor) strongly down-regulated Nrf2 at the protein level (Figure 27A). These experiments also included direct inhibition of Nrf2 by si-Nrf2 performed as a control. Furthermore, the inhibitory effect of

si-NOX1 and DPI on Nrf2 was confirmed at the Nrf2 target gene level employing an ARE reporter gene assay (Figure 27B). Down-regulation of Nrf2 by si-NOX1 could be prevented by the addition of the proteasome inhibitor MG-132, suggesting that NOX1-derived ROS interfere with the redox-dependent proteosomal degradation of Nrf2 (Figure 27C). Furthermore, real-time RT-PCR demonstrated that inhibition of NOX1 did not effect Nrf2 mRNA (data not shown) indicating that NOX1 controls Nrf2 directly at the protein levels.

To further confirm these results, we investigated the effect of NOX1 overexpression on Nrf2. Overexpression of NOX1 resulted in induction of Nrf2 as demonstrated by Nrf2 Western blot (Figure 27D, upper panel, left) and ARE reporter gene assay (Figure 27D, lower panel, left). Overexpression of NOX1 was validated by Western blot employing an HA-antibody for the detection of the HA-tagged NOX1 (Figure 27D, upper panel, right). Furthermore, also measurement of ROS (H_2O_2) concentrations by Amplex Red displayed significantly higher H_2O_2 level in cells transfected with NOX1-HA containing plasmid in comparison to empty vector (Figure 27D, lower panel, right).

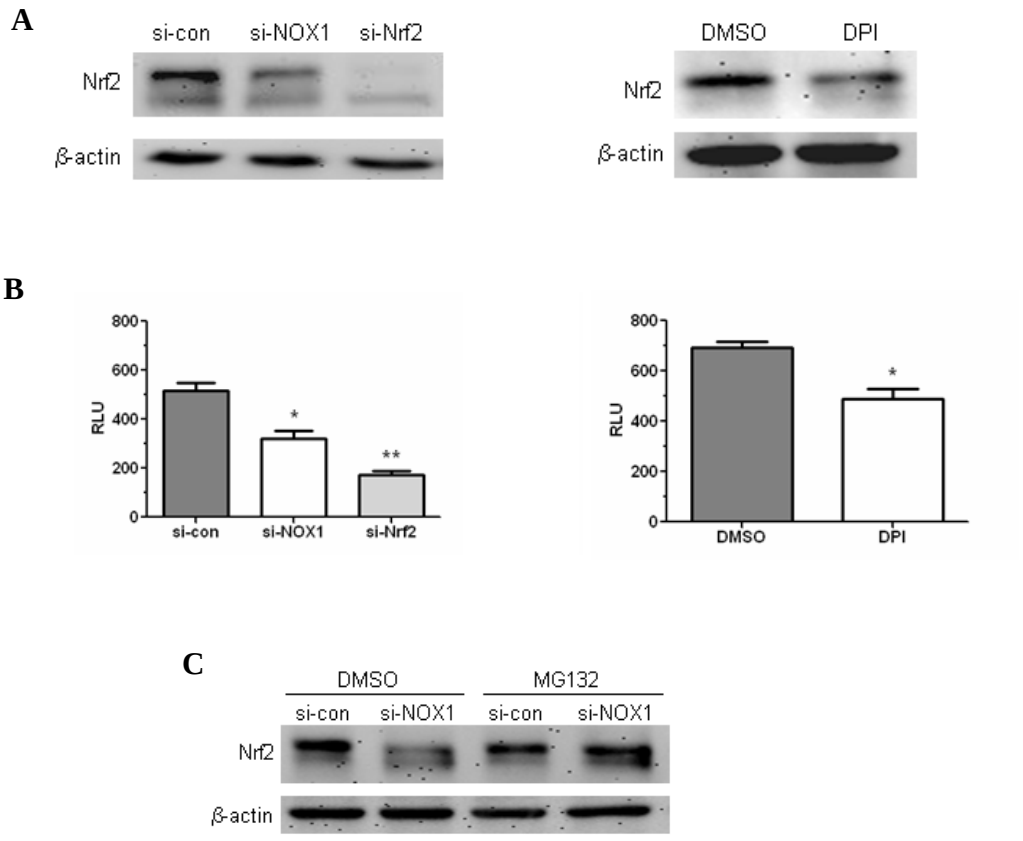

D

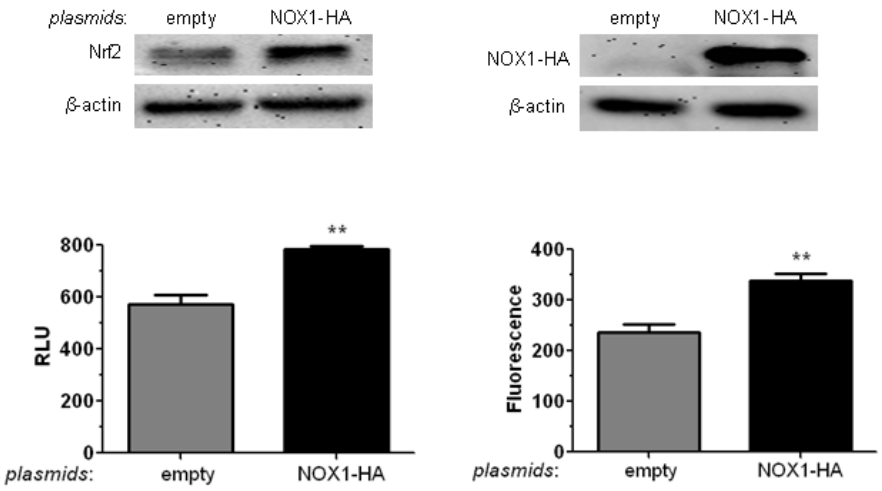

Figure 27: Regulation of Nrf2 by NOX1 in A549 cells
A) Western blot analysis of Nrf2 and **B)** ARE reporter gene analysis of Nrf2-dependent target genes in A549 cells transfected with si-NOX1 and with si-Nrf2 compared to si-con (left) and A549 cells treated by the NADPH oxidase inhibitor DPI (1 µM) or the solvent DMSO, which was used as control (right) (* $p<0.05$, ** $p<0.01$, n=3, unpaired t-test). **C)** Western blot analysis of Nrf2 in A549 cells transfected with si-NOX1 compared to si-con and treated by the proteasome inhibitor MG132 (25µM) or solvent DMSO used as control. **D)** Western blot analysis of Nrf2 (upper panels, left), and ARE reporter gene assay analysis (lower panels, left) in A549 cells transfected with tagged NOX1-HA or empty plasmid. Expression of NOX1-HA was validated by Western blot employing an HA antibody (upper panel, right) and by measurement of H_2O_2 concentration by Amplex Red (lower panel, right) (** $p<0.01$, n=3, unpaired t-test).

4.2.5 Regulation of Trx1 expression by NOX1

Next, we analyzed the effect of NOX1 on Trx1, a target gene of Nrf2. Accordingly, si-NOX1 treatment decreased Trx1 at the protein level as demonstrated by Western blot (Figure 28A) and mRNA level as demonstrated by real-time RT-PCR suggesting a transcription dependent regulation of Trx1 by NOX1 (Figure 28B). Also, these experiments included the inhibition of Nrf2 by si-Nrf2, and of Trx1 by si-Trx1 that were performed as controls (Figures 28A, B). *Vice verse*, NOX1 overexpression increased Trx1 at the protein level (Figure 28C). In order to prove that NOX1-dependent Trx1 regulation is mediated by Nrf2, we concomitantly overexpressed NOX1 and inhibited Nrf2 by siRNA (Figure 28D). Indeed, the NOX1-dependent induction of Trx1 was

completely abolished by Nrf2 inhibition which indicates that Nrf2 is the critical factor for Trx1 regulation by NOX1.

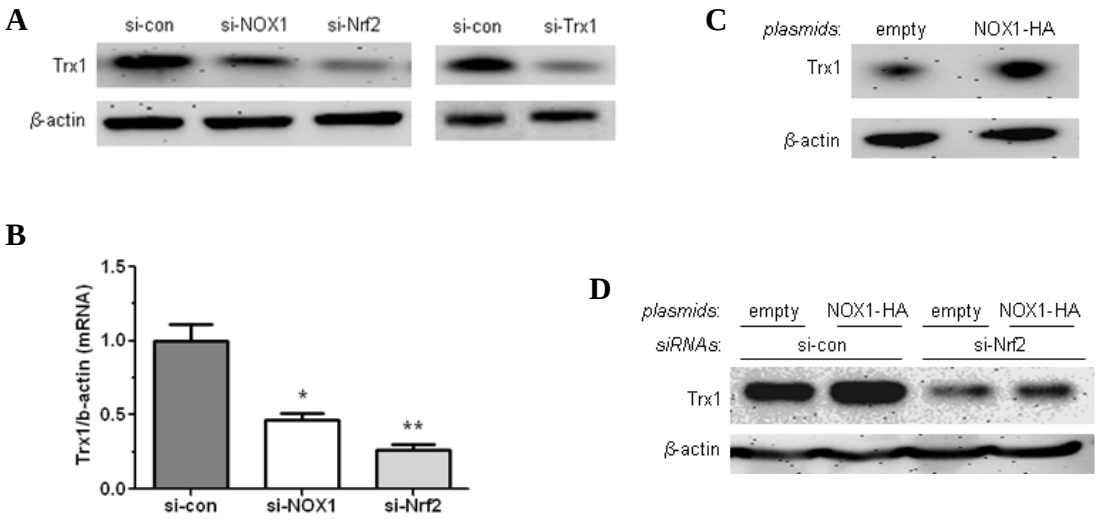

Figure 28: Regulation of Trx1 expression by NOX1 in A549 cells
A) Western blot analysis of Trx1 and **B)** real-time RT-PCR of Trx1 mRNA after inhibition of NOX1 by si-NOX and of Nrf2 by si-Nrf2 compared to si-con (* $p<0.05$, ** $p<0.01$, n=3, unpaired t-test). Trx1 inhibition by siRNA is included as a control. **C)** Western blot analysis of Trx1 from cells transfected by NOX1-HA plasmid compared to empty plasmid. **D)** Western blot analysis of Trx1 concomitantly transfected with empty plasmid or NOX1-HA plasmid and si-Nrf2 or si-con.

4.2.6 Regulation of Nrf2 and Trx1 expression by NOX1 under conditions of hypoxia-reoxygenation and intermittent hypoxia

The previous experiments revealed that Nrf2 and Trx1 expression depends on NOX1 under normoxic conditions (Figures 27 and 28). Initially, we observed a strong increase in Nrf2 and Trx1 expression in IH4R and IH6 (Figure 25B, C). Also, an up-regulation of NOX1 expression was observed in IH4R and IH6 (Figure 25B, C). Furthermore, NOX1-dependent ROS generation was more pronounced under these conditions (Figure 26B). Thus, we investigated the impact of NOX1 on Nrf2 and Trx1 in IH4R and IH6 (Figure 29). For this purpose, cells were transfected with si-con or si-NOX1 and subsequently Nrf2 and Trx1 expression was analyzed by Western blot. Indeed, si-NOX1 treatment caused most strong inhibition of Nrf2 and Trx1 under conditions of IH4R and IH6. In

particular, the Nrf2 and Trx1 protein decreased to the levels observed in normoxia after si-NOX1 treatment.

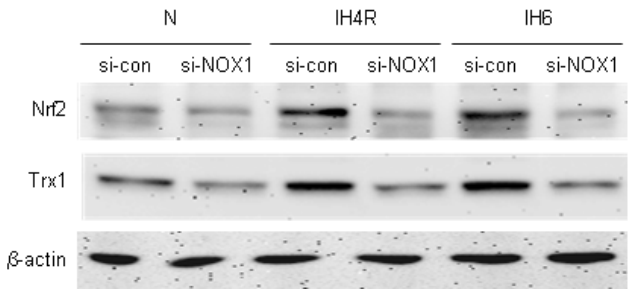

Figure 29: Regulation of Nrf2 and Trx1 expression by NOX1 under conditions of hypoxia-reoxygenation and intermittent hypoxia
Western blot analysis of Nrf2 and Trx1 after inhibition of NOX1 by si-NOX1 compared to si-con under conditions of IH4R and IH6 compared to N.

4.2.7 Regulation of HIF-1α by Nrf2, Trx1 and NOX1 under conditions of continuous and intermittent hypoxia

In the next step, we analyzed the effects of the inhibition of Nrf2, Trx1 and NOX1 on HIF-1α after continuous and intermittent hypoxic exposure (H2, H6, IH6). Treatment of cells with si-Nrf2, si-Trx1 and si-NOX1 resulted in significant down-regulation of HIF-1α expression in IH6, an effect that was less apparent in H2 and H6 as demonstrated by Western blot (Figure 30A) and HRE reporter gene assay (Figure 30B). IH6 displayed increased HIF-1 activity in comparison to H6 (Figure 30B, comparison of si-con (H6) to si-con (IH6), however this increase was not significant.

Furthermore, we demonstrated that overexpression of Trx1 induced HIF-1α both in continuous (H2, H6) and in intermittent hypoxia (IH6) (Figure 30C). Thus, increased Trx1 protein abundance (as observed endogenously in IH6) appears to be sufficient for the induction of HIF-1α, independently of other HIF-1α regulating mechanisms occurring in intermittent or continuous hypoxia. Also, these effects were evident when performing the HRE-dependent reporter gene assay measuring the accumulation of HIF-dependent target gene expression over the entire time periods studied (Figure 30D).

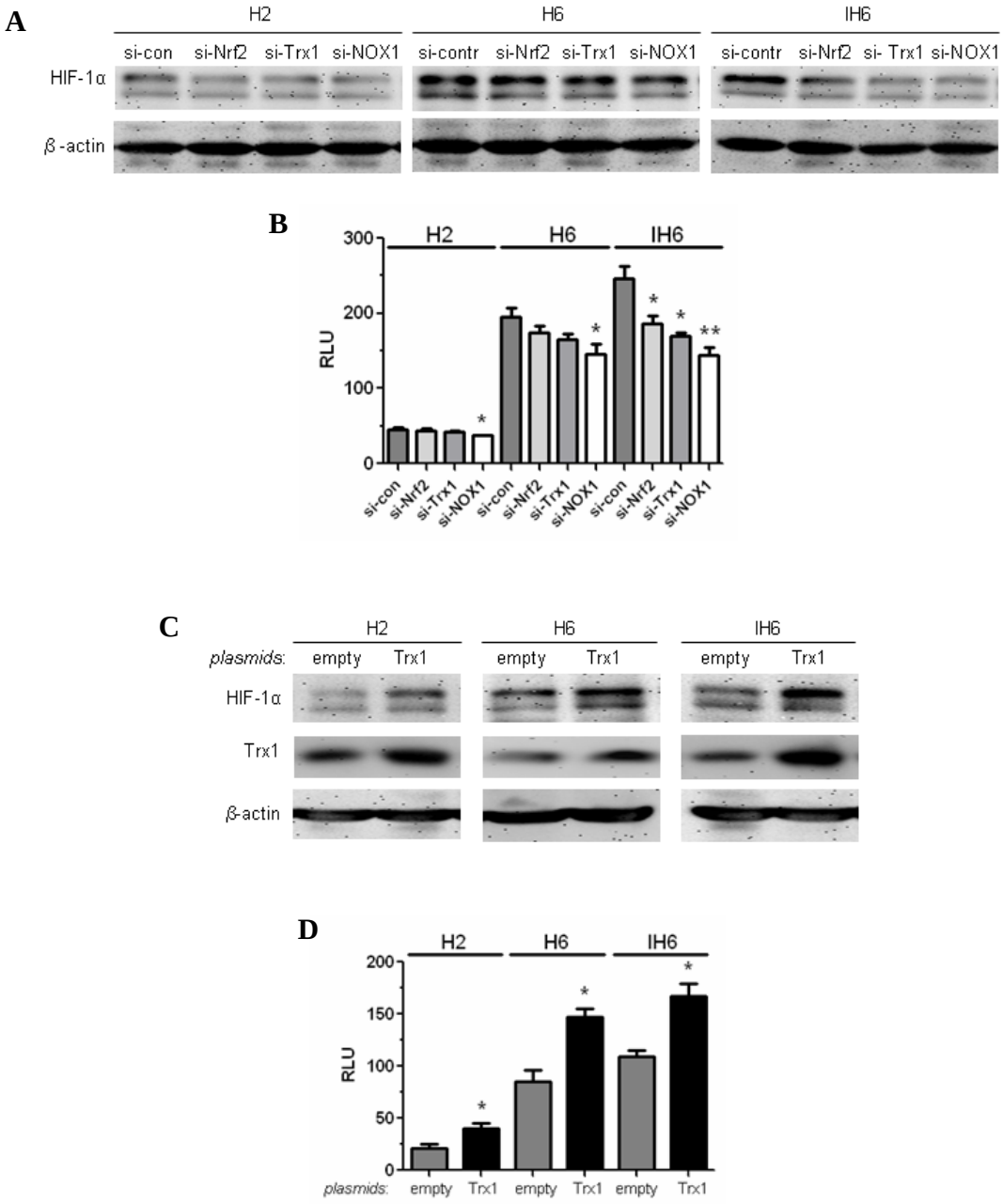

Figure 30: Regulation of HIF-1α by Nrf2, Trx1 and NOX1 under conditions of continuous and intermittent hypoxia

A) Western blot analysis of HIF-1α and **B)** HRE reporter gene assay in A549 cells after inhibition of Nrf2, Trx1 and NOX1 by si-Nrf2, si-Trx1, si-NOX1 compared to si-con under conditions of H2, H6 and IH6 (* $p<0.05$, ** $p<0.01$, n=3, unpaired t-test). **C)** Western blot analysis of HIF-1α and **D)** HRE reporter gene assay in A549 cells after transfection of Trx1 plasmid or empty plasmid (as validated by Trx1 Western blot) under conditions of H2, H6 and IH6 (* $p<0.05$, n=3, unpaired t-test).

4.2.8 Signaling pathway of NOX1 and Trx1 causing induction of HIF-1α in intermittent hypoxia

The following sequence of events causing the Nrf2-dependent induction of HIF-1α in intermittent hypoxia is suggested by our experiments: NOX1 induction in intermittent hypoxia causes an ROS elevation that subsequently induces Nrf2. In turn, Nrf2 induces its target Trx1 that leads to the induction of HIF-1α. In order to investigate whether Trx1 is the relevant downstream target of NOX1 enhancing HIF-1α in intermittent hypoxia (IH6), we performed both HIF-1α Western blot and HRE reporter gene assay from cells transfected with empty- or NOX1- or Trx1-plasmids and concomitantly with si-con or si-NOX1 or si-Trx1 (Figure 31A). Both overexpression of Trx1 (lane 2) and NOX1 (lane 3) displayed the typical induction of HIF-1α compared to the control (lane 1). Treatment of cells with si-NOX1 (lane 4) and si-Trx1 (lane 5) displayed down-regulation of HIF-1α expression compared to the control (lanes 1). However, treatment with si-NOX1 in Trx1-overexpressing cells (lane 6) did not result in the inhibition of HIF-1α, whereas treatment with si-Trx1 in NOX1-overexpressing cells (lane 7) was effective in the inhibition of HIF-1α, revealing that NOX1 is most likely upstream of Trx1. These HIF-1α Western blot results were in accordance with the HRE reporter gene assay organized exactly in the same way (Figure 31B). In particular, treatment of NOX1-overexpressing cells with si-Trx1 (lane 7) prevented the HRE induction (no significant induction compared to lane 1). In conclusion, the experiments strongly support a signal transduction pathway (Figure 32), that is relevant for HIF-1α induction under the given conditions of intermittent hypoxia.

A

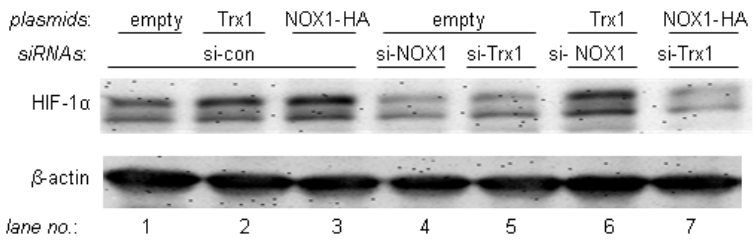

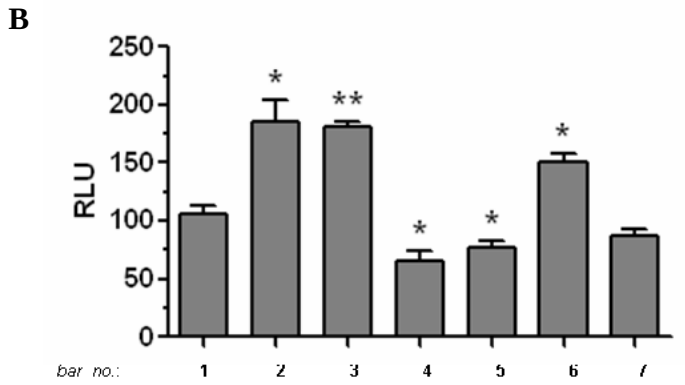

Figure 31: Signaling pathway of NOX1 and Trx1 causing the induction of HIF-1α after intermittent hypoxia exposure

A) Western blot analysis of HIF-1α and **B)** HRE reporter gene analysis in A549 cells transfected with empty or Trx1 or NOX1-HA plasmids with concomitant inhibition of NOX1 or Trx1 by si-NOX1 and si-Trx1 (* $p<0.05$, ** $p<0.01$, n=3, unpaired t-test).

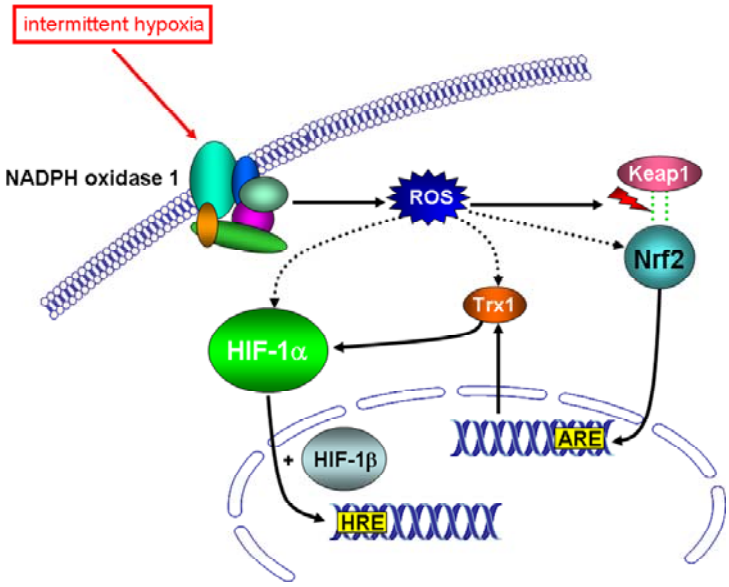

Figure 32: Schematic diagram of the regulation of HIF-1α by NOX1, Nrf2 and Trx1 during intermittent hypoxia exposure of A549 cells

ROS generated by NADPH oxidase 1 during intermittent hypoxia increase Nrf2 protein abundance likely by disruption of its interaction with Keap1. Nrf2 induction leads to enhanced Trx1 expression that subsequently stimulates HIF-1α . Alternatively, ROS may directly regulate Nrf2, Trx1 and HIF-1α by different mechanisms such as alteration of the redox state of the target molecules, phosphorylation or enhancement of translation.

5. Discussion

5.1 Detection of NOX1 and NOX4 proteins and analysis of NOX1- and NOX4-dependent ROS generation

In the first part of the work, we attempted to select the most suitable antibodies for the detection of NOX1 and NOX4 proteins since immuno-detection of these proteins is a commonly faced problem which complicates further structural and functional characterization of NOX1 and NOX4. Thus, several commercial and custom-made NOX1 and NOX4 antibodies were employed for Western blot analyses of total cell lysates and fractions of different cell compartments of A549 and other cell types expressing high levels of NOX1 or NOX4. In parallel with these approaches, we developed efficient siRNAs for specific knock-down of NOX1 and NOX4, and also attempted to purify and identify some of NOX1 and NOX4 proteins by HPLC/2D-GE followed by MALDI-TOF MS. Finally, we characterized the relative contribution of NOX1 and NOX4 to ROS generation in A549 cells.

5.1.1 Detection and analysis of cellular localization of NOX1 and NOX4 proteins using different antibodies

5.1.1.2 NOX1

The NOX1 antibodies immunoreactive proteins were analyzed in A549 and CaCo2 cells. Both cell types (but particularly CaCo2) are suggested to express considerable levels of NOX1. In accordance to our studies, CaCo2 cells displayed a higher NOX1 mRNA level than A549 cells as detected by real-time RT-PCR (Figure 8A). Five different NOX1 antibodies were employed for the detection of NOX1. However, no common bands in the range of the predicted NOX1 size could be detected with these antibodies (Figure 10A and 11A). The predicted molecule weight from the open reading frame sequence of NOX1 is 65kDa. However, commonly detected bands have been observed in the range of 50-65kDa [14], [15], [16], [17], [18], [19]. Deviations from the predicted NOX1 molecular weight may have different reasons:

1. altered migration of NOX1 proteins in SDS-PAGE based on their specific physical-chemical properties
2. cleavage of an N-terminal signal peptide or other proteolytic processing of NOX1
3. translation from different start codons in the NOX1 mRNA
4. alternative splice products of the NOX1 gene
5. immunoreactive NOX1 antibodies bands not related to NOX1

The characteristic immunoreactive patterns of the different NOX1 antibodies employed in Western blots are described below.

NOX1wch

NOX1wch (Dr.W.Chamulitrat, University Heidelberg) was the only antibody that detected some bands near to the predicted size of NOX1, both in total cell lysate and subcellular fractions of both A549 and CaCo2 cells. Finally, this polyclonal antibody appeared to be the most suitable antibody for the detection of NOX1. It was developed against a synthetic NOX1-derived peptide (Figure 9A) that was used also by other groups for raising NOX1 antibodies [206], [207], [208], [209]. In particular, NOX1wch detected bands at 55kDa and 65kDa that were more strongly abundant in CaCo2 than in A549 cells. The sizes of these bands were the same as those detected in immortalized human gingival keratinocytes using this antibody [29], [14].

When different techniques for subcellular fractionation were used, both the 55kDa and 65kDa bands were localized predominantly in the cytoskeleton of A549 and CaCo2 cells (Figure 11A, 12A, 16A). The detection of these proteins in a particular fraction also depended on the method of fractionation and was not always consistent. For example, when the *Complete Cell Fractionation Kit* was used the 55kDa and 65kDa bands were strongly present in the cytoskeleton and weakly in the nuclei of these cell lines (Figure 11A). When the *Nuclear and Cytoplasmic Extraction Reagent* was employed, the 65kDa band of CaCo2 cells was mainly detected in the nuclear insoluble fraction representing the cytoskeleton and the 55kDa band was also strongly present in the nuclear soluble fraction representing nuclear proteins (Figure 16A). However, when the same kit was used for A549 cells, the 65kDa band was mainly in the nuclear insoluble fraction but the

55kDa band was detected only in the nuclear soluble fraction (Figure 16A). These inconsistent observations make it difficult to draw clear conclusions regarding the accurate subcellular localization of NOX1.

The strong cytoskeletal and the weak nuclear NOX1 localizations appear to be in contrast to previous reports, where NOX1 was commonly detected in the plasma membrane [27], [21], [22], [23], [24]. Interestingly, the NOX1 homologs NOX2 and NOX4 were both found in the Tx-100 insoluble fraction (containing mainly cytoskeleton proteins) and NOX4 was also colocalized with focal adhesions [210], [18]. The subcellular localization of these homologs seems to be dependent on the type of cells. For example, in neutrophils NOX2 associates with the plasma membrane [211], [212], whereas in HUVEC NOX2 is predominantly localized intracellular at the cytoskeleton and in the nuclei [210]. However in our experiments, NOX1wch detected bands in both A549 and CaCo2 cells in the cytoskeleton but not in the membrane fraction. One current study from Gianni et al. is partially supporting our observations. This study has shown that recombinant NOX1 is colocalized with F-actin and cortactin in invadopodia (i.e. protrusion in the plasma membrane) of DLD1 colon cancer cells [28]. Interestingly, also our experiments with recombinant NOX1 demonstrated that HA-tagged NOX1 protein was localized mainly in the Tx-100 insoluble fraction (Figure 15A). One possible explanation of this observation could be that NOX1 is localized in the plasma membrane where it interacts with the cytoskeleton or focal adhesions and thus it may be difficult to recover NOX1 from the membrane fraction (i.e. to separate it from the cytoskeleton) by common biochemical techniques. Additional approaches such as immunocytology employing suitable antibodies for the analysis of NOX1 protein localization could be helpful in this regard. However, this approach was not applicable with NOX1wch since several additional proteins of lower molecular weight were detected with this antibody. Also, detection of recombinant NOX1-HA with HA-antibody was not applicable since it displayed several degradation products that might interfere with the localization of NOX1-HA “full length” protein.

NOX1wch typically detected bands at 55kDa and 65kDa. The band at 55kDa in A549 and CaCo2 cells was stronger than the 65kDa band. Both bands were sensitive to si-NOX1 treatment (Figure 14A), thus both these proteins were considered as NOX1. The

55kDa band was unlikely representing NOX1v (i.e. NOX1 splice variant, Mw = 59kDa) since, firstly, this variant was almost undetectable at the mRNA level in A549 and CaCo2 cells and secondly, one previous study showed that transfection of immortalized human gingival keratinocytes by recombinant NOX1 increased the abundance of both the 65kDa and 55kDa bands when using the NOX1wch antibody [14]. Thus, the 55kDa band may rather represent an endogenous proteolyticly processed product, for example, after signal peptide cleavage as suggested by Helmecke et al. [21]. However, the predicted signal peptide of NOX1 protein would contain the first 29 amino acids of the N-terminus (ExPASy Proteomics Server, Post-translational modification prediction), which does not fit to the difference of 10kDa between the predicted size of 65kDa and the detected of 55kDa. An additional explanation of this observation could be based on the physical-chemical properties of the NOX1 protein. Proteins containing membrane domains are typically migrating faster in SDS-PAGE since they may bound higher amount of SDS [213]. Signal peptide cleavage could alter the hydrophobicity of NOX1 and thus proteolyticly processed NOX1 would migrate faster than the non-processed. The presence of two differently processed NOX1 proteins (55 and 65kDa) may affect NOX1 localization and function. In this context is interesting, that deglycosylation of NOX1 homolog NOX2, that in glycosylated form migrates as a 91kDa protein, shifted the apparent molecular weight not to the predicted 65kDa but to 55kDa [214], [215].

A further explanation could be that different start codons of NOX1 mRNA for translation are functional. In fact, if the translation of NOX1 mRNA would start at the second start codon (Met-107) in frame, the protein would have a size of 53kDa. However, this start position is speculative since the second AUG unlike the first one does not exhibit any Kozak-related sequence (A/GxxAUGG) that would favour initiation of translation at this position (Molecular biology of the cell, Alberts et al., 2002).

Thus, in the next part of our work, we performed proteomic analyses in order to get more information about the amino acid sequence and identity of these two proteins.

In sum, NOX1wch detected protein bands near to the predicted size of NOX1 (55kDa and 65kDa) both in A549 and in CaCo2 cells. Both proteins were stronger expressed in CaCo2 than in A549 cells (Figure 10A). These bands were sensitive to inhibition by specific si-NOX1 (Figure 14A). Furthermore, this antibody detected fragments of the

NOX1 recombinant protein (Figure 15A). We concluded that this antibody was the most suitable for NOX1 protein detection in Western blot when compared to the other antibodies.

NOX1ab55831

NOX1ab55831 (Abcam) detected a band at position of 60kDa. However, this band was considered to be unlikely NOX1 since, firstly, it was expressed in A549 cells at a higher level than in CaCo2 cells (Figure 10A, 11A, 12A), secondly, it was present in the cytosolic fraction (Figure 11A, 13A) and thirdly this protein was not sensitive to siRNA mediated NOX1 knock-down (Figure 14A). Also treatment of samples with Tx-100 did not show any changes in the localization of this protein (Figure 12A), which indicated that this protein was not membrane associated.

MOX1 H-15

MOX1 H-15 (Santa Cruz Biotechnology) is a frequently used antibody for the detection of NOX1 [200], [20] [201], [216], [217], [21], [218]. This antibody interacted with the NOX1 recombinantly expressed protein (data not shown) however the detection of endogenous NOX1 was problematic. Employing an older batch of MOX1 H-15, a band at 60kDa was detected in the cytosolic fraction of A549 (Figure 19, 110000g supernatant). This band seemed to be identical with the 60kDa band detected with NOX1ab55831 since both antibodies have been raised against peptides that had overlaping amino acid sequences (Figure 9A). However with the new batch of the antibody, the band at 60kDa was undetectable in total cell lysate (Figure 10A) and weakly detectable in cell fractions (Figure 11A). In contrast, the new batch of MOX1 H-15 visualized a band at 68kDa in the nuclear fraction both in A549 and CaCo2 (Figure 11A) cells. However, because this band was not detected in the total cell lysate, the antibody was not useful for further validation such as the inhibition of NOX1 by siRNAs.

MOX1 H-75

MOX1 H-75 (Santa Cruz Biotechnology) was described to detect recombinant NOX1 in one study [219]. In our studies, the antibody detected a band at 50kDa (Figure 10A, 11A) - an observation that was not always reproducible (Figure 12A). This antibody was raised

to a relative long peptide of 75 amino acids at the N-terminal part of NOX1, and thus it is more likely that the antibody detects also related proteins.

NOX1jh

NOX1jh (Dr.J.Hänze, University Giessen) antibody detected a band at 95kDa in both cell types, however at a higher level in A549 than in CaCo2 cells (Figure 10A). This band was very strong and was detectable in cytosolic, membrane and nuclear fractions (Figure 11A). Tx-100 treatment appeared to release the protein from the pellet to the supernatant which may indicate that it was a membrane associated protein (Figure 12A). Based on its molecular weight (95kDa), the protein could represent a dimer of NOX1 with p22phox but this explanation seems to be unlikely since reducing and denaturing conditions should disrupt the interaction of NOX1 and p22phox. Also, si-NOX1 treatment did not decrease the level of this protein (Figure 14A).

A polyclonal antibody raised against the identical NOX1-derived peptide as NOX1jh was also used by another group. However, in this study the antibody functionality was not properly validated [19].

mAb54.1

mAb54.1 (Dr.J.Buritt, Montana State University, USA) is a monoclonal antibody raised against a NOX2-derived peptide. This antibody is well established for the detection of NOX2 [220], [221], [222], [223]. In addition, one study showed that mAb54.1 also detected fragments of recombinant proteins of NOX1, NOX3 and NOX4 [199]. This was likely based on similarities in the amino acid sequences between different NOX proteins in the epitop that was used as immunoreactive peptide. This antibody detected a strong band at 55kDa (Figure 10A) that was previously determined as GRP 58 [199]. When subcellular fractionation was performed, the mAb54.1 was the only antibody detecting proteins close to 65kDa in the membrane fraction of A549 cells (Figure 11A). Since this protein was almost not present in the membrane of CaCo2 cells, we supposed that it represents rather NOX2 than NOX1. Limited amount of mAb54.1 did not allow to perform further experiments with this antibody.

5.1.1.3 NOX4

Three different NOX4 antibodies were employed for the detection of NOX4 in A549 cells and HUVEC in our study. HUVEC were used as a positive control for NOX4 expression since these cells have been described to express high level of NOX4 [65], [74], [224]. Indeed, NOX4 mRNA analysis by real-time RT-PCR revealed higher level of NOX4 mRNA in HUVEC than in A549 cells (Figure 8B). Employing different NOX4 antibodies, bands near to the predicted size of 67kDa and an additional band in the range of 75-80kDa have been commonly detected [60], [18], [61], [62], [63], [64]. The higher molecular weight may represent posttranslational modifications of NOX4. In fact, several N-glycosylation sites in NOX4 protein are predicted (ExPASy Proteomics Server, Post-translational modification prediction). However, treatment of the cell lysate with N-glycosidase F did not reduce the molecular weight of the 80kDa band [60] making N-glycosylation of NOX4 not very likely. Thus, the reason of this shift in molecular weight of NOX4 remains unexplained.

Similarly to the NOX1 antibodies, comparison between the different NOX4 antibodies revealed no common band in Western blot analysis of cell lysates from A549 cells and HUVEC. The characteristic immunoreactive patterns of the different NOX4 antibodies are presented below.

NOX4jh

NOX4jh (Dr.J.Hänze, University Giessen) turned out to be the most suitable antibody for NOX4 detection. This antibody detected bands at 62kDa and 67kDa in A549 cells and bands at 50kDa, 67kDa and 80kDa in HUVEC (Figure 10B). In addition, several protein species of lower molecular weight were observed. In contrast to the 62kDa band, the 67kDa band was efficiently inhibited by NOX4 siRNA (Figure 14B) supporting the identity of this band as NOX4. In accordance with some previous studies [18], [64], [66] the NOX4 67kDa band was found in the cytoskeleton fraction of A549 cells (Figure 11B, 12B). Interestingly when fractions from HUVEC were analysed, NOX4 was present in the cytoskeleton and in the nuclear fraction (Figure 11B). This was confirmed by isolation of the nuclear fraction employing different kit systems (Figure 16B). The NOX4

localization in nuclei was also observed by other groups [65], [18], [62]. Accordingly, the isolation of Tx-100 soluble and insoluble fractions revealed NOX4 both in the supernatant and pellet in HUVEC but only in the pellet of A549 cells (Figure 12B). These different results of the biochemical separation between A549 cells and HUVEC may also be caused by different solubility of the cytoskeletons. In contrast to our results, other groups demonstrated that NOX4 is localized in the ER [21], [62], [25]. This may be explained by different localization of NOX4 in dependency on the cell type or on presence of different isoforms (splice variants) of NOX4 in cells or on NOX4 posttranslational modification(s) or by use of different techniques for analysis of subcellular localization of NOX4 or by a low specificity of the antibodies. In HUVEC cells we observed an additional 80kDa NOX4 band that was present in the cytosolic but not in the membrane or cytoskeleton fraction (Figure 11B) (confirmed also by separation of Tx-100 soluble and insoluble fraction, Figure 12B). In contrast to our results, one recent study described the 80kDa band as NOX4 that was localized in focal adhesions, stress fibres and nuclei [64], and another study that demonstrated this band localized both in Tx-100 soluble and insoluble fractions [18].

In order to identify all NOX4jh antibody immunoreactive bands that may represent different posttranslational modifications or splice variants of NOX4, further proteomic analyses of these proteins were performed.

In sum, the NOX4jh antibody was suitable for the detection of NOX4 protein since it reacted with a band of the expected 67kDa (Figure 10B) and this band was sensitive to knock-down by si-NOX4 (Figure 14B). Moreover, the 67kDa protein was stronger expressed in HUVEC than in A549 cells (Figure 10B) which was in accordance with NOX4 mRNA quantification in these types of cells (Figure 8B).

NOX4 N-15 & NOX4 H-300

Also, the antibodies NOX4 N-15 and NOX4 H-300 (Santa Cruz biotechnology) were employed for the analysis of expression of potential NOX4 proteins. However, these antibodies did not detect any band in common with NOX4jh. Additionally, these antibodies turned out not to be very sensitive since they did not detect any strong band in the total cell lysate (Figure 10B). NOX4 N-15 has been described to detect NOX4 in

several studies [201], [200], [216], [217]. However, in our experiments, not any bands were detected at all. The reasons for this are not clear. In contrast to NOX4 N-15, NOX4 H-300 detected a few bands near to the predicted size of NOX4 in subcellular fractions of A549 cells but not of HUVEC (Figure 11B). NOX4 H-300 was used in one recent study. However, in this study the immunoreactivity of the antibody with NOX4 protein was not clearly confirmed [224].

In conclusion, NOX4 N-15 and NOX4 H-300 were not useful for the detection of NOX4 in our Western blot experiments.

5.1.2 Detection of p22phox and NOXO1 proteins in different cell compartments

p22phox and NOXO1 are essential components for NADPH oxidase 1 function. Their expressions were analysed along with NOX1 by Western blot. Previous studies demonstrated that p22phox is localized in different cell membranes [26], [225], [226], [24], [212] and NOXO1 in the plasma membrane and cytosol [226], [24], [23]. Accordingly, we detected p22phox mainly in the membrane (Figure 11C, 13A) and the nuclear fraction (Figure 11C). The membrane association of p22phox was also suggested from experiments where Tx-100 treatment of cell lysate released p22phox at least partially into the supernatant (Figure 12C). The non complete release of p22phox from the pellet after treatment by Tx-100 suggested that p22phox also interacted with components of the cytoskeleton. Also, Li et al. [210] observed p22phox in the Tx-100 insoluble fraction of HUVEC. Additionally, our experiments showed that p22phox was almost not present in the pure plasma membrane fraction of A549 cells (Figure 13A) which indicates that also NOX1 should not be in this fraction since p22phox-NOX1 interaction is important for the function of NADPH oxidase 1 [26], [25].

The NOXO1 antibody detected a band with a molecular weight of the expected 41kDa (emerging sometimes as a double band) and no further bands were visible. Employing several approaches, our studies demonstrated NOXO1 mainly in the cytoskeleton fraction (Figure 11C, 16C). Tx-100 treatment partially released NOX1 from the cytoskeleton indicating a possible association of NOXO1 with membranes (Figures 12C). The localization of NOXO1 in the cytoskeleton fraction was in accordance with the NOX1

localization (using NOX1wch antibody) and supports the functional interaction between these two proteins.

5.1.3 Effect of p22phox knock-down on NOX1 and NOX4 stability

p22phox is also suggested to stabilize NOX proteins during their folding in the ER. It has been shown that p22phox is critical for maturation and function of NOX2 [78], [77], [82]. An inhibitory effect of p22phox knock-down on recombinant NOX1 but not NOX4 protein expression has also been demonstrated [82]. Thus, our further aims were to investigate effect of p22phox knock-down on expression of proteins that we determined as NOX1 and NOX4 and *vice-versa*, effect of NOX1 and NOX4 knock-down on p22phox protein expression.

An inhibition of p22phox by specific siRNA did not display any effect on the expression levels of endogenous NOX1 and NOX4 proteins (Figure 17A). When the same experiment with recombinantly expressed NOX1 and NOX4 proteins was performed, the down regulatory effect of p22phox inhibition on NOX1 and NOX4 proteins levels was strongly apparent (Figure 17B). This effect was partially cancelled by treatment of cells with a proteasome inhibitor (MG132) indicating that p22phox influences NOX1 and NOX4 protein stability by proteasome degradation. Conversely, inhibition of NOX1 but almost not of NOX4 led to a decrease of p22phox protein expression (Figure 17C). Theses results indicate that p22phox is important for NOX1 and NOX4 protein stabilization under the conditions when NOX1 and NOX4 protein synthesis is induced, and secondly, that NOX1 is more important than NOX4 for stabilization of p22phox protein in A549. The second observation may be based simply on the fact that in A549 cells NOX1 is expressed at a much higher level than NOX4 (Figure 8C, comparison of quantity of NOX1 and NOX4 mRNAs in A549 cells) and thus NOX1 may be more important than NOX4 for p22phox stabilization.

5.1.4 Purification of putative NOX1 and NOX4 proteins

Different NOX1 antibodies displayed different patterns of NOX1 immunoreactive bands. The NOX1wch antibody detected two specific bands of 55kDa and 65kDa in A549 cells.

The NOX4jh antibody detected at least two specific bands of 67kDa and 80kDa in HUVEC. Furthermore, both antibodies detected several additional bands of lower molecular weights that also may represent NOX proteins. Thus, we aimed to further identify all these bands by proteomic approaches.

Isolation of the proteins bands after subcellular fractionation from the polyacryl-amid gel or PVDF membrane did not allow the identification of NOX related proteins by MALDI-TOF MS analysis. This was likely because of the low abundance and purity of the investigated proteins in single bands isolated from the polyacryal-amid gel or PVDF membrane. Thus, we performed several additional purification steps. After subcellular fractionation, two HPLC purification steps were performed, i.e. anion exchange chromatography (AEC) and reverse phase chromatography (RPC), followed by Western blot analysis of all HPLC fractions and final analysis of the relevant proteins bands isolated from the gel or PVDF membrane by MALDI-TOF MS. An alternative purification procedure included 2D gel electrophoresis (2D-GE) instead of one or both HPLC purification steps. The strategy of purification is depicted on Figure 18.

However, in spite of performing these additional purification steps, we did not identify any of the immunoreactive bands as NOX1 or NOX4 proteins.

The limitations of the protein purification and identification procedures may be caused by the following reasons:

Firstly, the MALDI-TOF MS technique turned out to have an insufficient sensitivity when compared to the immunodetection of NOX1 and NOX4 employing UV based visualization of protein bands on the PVDF membrane. This was, for example, demonstrated by experiment where the p22phox immunoreactive band was cut out from the PVDF membrane and MALDI-TOF MS analysis of the protein digest did not identify the p22phox protein (Figure 20F). Furthermore, the sample preparation and efficiency of protein extraction from the gel or PVDF membrane may also be critical in protein identification by MALDI-TOF MS. Another technical challenge of the purification procedure represented the optimization of HPLC. Since each step of HPLC purification decreased the amount of the analyzed protein significantly, high amounts of relative pure protein material (several tens of milligrams of proteins) had to be used for each run of chromatography. This limited numbers of repetition of purification experiments and use

of low capacity binding semi-preparative columns that are normally suitable for protein purifications. Particularly at RPC, amount of proteins loaded on column turned out to be problematic. Thus, an additional purification step such as cation exchange chromatography or ultrafiltration should be included before applying samples on RPC column.

As an alternative purification procedure, 2D-GE was performed. However, also this approach appeared to be inappropriate. In particular, after 2D-GE separation, we did not detected proteins of interest at their expected or near to the expected molecular weight (Figure 20B, C, D, H). This might be explained, for example, by degradation or not proper solubility of the proteins of interest in the 2D-GE sample buffer or by insufficient transfer of protein to the PVDF membrane or by use of an improper pH-gradient. Another explanation could also be that, in general, membrane and hydrophobic proteins are often poorly represented in the second dimension of 2D gel. This phenomenon is not completely understood yet, but it may be based on protein-gel interactions during IEF [227].

Up to now, only two groups have managed to purify endogenously expressed NOX family proteins. The DUOX2 protein was purified from pig thyroid membrane [228]. Solubilized membrane proteins were subjected to cation exchange chromatography, followed by an FAD-based affinity chromatography. Specific protein bands being immunoreactive with a DUOX antibody were cut from the gel, digested by trypsin and the peptides were separated on a RPC column and identify by MALDI-TOF MS. This purification procedure could be suitable for purification of NOX proteins generally since also other NOXs have a FAD binding domain.

Also, the NOX2 protein in complex with p22phox (i.e. flavocytochrome b_{558}) was purified from neutrophil membranes and identified by MALDI-TOF MS [229], [230]. The method was based on immuno-affinity chromatography purification of NOX2 by an anti-NOX2 monoclonal antibody coupled to A-sepharose. In contrast to our purification procedure of NOX1 or NOX4, this approach enables to recover a high amount (several tens of micrograms) of purified flavocytochrome b_{558} that allows detection by MS.

Despite of the fact that finally the NOX1 and NOX4 proteins could not be identified and other strategies of purification would have to be employed or developed for succeeding in this, several interesting observations were made:

1. MOX1 H-15 detected strong bands at 60kDa and 45kDa in A549 cells. These bands or other bands near to the predicted size were previously described as NOX1 [18], [200], [20], [201], [216], [217], [218]. However, after performing the complete HPLC-based purification process, these bands were identified as pyruvate kinase and β-actin. Moreover, this antibody did not detect any band close to the predicted size in CaCo2 cells. Thus, it is questioned whether the MOX1 H-15 antibody is suitable for the detection of endogenous NOX1.

2. The 65kDa and 55kDa bands detected by NOX1wch (both in A549 and CaCo2 cells) were found in the flow through after AEC. AEC was used since most of the proteins have a pI in the neutral pH range (Molecular biology of the cell, Alberts et al., 2002) and thus, buffers with high pH (commonly used in AEC) would ensure their negative charge and good solubility. NOX1 is a basic protein with a pI of 8.8 (ExPASy proteomic server, Identification of isoelectric point, molecular weight and/or amino acid composition) and thus it would have a zero net charge in the chromatographic buffer used (Tris-HCl, pH = 8.8). Since binding of the uncharged protein to the ion exchange chromatography column is unlikely, the recovery of NOX1 (detected with NOX1wch) in the flow through could be expected. However, MOX1 H-15 positive bands were eluated in certain fractions and not in the flow through. Similarly to the pI of NOX1, the theoretically predicted pI of NOX4, NOX2 and p22phox is higher than 8.8. Thus, the immunodetection of NOX4 (67kDa), NOX2 (70kDa) and p22phox (22kDa) in the flow through after AEC was not very surprising (Figure 20C, E, F). On the other hand, posttranslation modifications such as glycosylation may decrease the pI of the protein. In accordance with this, the 80kDa band of NOX4 and the 90kDa band of NOX2 possibly representing glycosylated forms of these proteins were binding to the AEC column (Figure 20D, E).

5.1.5 Contribution of NOX1 and NOX4 to ROS generation in A549 cells

Initially, we showed that NOX1 mRNA was expressed in A549 at a significant higher level than NOX4 mRNA (Figure 8C).

Based on this observation, we were further interested in the relative contribution of NOX1- and NOX4-containing NADPH oxidases to ROS production in A549 cells.
Measurement of H_2O_2 by Amplex Red reagent in the total cell lysate showed that knock-down of NOX1 by siRNA significantly decreased the H_2O_2 concentration (about 20%), whereas knock-down of NOX4 did not display any significant ROS decrease. This observation may reflect that NOX1 is more strongly expressed than NOX4 in A549 cells. In this regard, of interest are studies demonstrating that NADPH oxidase 1 is primary producing $O_2^{\cdot-}$ whereas NADPH oxidase 4 is producing H_2O_2 [21], [231]. In our study, only H_2O_2 was measured since $O_2^{\cdot-}$ is suggested to be rapidly converted to H_2O_2. Additionally, also other groups have shown NOX1-dependent H_2O_2 generation [34], [232], [233]. Thus, measurement of H_2O_2 as product of both NOX1 and NOX4 appears to be relevant.

5.2 Regulation and cross-talk of NOX1, Nrf2, Trx1 and HIF-1α under different oxygenation conditions

Hypoxia and fluctuations of oxygenation resulting in intermittent hypoxia occur as consequences of different phathological states of organism. In particular, oxygen level fluctuations are typical characteristics of solid tumors [234], [235]. NADPH oxidase 1 is highly expressed in several adenocarcinoma cells (including A549 cells) and is of importance in cellular signaling possibly targeting the ROS- and oxygen- dependent transcription factors HIF-1 and Nrf2. Thus, we analysed the expression of NOX1, HIF-1α, Nrf2 and the Nrf2 target Trx1 under different conditions of oxygenation. In particular, we investigated the regulation and a possible cross-talk between Nrf2 and HIF-1α with regard to NOX-dependent ROS signaling in continuous and intermittent hypoxia.

5.2.1 NOX1, NOX4, HIF-1α and Nrf2 expression, and NOX1-dependent ROS generation under different hypoxic conditions

Initially**,** the expression of NOX1 mRNA and protein was analyzed in comparison to NOX4 under the different hypoxic conditions in A549 cells. The results showed that continuous long term hypoxia (H24) and intermittent hypoxia (IH6) induced NOX1 mRNA and proteins to a similar degree (Figure 22A). An apparent increase of NOX1 protein level was also visible after 12 hours of hypoxia. The induction of NOX1 expression or activity under conditions of continuous hypoxia has also been described previously [236], [155], [237]. In contrast, NOX4 expression in A549 cells was not induced under the hypoxic conditions investigated (Figure 22B). In accordance with the induction of NOX1 expression under the different hypoxic conditions, also ROS derived from NOX1 displayed a most significantly increased level in IH6 and H24 (Figure 23B). Based on these studies, we conclude that intermittent hypoxia enhanced NOX1 expression and NOX1-dependent ROS generation more rapidly than continuous hypoxia does.

Furthermore, HIF-1α levels were increased both in continuous long term and intermittent hypoxia whereas Nrf2 was increased only in intermittent hypoxia (Figure 24A). Interestingly, Nrf2 knock-down revealed strong down-regulation of HIF-1α in intermittent hypoxia but not in continuous long term hypoxia (Figure 24B).

5.2.2 Intermittent hypoxia and its relevance for physiological and pathophysiological conditions

Cellular oxygenation in higher organisms is dynamic displaying alternations between stages of hypoxia and reoxygenation termed intermittent hypoxia. These conditions are observed under normal physiologic conditions (development, physical activity, exposure to hypoxic environment) and are also related to various pathophysiological conditions among them are pulmonary, cardial and vascular diseases, inflammation, transplantation and cancer.

In particular, solid tumors are characterized by a hypoxic microenvironment that is caused by a high oxygen consumption rate due to the high metabolic rate of proliferating

cells, and due to structural deficiencies of tumor vessels that are not able to ensure stable oxygen supply [238], [239]. These hypoxic tumor areas are not stable since the oxygen concentrations in the tumor fluctuate in a temporal and spatial pattern, due to the dynamics of tumor progression and tumor angiogenesis, two processes that cause and counteract hypoxia [240]. Also, vasomotion of tumor arterioles, changes in the distribution and flux of red blood cells, and a progressive longitudinal decline in hemoglobin saturation play a role. These different phenomena result in conditions of intermittent hypoxia, where hypoxia and reoxygenation alternate with time, with periods ranging from minutes to days that are superimposed [241].

In this context, we selected different sequences of hypoxic and normoxic intervals of 2 h (Figure 25A) principally mimicking intermittent hypoxia particular in vascularized tumors [242], [234], [235], [243], [244], [240]. Our protocol of intermittent hypoxia was also based on other cell culture studies where similar oxygenation conditions were used [245], [246], [247], [248] and on the presumption that HIF-1- and Nrf2-dependent gene regulatory pathways characterized by *de novo* mRNA and protein synthesis become effective in the range of hours. For example, induction of the Nrf2-dependent target gene peroxiredoxin 1, reflected by an increased protein level of this target, required about 2 h after switching from hypoxia to reoxygenation [202].

Intermittent hypoxia is accompanied by elevated ROS generation, affecting signal transduction and gene regulation by both HIF-1α and Nrf2. In this regard, it is of note that Trx1 an Nrf2-dependent target gene has been demonstrated to induce HIF-1α [249], [161], [123], [196] thus Trx1 may represent a possible link between Nrf2 and HIF-1α**.**

5.2.2.1 Regulation of HIF-1α, Nrf2, Trx1 and NOX1 expression, and NOX1-dependent ROS generation in A549 cells treated by different alternating hypoxic and normoxic intervals

Induction of HIF-1α was progressively enhanced after each cycle of 2 hours of hypoxia and 2 hours of reoxygenation in spite of the fact that during the reoxygenation period, the HIF-1α signal was almost not detectable (Figure 25B). This suggests that HIF-1α becomes more responsive to the induction after two hours of hypoxic exposure in the

later stages of intermittent hypoxia, resulting in a comparable HIF-1α protein level induction as observed after six hours of continuous hypoxic exposure. In contrast to IH6, where HIF-1α can accumulate only over a 2h of hypoxic stage (disappearing after each 2h of reoxygenation step), in H6, HIF-1α can accumulate over a 6h of hypoxic stage.

One study demonstrated that intermittent hypoxia (performed with three cycles of hypoxia (1 hour) interrupted by reoxygenation (0.5 hour) increased cell migration and cell survival of endothelial cells in a HIF-1α-dependent manner. Also, this study demonstrated that intermittent hypoxia enhanced the resistance of endothelial and tumor cells towards apoptosis caused by irradiation [245]. A further study showed that the phosphoinositide-3 kinase pathway and stimulation of mitochondrial respiration triggered the stabilization of HIF-1α in endothelial cells in this pattern of intermittent hypoxia [246]. Another study identified protein kinase A as relevant for the progressive increase of phosphorylated HIF-1α observed in intermittent hypoxia in endothelial cells [247]. Furthermore, angiogenesis as indicated by cell migration and tubulogenesis of endothelial cells was enhanced in intermittent hypoxia in a HIF-1α dependent manner. This study also included analysis of Nrf2 that was observed not to be induced [248]. These observations suggest different mechanisms contributing to the enhancement of HIF-1α induction in intermittent hypoxia. In this context, our study employing patterns of intermittent hypoxia with stages of hypoxia and reoxygenation in the range of hours, demonstrated augmented HIF-1α signaling caused by Nrf2 in NOX1 expressing adenocarcinoma cells.

HIF-1α was induced in both continuous and intermittent hypoxia, whereas Nrf2 was induced only in intermittent hypoxia but not in continuous hypoxic exposure (Figure 25B). The Nrf2 target Trx1 that is known to induce HIF-1α was regulated accordingly (Figure 25B). This suggests that Nrf2 may enhance HIF-1α accumulation by Trx1 in the progressive hypoxic stages (2h) of intermittent hypoxia (IH6) to a similar extent as HIF-1α accumulation occurring after 6h of continuous hypoxia (H6). The observation that HIF-1α is induced both in IH6 and H6 whereas Nrf2 and Trx1 are induced only in IH6 suggests that different mechanisms are involved in HIF-1α induction. The contribution of different relevant mechanisms to HIF-1α induction may depend on the specific

conditions. These mechanisms include the control of HIF-1α degradation by PHD, HIF-1α transactivation by FIH [250], degree of HIF-1α synthesis (e.g. translational control by mTOR) [160], posttranslational modifications of HIF-1α (e.g. phosphorylation [204], [251]) and regulation of the redox state of HIF-1α by Trx1 and Ref1 [161], [123]. Thus, we suggest that Trx1 plays a critical role in HIF-1α induction in intermittent hypoxia whereas other mechanisms dominate under conditions of continuous hypoxia.

The total cellular ROS levels were elevated to a similar extent after IH6 and H6 (Figure 26A). However, specific NOX1-derived ROS were most significantly increased after intermittent hypoxic exposure but not after continuous hypoxic exposure (Figure 26C). Overall, this observation reflects that other ROS sources beside NOX1 contribute to the total cellular ROS levels to a higher extent in continuous hypoxia (H6) than in intermittent hypoxia (IH6). Furthermore, it was striking that the NOX1-derived ROS levels matched the regulatory pattern of Nrf2 and Trx1 being most strongly up-regulated in IH6 (Figure 25B). This NOX1-derived ROS increase was likely caused by increased NOX1 protein expression due to increased NOX1 mRNA levels (Figure 25B, C). Accordingly, also A549 cells overexpressing NOX1 displayed significantly increased ROS level (Figure 27D).

The mechanisms of endogenous NOX1 mRNA and protein up-regulation in intermittent hypoxia are unclear. Several transcription factors regulating NOX1 have been identified [57], [53], however the relevance of these factors for NOX1 expression in the conditions investigated in our study is not clear. In addition, increased ROS generation by a NOX1-containing NADPH oxidase may be caused at the regulatory level of other participating NADPH oxidase subunits or by posttranslational modifications resulting in the activation of the NADPH oxidase complex. Such mechanisms have been described for NOX1 [252], [253], [23].

5.2.2.2 Regulation Nrf2 and Trx1 expression by NOX1

Nrf2 induction at the protein level was dependent on NOX1 as shown by overexpression and inhibition of NOX1 (Figure 27A, B, D). Accordingly, the Nrf2 target gene Trx1 was regulated by NOX1 (Figure 28A, B, C) at the transcriptional level (Figure 22B) as

demonstrated by inhibition and overexpression of NOX1 (Figure 22D). Thus, in this study a link between NOX1 and Nrf2 dependent gene expression was explored as a new observation.

Interestingly, the dependence of Nrf2 and Trx1 on NOX1 was most strongly pronounced in intermittent hypoxia, as demonstrated by inhibition of NOX1 (Figure 29) which indicated that an elevation of Nrf2 and Trx1 protein levels was caused by induction of endogenous NOX1 under these conditions. On the other hand, an induction of NOX1 is probably not the only mechanism regulating Nrf2 protein expression, since exposure of cells to continuous long term hypoxia (H24) led to an NOX1 up-regulation without concomitant Nrf2 induction (Figure 22A and 24A). This may suggest the presence of additional mechanism(s) activated during intermittent hypoxia that are involved in Nrf2 stabilization or on the presence of additional mechanism(s) that are involved in Nrf2 destabilization in continuous long term hypoxia. Nevertheless, NOX1 appears to be one of the essential factors stimulating Nrf2 activity during intermittent hypoxia.

Accordingly, NOX1 inhibition by DPI (i.e. NADPH oxidase inhibitor) led to a decrease of Nrf2 protein level (Figure 27A, B) and NOX1 overexpression increased Nrf2 protein abundance (Figure 21D). These results strongly indicate a dependence of Nrf2 on NOX1-derived ROS. The NOX1-dependent Nrf2 induction appeared to be mediated by the redox-dependent interaction of Keap1 with Nrf2, controlling its proteasomal degradation, since Nrf2 protein down-regulation after si-NOX1 treatment was prevented by a proteasome inhibitor (Figure 21C). Of note is that Keap1 is mutated in A549 cells. Thus, the interaction between Nrf2 and Keap1 and subsequent proteasomal degradation of Nrf2 are diminished [185]. Howerver, it has been demonstrated that Nrf2 is induced by H_2O_2 and that the Nrf2 target gene peroxiredoxin 6 is induced by siRNA ablation of Keap1 in A549 cells [254]. Thus Keap1 plays a significant role for the redox-dependent Nrf2 turnover in A549 cells.

5.2.2.3 Trx1 mediated regulation of HIF-1α by Nrf2 in NOX1-dependent manner

In our experiments, Nrf2 ablation caused a decrease of Trx1 expression (Figure 28A). This is in accordance with other studies that described the ARE-dependent regulation of

Trx1 by Nrf2 [187], [186]. The inhibition of Nrf2 caused pronounced reduction in HIF-1α levels in intermittent hypoxia. Also, the inhibition of Trx1 and NOX1 attenuated HIF-1α, and these effects were pronounced in intermittent rather than continuous hypoxic exposure (Figure 30A, B).

The sequence of signaling events leading to the enhancement of HIF-1α expression in intermittent hypoxic exposure is suggested from an experiment where overexpression of NOX1 and Trx1 was combined with the down-regulation of Trx1 and NOX1 expression by siRNA (Figure 31A, B). This experiment is based on the suggestion that NOX1 is the initial player (regulating Trx1 expression), and Trx1 the final player in exerting effects on HIF-1α in intermittent hypoxic exposure with Nrf2 as the crucial factor linking NOX1 with Trx1. Accordingly, the inhibition of Trx1 in NOX1-overexpressing cells abolished the induction of HIF-1α, whereas inhibition of NOX1 in Trx1-overexpressing cells had no inhibitory effect on HIF-1α expression. It is also important to say that based on our results, other mechanisms of a cross-talk between NOX1 and Trx1 influencing HIF-1α activity cannot be excluded. For example, ROS generated by NOX1 may affect the redox-state and thus the function of Trx1.

In this regard, also Trx1-dependent HIF-1α induction was demonstrated to be redox state dependent. This is likely based on the Trx1-mediated redox state regulation of cysteine residues within the transactivation domain of HIF-1α that consequently is critical for the binding of transcription factor coactivators, such as CBP/p300, to this domain [161]. Another study demonstrated that Trx1 overexpression led to an increased phosphorylation of translation activators 4E-BP1 and p70S6K, two well-known targets of mTOR [196]. This could result in an increase of HIF-1α synthesis. Our results showed that overexpression of Trx1 in both continuous and intermittent hypoxia induces HIF-1α to a similar extent (Figure 30C, D). This suggests that Trx1 is able to induce HIF-1α both in continuous and in intermittent hypoxia. However, HIF-1α induction by endogenous Trx1 is predominantly relevant in intermittent hypoxia since Trx1 is up-regulated only in this situation. This aspect is noteworthy regarding the occurrence of cancer drug resistance in hypoxic tumor areas, since several anticancer drugs are activators of Nrf2

[168], [181], [255], connecting this cytoprotective transcription factor by its target Trx1 with HIF-1α.

An interesting question is, whether NOX1 induces HIF-1α only through the Nrf2-Trx1 pathway. In fact, this pathway seems to be relevant in our conditions of intermittent hypoxia that proceeded over several hours rather than minutes. The effects of ROS on HIF-1α are complex and are dependent on the source, type and kinetic of generation of ROS. In our work, we have observed a significant elevation of NOX1-dependent ROS levels after tens of hours of continuous hypoxia. Thus it is unlike that NOX1 derived ROS would be involved in signaling pathways leading to rapid HIF-1α activation. Nevertheless, additional mechanisms of HIF-1α induction by NOX1 both in intermittent and continuous hypoxia cannot be excluded.

In sum, we identified a signal transduction pathway that causes the enhancement of HIF-1α by Nrf2 in response to the studied pattern of intermittent hypoxia. In particular, this mechanism is relevant in adenocarcinoma cells expressing NOX1. ROS production by NOX1 was demonstrated to induce Nrf2 and Trx1 resulting in enhancement of HIF-1α induction. As a consequence, NOX1-expressing tumors may favor therapy resistance by increasing Nrf2 and HIF-1α in a tumor microenvironment exposed to conditions of intermittent hypoxia. Thus, therapeutic approaches for targeting of NOX1, Nrf2 and Trx1 may be valid to eliminate therapy-resistant cancer cells.

6. Summary

NADPH oxidase 1 and 4 are ROS generating enzyme complexes that play an important role in cellular signaling. The core subunits of NADPH oxidase 1 and 4 are NOX1 and NOX4, respectively.

The immuno-detection of NOX1 and NOX4 proteins is a commonly faced problem. Protein bands of different molecular weights suggested to represent NOX1 and NOX4 have been described in previous studies. These bands could represent, for example, different NOX splice variants, posttranslational modifications, proteolytic products or non-specifically immunoreacting proteins. Thus, well validated NOX1 and NOX4 antibodies are critical for further functional and structural characterization of these proteins. Based on this, the aims of the first part of the work were: 1. To test and to select most suitable antibodies for the detection of NOX1 and NOX4 in human adenocarcinoma A549, CaCo2 cells and HUVEC, 2. To determine the subcellular localization of NOX1 and NOX4, 3. To identify putative NOX1 and NOX4 proteins by mass spectroscopic (MS) analysis.

Employing several commercially available and custom made NOX1 and NOX4 antibodies it was obvious that neither of the antibodies detected any common band. Further, by employing specific siRNAs, custom made antibodies termed NOX1wch and NOX4jh were identified as suitable for NOX1 and NOX4 detection. Using these antibodies we also determined the presence of NOX1 and NOX4 in certain subcellular fractions. The results showed that both NOX1 and NOX4 were predominantly localized in the cytoskeleton fraction of A549 cells. This observation was partially in contrast to previous studies demonstrating the presence of endogenous NOX1 in the membrane fraction of different cell types including those that we used.

In addition to proteins of the predicted size, the NOX1wch and NOX4jh antibodies also detected other protein species of lower or higher molecular weight. To identify these additional bands and to confirm the identity of NOX1 and NOX4 full length proteins, purification and MALDI-TOF MS analysis was performed. However, neither of the analysed proteins were identified as NOX-related which does not mean that this is not the

case. This might be explained, for example, by low abundance of NOX1 and NOX4 proteins, or by technical limits of the protein purification and identification procedure.
Furthermore, we determined that NOX1 predominates in ROS generation in comparison to NOX4 in A549 cells which was in accordance with a higher expression level of NOX1 mRNA than NOX4 mRNA in A549 cells.
In conclusion, this part of the work identified NOX1 and NOX4 antibodies that are suitable for the detection of NOX1 and NOX4 by Western blot. These antibodies were employed for the detection of NOX1 and NOX4 proteins in certain biochemical fractions representing different subcellular compartments. Furthermore, the open attempt for the purification and identification of NOX1 and NOX4 proteins was performed, and these results may be considered as the basis for further proteomic experiments.

NADPH oxidase 1 is a significant source of ROS in A549 cells. ROS are involved in the regulation of the transcription factors HIF-1 and Nrf2. Trx1 represents a target gene of Nrf2 that is known to induce HIF-1α. Intermittent hypoxia occurs in different pathophysiological conditions and is characterized by fluctuations of oxygen and ROS levels with impact on both HIF-1 and Nrf2.
In this context, the aims of this part of the study were: 1. To analyse the expression of NOX1, HIF-1α , Nrf2 and Trx1 under different conditions of oxygenation in A549 cells, 2. To analyse possible cross-talk(s) between these components, particularly under conditions of intermittent hypoxia.
Initial experiments revealed, that whereas HIF-1α was up-regulated both in continuous and intermittent hypoxias, the Nrf2, Trx1 and NOX1 as well as NOX1-derived ROS were only up-regulated in intermittent hypoxia. NOX1 was determined as crucial for enhanced ROS production in intermittent hypoxia that in turn mediated induction of Nrf2 and Trx1. The regulation of Nrf2 and Trx1 by NOX1 was confirmed by both inhibition of endogenous NOX1 and overexpression of recombinant NOX1 protein. Employing a proteosomal inhibitor, NOX1 was demonstrated to activate Nrf2 at the level of protein stability. Subsequently, Nrf2-dependent Trx1 induction turned out to enhance HIF-1α signaling in intermittent hypoxia.

In sum, we identified a signal transduction pathway that causes the enhancement of HIF-1α mediated by NOX1, Nrf2 and Trx1 in response to intermittent hypoxia.

7. Zusammenfassung

NADPH Oxidase 1 und 4 sind ROS generierende Enzymkomplexe mit einer wichtigen Funktion in der Signaltransduktion. Die wesentlichen Untereinheiten sind NOX1 und NOX4.

Die Immunodetektion von NOX1 und NOX4 ist problematisch. Proteinbanden mit verschiedenem Molekulargewicht wurden beschrieben. Diese Banden könnten verschiedene Splicevarianten, posttranslationale Modifikationen, proteolytische Spaltprodukte oder unspezifische Proteine darstellen. Daher sind gut validierte NOX1 und NOX4 Antikörper wesentlich für weitere funktionelle und strukturelle Untersuchungen von NOX1 und NOX4. Darauf basierend waren die Ziele des ersten Teils der Arbeit 1. Verschiedene Antikörper für NOX1 und NOX4 zu testen und möglichst geeignete Antikörper für den Nachweis von NOX1 und NOX4 in humanen Adenokarzinom- und HUVEC Zellen auszuwählen, 2. Die subzelluläre Lokalisation von NOX1 und NOX4 zu identifizieren, 3. Mögliche NOX1 und NOX4 Proteine durch Massenspektroskopie zu identifizieren

Unter Einsatz verschiedener kommerziell erhältlicher und *custom made* NOX1 und NOX4 Antikörper war es offensichtlich, dass mit keiner der verwendeten Antikörper übereinstimmende Banden detektiert wurden. Basierend auf der spezifischen Inhibition von NOX1 und NOX4 mit siRNA wurde ein NOX1 Antikörper (NOX1wch) und ein NOX4 Antikörper (NOX4jh) als geeignet für den Nachweis von NOX1 und NOX4 identifiziert. Mit diesen Antikörpern wurden NOX1 und NOX4 in verschiedenen subzellulären Fraktionen detektiert und analysiert. Dabei zeigte sich, dass sowohl NOX1 als auch NOX4 vorwiegend in Fraktionen des Zytoskeletts enthalten war. Diese Beobachtung steht teilweise im Kontrast zu Studien, die das Vorhandensein von NOX1 und NOX4 in den Membranfraktionen verschiedener Zelltypen (die von uns benutzten eingeschlossen) fanden.

Außerdem wurden mit den Antikörpern NOX1wch und NOX4jh andere Proteinspezies mit abweichenden Molekulargewichten detektiert. Diese Proteine und die mit erwartetem Molekulargewicht wurden nach verschiedenen Aufreinigungsschritten mit MALDI-TOF MS analysiert. Jedoch konnte keiner dieser Proteinbanden als NOX Protein identifiziert werden, was jedoch nicht heißt, dass es sich nicht um NOX Proteine handelt. Dies kann durch das geringe Vorkommen von NOX1 und NOX4 oder durch die Grenzen der verwendeten Proteinaufreinigung und Identifizierung bedingt sein.
Außerdem wurde in der Studie aufgezeigt, dass NOX1 im Vergleich zu NOX4 die wesentliche ROS Quelle in A549 Zellen darstellt, was im Einklang mit den erhöhten mRNA Spiegeln von NOX1 im Vergleich zu NOX4 ist.
Zusammenfassend wurden in diesem Teil der Arbeit Antikörper gegen NOX1 und NOX4 identifiziert, die geeignet sind für den Nachweis von NOX1 und NOX4 im Western Blot. Diese Antikörper wurden dazu genutzt, um NOX1 und NOX4 Proteine in biochemischen Fraktionen, die verschiedene subzelluläre Kompartimente repräsentieren nachzuweisen. Außerdem wurde der noch offene Versuch der Aufreinigung und Identifizierung von NOX1 und NOX4 Proteinen durchgeführt, dessen Ergebnisse, die Grundlage für weitergehende Experimente in diese Richtung darstellen.

NADPH Oxidase 1 ist eine signifikante Quelle von ROS in A549 Zellen. ROS sind an der Regulation der Transkriptionsfaktoren HIF-1 und Nrf2 beteiligt. Trx1 repräsentiert ein Zielgen von Nrf2, das bekanntermaßen HIF-1 induziert. Der zyklische Wechsel von Normoxie und Hypoxie (*intermittent hypoxia*) kommt unter verschiedenen pathophysiologischen Bedingungen vor und ist durch Fluktuationen der Sauerstoff und ROS Spiegel mit Einfluss auf HIF-1 und Nrf2 gekennzeichnet. In diesem Zusammenhang waren die Ziele dieses Teils der Arbeit: 1. Die Expression von NOX1, HIF-1α , Nrf2 and Trx1 unter verschiedenen Oxygenierungsbedingungen in A549 Zellen zu analysieren, 2. Eine mögliche Interaktion dieser Komponenten insbesondere in *intermittent hypoxia* zu untersuchen. Es zeigte sich, dass HIF-1α sowohl nach andauernder Hypoxie als auch nach *intermittent hypoxia* hoch reguliert war während Nrf2, Trx1, NOX1 und NOX1-abgeleitete ROS nur nach *intermittent hypoxia* hoch reguliert waren. NOX1 erwies sich dabei als entscheidend für die erhöhte ROS Generierung in *intermittent hypoxia*, die

nachfolgend für die Induktion von Nrf2 und Trx1 relevant war. Die Regulation von Nrf2 und NOX1 wurde bestätigt durch die Inhibition von endogenem NOX1 und die Überexpression von rekombinantem NOX1. Durch Verwendung eines Proteasom Inhibitors konnte gezeigt werden, dass NOX1 Nrf2 auf der Ebene der Proteinstabilität induziert. Nachfolgend, verstärkt die Nrf2-abhängige Induktion von Trx1 die HIF-1α Antwort in *intermittent hypoxia*.

Zusammenfassend wurde ein Signaltransduktionsweg aufgezeigt, der die HIF-1α Antwort in NOX1-, Nrf2- und Trx1-abhängiger Weise unter Bedingungen von *intermittent hypoxia* verstärkt.

8. References

[1] Cheng, G.; Cao, Z.; Xu, X.; van Meir, E. G.; Lambeth, J. D. Homologs of gp91phox: cloning and tissue expression of Nox3, Nox4, and Nox5. *Gene* **269:**131-140; 2001.
[2] De Deken, X.; Wang, D.; Many, M. C.; Costagliola, S.; Libert, F.; Vassart, G.; Dumont, J. E.; Miot, F. Cloning of two human thyroid cDNAs encoding new members of the NADPH oxidase family. *J Biol Chem* **275:**23227-23233; 2000.
[3] De Deken, X.; Wang, D.; Dumont, J. E.; Miot, F. Characterization of ThOX proteins as components of the thyroid H(2)O(2)-generating system. *Exp Cell Res* **273:**187-196; 2002.
[4] Lambeth, J. D. NOX enzymes and the biology of reactive oxygen. *Nat Rev Immunol* **4:**181-189; 2004.
[5] Bedard, K.; Krause, K. H. The NOX family of ROS-generating NADPH oxidases: physiology and pathophysiology. *Physiol Rev* **87:**245-313; 2007.
[6] Vignais, P. V. The superoxide-generating NADPH oxidase: structural aspects and activation mechanism. *Cell Mol Life Sci* **59:**1428-1459; 2002.
[7] Han, C. H.; Nisimoto, Y.; Lee, S. H.; Kim, E. T.; Lambeth, J. D. Characterization of the flavoprotein domain of gp91phox which has NADPH diaphorase activity. *J Biochem* **129:**513-520; 2001.
[8] Pessach, I.; Levy, R. The NADPH oxidase diaphorase activity in permeabilized human neutrophils and granulocytic like PLB-985 cells. *Adv Exp Med Biol* **479:**107-114; 2000.
[9] Maturana, A.; Krause, K. H.; Demaurex, N. NOX family NADPH oxidases: do they have built-in proton channels? *J Gen Physiol* **120:**781-786; 2002.
[10] Banfi, B.; Schrenzel, J.; Nusse, O.; Lew, D. P.; Ligeti, E.; Krause, K. H.; Demaurex, N. A novel H(+) conductance in eosinophils: unique characteristics and absence in chronic granulomatous disease. *J Exp Med* **190:**183-194; 1999.
[11] Mankelow, T. J.; Henderson, L. M. Proton conduction through full-length gp91phox requires histidine 115. *Protoplasma* **221:**101-108; 2003.
[12] Geiszt, M.; Lekstrom, K.; Leto, T. L. Analysis of mRNA transcripts from the NAD(P)H oxidase 1 (Nox1) gene. Evidence against production of the NADPH oxidase homolog-1 short (NOH-1S) transcript variant. *J Biol Chem* **279:**51661-51668; 2004.
[13] Lambeth, J. D.; Kawahara, T.; Diebold, B. Regulation of Nox and Duox enzymatic activity and expression. *Free Radic Biol Med* **43:**319-331; 2007.
[14] Chamulitrat, W.; Huber, A.; Riedel, H. D.; Stremmel, W. Nox1 induces differentiation resistance in immortalized human keratinocytes generating cells that express simple epithelial keratins. *J Invest Dermatol* **127:**2171-2183; 2007.
[15] Dikalova, A.; Clempus, R.; Lassegue, B.; Cheng, G.; McCoy, J.; Dikalov, S.; San Martin, A.; Lyle, A.; Weber, D. S.; Weiss, D.; Taylor, W. R.; Schmidt, H. H.; Owens, G. K.; Lambeth, J. D.; Griendling, K. K. Nox1 overexpression potentiates angiotensin II-induced hypertension and vascular smooth muscle hypertrophy in transgenic mice. *Circulation* **112:**2668-2676; 2005.
[16] Arnold, R. S.; He, J.; Remo, A.; Ritsick, D.; Yin-Goen, Q.; Lambeth, J. D.; Datta, M. W.; Young, A. N.; Petros, J. A. Nox1 expression determines cellular reactive oxygen

and modulates c-fos-induced growth factor, interleukin-8, and Cav-1. *Am J Pathol* **171:**2021-2032; 2007.
[17] Kim, Y. S.; Morgan, M. J.; Choksi, S.; Liu, Z. G. TNF-induced activation of the Nox1 NADPH oxidase and its role in the induction of necrotic cell death. *Mol Cell* **26:**675-687; 2007.
[18] Hilenski, L. L.; Clempus, R. E.; Quinn, M. T.; Lambeth, J. D.; Griendling, K. K. Distinct subcellular localizations of Nox1 and Nox4 in vascular smooth muscle cells. *Arterioscler Thromb Vasc Biol* **24:**677-683; 2004.
[19] Cui, X. L.; Brockman, D.; Campos, B.; Myatt, L. Expression of NADPH oxidase isoform 1 (Nox1) in human placenta: involvement in preeclampsia. *Placenta* **27:**422-431; 2006.
[20] Lavrentyev, E. N.; Malik, K. U. High glucose-induced Nox1-derived superoxides downregulate PKC-betaII, which subsequently decreases ACE2 expression and ANG(1-7) formation in rat VSMCs. *Am J Physiol Heart Circ Physiol* **296:**H106-118; 2009.
[21] Helmcke, I.; Heumuller, S.; Tikkanen, R.; Schroder, K.; Brandes, R. P. Identification of structural elements in Nox1 and Nox4 controlling localization and activity. *Antioxid Redox Signal* **11:**1279-1287; 2009.
[22] Chen, W.; Shang, W. H.; Adachi, Y.; Hirose, K.; Ferrari, D. M.; Kamata, T. A possible biochemical link between NADPH oxidase (Nox) 1 redox-signalling and ERp72. *Biochem J* **416:**55-63; 2008.
[23] Cheng, G.; Lambeth, J. D. NOXO1, regulation of lipid binding, localization, and activation of Nox1 by the Phox homology (PX) domain. *J Biol Chem* **279:**4737-4742; 2004.
[24] Ueyama, T.; Geiszt, M.; Leto, T. L. Involvement of Rac1 in activation of multicomponent Nox1- and Nox3-based NADPH oxidases. *Mol Cell Biol* **26:**2160-2174; 2006.
[25] Ambasta, R. K.; Kumar, P.; Griendling, K. K.; Schmidt, H. H.; Busse, R.; Brandes, R. P. Direct interaction of the novel Nox proteins with p22phox is required for the formation of a functionally active NADPH oxidase. *J Biol Chem* **279:**45935-45941; 2004.
[26] Hanna, I. R.; Hilenski, L. L.; Dikalova, A.; Taniyama, Y.; Dikalov, S.; Lyle, A.; Quinn, M. T.; Lassegue, B.; Griendling, K. K. Functional association of nox1 with p22phox in vascular smooth muscle cells. *Free Radic Biol Med* **37:**1542-1549; 2004.
[27] Nisimoto, Y.; Tsubouchi, R.; Diebold, B. A.; Qiao, S.; Ogawa, H.; Ohara, T.; Tamura, M. Activation of NADPH oxidase 1 in tumour colon epithelial cells. *Biochem J* **415:**57-65; 2008.
[28] Gianni, D.; Diaz, B.; Taulet, N.; Fowler, B.; Courtneidge, S. A.; Bokoch, G. M. Novel p47(phox)-related organizers regulate localized NADPH oxidase 1 (Nox1) activity. *Sci Signal* **2:**ra54; 2009.
[29] Chamulitrat, W.; Schmidt, R.; Tomakidi, P.; Stremmel, W.; Chunglok, W.; Kawahara, T.; Rokutan, K. Association of gp91phox homolog Nox1 with anchorage-independent growth and MAP kinase-activation of transformed human keratinocytes. *Oncogene* **22:**6045-6053; 2003.
[30] Desouki, M. M.; Kulawiec, M.; Bansal, S.; Das, G. M.; Singh, K. K. Cross talk between mitochondria and superoxide generating NADPH oxidase in breast and ovarian tumors. *Cancer Biol Ther* **4:**1367-1373; 2005.

[31] Szanto, I.; Rubbia-Brandt, L.; Kiss, P.; Steger, K.; Banfi, B.; Kovari, E.; Herrmann, F.; Hadengue, A.; Krause, K. H. Expression of NOX1, a superoxide-generating NADPH oxidase, in colon cancer and inflammatory bowel disease. *J Pathol* **207:**164-176; 2005.
[32] Suh, Y. A.; Arnold, R. S.; Lassegue, B.; Shi, J.; Xu, X.; Sorescu, D.; Chung, A. B.; Griendling, K. K.; Lambeth, J. D. Cell transformation by the superoxide-generating oxidase Mox1. *Nature* **401:**79-82; 1999.
[33] Banfi, B.; Clark, R. A.; Steger, K.; Krause, K. H. Two novel proteins activate superoxide generation by the NADPH oxidase NOX1. *J Biol Chem* **278:**3510-3513; 2003.
[34] Arnold, R. S.; Shi, J.; Murad, E.; Whalen, A. M.; Sun, C. Q.; Polavarapu, R.; Parthasarathy, S.; Petros, J. A.; Lambeth, J. D. Hydrogen peroxide mediates the cell growth and transformation caused by the mitogenic oxidase Nox1. *Proc Natl Acad Sci U S A* **98:**5550-5555; 2001.
[35] Mitsushita, J.; Lambeth, J. D.; Kamata, T. The superoxide-generating oxidase Nox1 is functionally required for Ras oncogene transformation. *Cancer Res* **64:**3580-3585; 2004.
[36] Komatsu, D.; Kato, M.; Nakayama, J.; Miyagawa, S.; Kamata, T. NADPH oxidase 1 plays a critical mediating role in oncogenic Ras-induced vascular endothelial growth factor expression. *Oncogene* **27:**4724-4732; 2008.
[37] Kamata, T. Roles of Nox1 and other Nox isoforms in cancer development. *Cancer Sci* **100:**1382-1388; 2009.
[38] Kanterewicz, B. I.; Knapp, L. T.; Klann, E. Stimulation of p42 and p44 mitogen-activated protein kinases by reactive oxygen species and nitric oxide in hippocampus. *J Neurochem* **70:**1009-1016; 1998.
[39] Schafer, M.; Schafer, C.; Ewald, N.; Piper, H. M.; Noll, T. Role of redox signaling in the autonomous proliferative response of endothelial cells to hypoxia. *Circ Res* **92:**1010-1015; 2003.
[40] Wang, Y.; Zeigler, M. M.; Lam, G. K.; Hunter, M. G.; Eubank, T. D.; Khramtsov, V. V.; Tridandapani, S.; Sen, C. K.; Marsh, C. B. The role of the NADPH oxidase complex, p38 MAPK, and Akt in regulating human monocyte/macrophage survival. *Am J Respir Cell Mol Biol* **36:**68-77; 2007.
[41] Kulisz, A.; Chen, N.; Chandel, N. S.; Shao, Z.; Schumacker, P. T. Mitochondrial ROS initiate phosphorylation of p38 MAP kinase during hypoxia in cardiomyocytes. *Am J Physiol Lung Cell Mol Physiol* **282:**L1324-1329; 2002.
[42] Lauzier, M. C.; Page, E. L.; Michaud, M. D.; Richard, D. E. Differential regulation of hypoxia-inducible factor-1 through receptor tyrosine kinase transactivation in vascular smooth muscle cells. *Endocrinology* **148:**4023-4031; 2007.
[43] Nakajima, H.; Takenaka, M.; Kaimori, J. Y.; Hamano, T.; Iwatani, H.; Sugaya, T.; Ito, T.; Hori, M.; Imai, E. Activation of the signal transducer and activator of transcription signaling pathway in renal proximal tubular cells by albumin. *J Am Soc Nephrol* **15:**276-285; 2004.
[44] Arbiser, J. L.; Petros, J.; Klafter, R.; Govindajaran, B.; McLaughlin, E. R.; Brown, L. F.; Cohen, C.; Moses, M.; Kilroy, S.; Arnold, R. S.; Lambeth, J. D. Reactive oxygen generated by Nox1 triggers the angiogenic switch. *Proc Natl Acad Sci U S A* **99:**715-720; 2002.

[45] Esposito, F.; Chirico, G.; Montesano Gesualdi, N.; Posadas, I.; Ammendola, R.; Russo, T.; Cirino, G.; Cimino, F. Protein kinase B activation by reactive oxygen species is independent of tyrosine kinase receptor phosphorylation and requires SRC activity. *J Biol Chem* **278:**20828-20834; 2003.
[46] Bogeski, I.; Bozem, M.; Sternfeld, L.; Hofer, H. W.; Schulz, I. Inhibition of protein tyrosine phosphatase 1B by reactive oxygen species leads to maintenance of Ca2+ influx following store depletion in HEK 293 cells. *Cell Calcium* **40:**1-10; 2006.
[47] Brar, S. S.; Kennedy, T. P.; Quinn, M.; Hoidal, J. R. Redox signaling of NF-kappaB by membrane NAD(P)H oxidases in normal and malignant cells. *Protoplasma* **221:**117-127; 2003.
[48] Chandel, N. S.; Trzyna, W. C.; McClintock, D. S.; Schumacker, P. T. Role of oxidants in NF-kappa B activation and TNF-alpha gene transcription induced by hypoxia and endotoxin. *J Immunol* **165:**1013-1021; 2000.
[49] Dodd, S. L.; Gagnon, B. J.; Senf, S. M.; Hain, B. A.; Judge, A. R. Ros-mediated activation of NF-kappaB and Foxo during muscle disuse. *Muscle Nerve*; 2009.
[50] Wu, S.; Gao, J.; Ohlemeyer, C.; Roos, D.; Niessen, H.; Kottgen, E.; Gessner, R. Activation of AP-1 through reactive oxygen species by angiotensin II in rat cardiomyocytes. *Free Radic Biol Med* **39:**1601-1610; 2005.
[51] Fan, C. Y.; Katsuyama, M.; Yabe-Nishimura, C. PKCdelta mediates up-regulation of NOX1, a catalytic subunit of NADPH oxidase, via transactivation of the EGF receptor: possible involvement of PKCdelta in vascular hypertrophy. *Biochem J* **390:**761-767; 2005.
[52] Fan, C.; Katsuyama, M.; Nishinaka, T.; Yabe-Nishimura, C. Transactivation of the EGF receptor and a PI3 kinase-ATF-1 pathway is involved in the upregulation of NOX1, a catalytic subunit of NADPH oxidase. *FEBS Lett* **579:**1301-1305; 2005.
[53] Katsuyama, M.; Fan, C.; Arakawa, N.; Nishinaka, T.; Miyagishi, M.; Taira, K.; Yabe-Nishimura, C. Essential role of ATF-1 in induction of NOX1, a catalytic subunit of NADPH oxidase: involvement of mitochondrial respiratory chain. *Biochem J* **386:**255-261; 2005.
[54] Park, H. S.; Lee, S. H.; Park, D.; Lee, J. S.; Ryu, S. H.; Lee, W. J.; Rhee, S. G.; Bae, Y. S. Sequential activation of phosphatidylinositol 3-kinase, beta Pix, Rac1, and Nox1 in growth factor-induced production of H2O2. *Mol Cell Biol* **24:**4384-4394; 2004.
[55] Lassegue, B.; Sorescu, D.; Szocs, K.; Yin, Q.; Akers, M.; Zhang, Y.; Grant, S. L.; Lambeth, J. D.; Griendling, K. K. Novel gp91(phox) homologues in vascular smooth muscle cells : nox1 mediates angiotensin II-induced superoxide formation and redox-sensitive signaling pathways. *Circ Res* **88:**888-894; 2001.
[56] Mollnau, H.; Wendt, M.; Szocs, K.; Lassegue, B.; Schulz, E.; Oelze, M.; Li, H.; Bodenschatz, M.; August, M.; Kleschyov, A. L.; Tsilimingas, N.; Walter, U.; Forstermann, U.; Meinertz, T.; Griendling, K.; Munzel, T. Effects of angiotensin II infusion on the expression and function of NAD(P)H oxidase and components of nitric oxide/cGMP signaling. *Circ Res* **90:**E58-65; 2002.
[57] Adachi, Y.; Shibai, Y.; Mitsushita, J.; Shang, W. H.; Hirose, K.; Kamata, T. Oncogenic Ras upregulates NADPH oxidase 1 gene expression through MEK-ERK-dependent phosphorylation of GATA-6. *Oncogene* **27:**4921-4932; 2008.
[58] Geiszt, M.; Kopp, J. B.; Varnai, P.; Leto, T. L. Identification of renox, an NAD(P)H oxidase in kidney. *Proc Natl Acad Sci U S A* **97:**8010-8014; 2000.

[59] Goyal, P.; Weissmann, N.; Rose, F.; Grimminger, F.; Schafers, H. J.; Seeger, W.; Hanze, J. Identification of novel Nox4 splice variants with impact on ROS levels in A549 cells. *Biochem Biophys Res Commun* **329:**32-39; 2005.
[60] Shiose, A.; Kuroda, J.; Tsuruya, K.; Hirai, M.; Hirakata, H.; Naito, S.; Hattori, M.; Sakaki, Y.; Sumimoto, H. A novel superoxide-producing NAD(P)H oxidase in kidney. *J Biol Chem* **276:**1417-1423; 2001.
[61] Hwang, J.; Kleinhenz, D. J.; Lassegue, B.; Griendling, K. K.; Dikalov, S.; Hart, C. M. Peroxisome proliferator-activated receptor-gamma ligands regulate endothelial membrane superoxide production. *Am J Physiol Cell Physiol* **288:**C899-905; 2005.
[62] Sturrock, A.; Huecksteadt, T. P.; Norman, K.; Sanders, K.; Murphy, T. M.; Chitano, P.; Wilson, K.; Hoidal, J. R.; Kennedy, T. P. Nox4 mediates TGF-beta1-induced retinoblastoma protein phosphorylation, proliferation, and hypertrophy in human airway smooth muscle cells. *Am J Physiol Lung Cell Mol Physiol* **292:**L1543-1555; 2007.
[63] Gupte, S. A.; Kaminski, P. M.; Floyd, B.; Agarwal, R.; Ali, N.; Ahmad, M.; Edwards, J.; Wolin, M. S. Cytosolic NADPH may regulate differences in basal Nox oxidase-derived superoxide generation in bovine coronary and pulmonary arteries. *Am J Physiol Heart Circ Physiol* **288:**H13-21; 2005.
[64] Lyle, A. N.; Deshpande, N. N.; Taniyama, Y.; Seidel-Rogol, B.; Pounkova, L.; Du, P.; Papaharalambus, C.; Lassegue, B.; Griendling, K. K. Poldip2, a novel regulator of Nox4 and cytoskeletal integrity in vascular smooth muscle cells. *Circ Res* **105:**249-259; 2009.
[65] Kuroda, J.; Nakagawa, K.; Yamasaki, T.; Nakamura, K.; Takeya, R.; Kuribayashi, F.; Imajoh-Ohmi, S.; Igarashi, K.; Shibata, Y.; Sueishi, K.; Sumimoto, H. The superoxide-producing NAD(P)H oxidase Nox4 in the nucleus of human vascular endothelial cells. *Genes Cells* **10:**1139-1151; 2005.
[66] Clempus, R. E.; Sorescu, D.; Dikalova, A. E.; Pounkova, L.; Jo, P.; Sorescu, G. P.; Schmidt, H. H.; Lassegue, B.; Griendling, K. K. Nox4 is required for maintenance of the differentiated vascular smooth muscle cell phenotype. *Arterioscler Thromb Vasc Biol* **27:**42-48; 2007.
[67] Martyn, K. D.; Frederick, L. M.; von Loehneysen, K.; Dinauer, M. C.; Knaus, U. G. Functional analysis of Nox4 reveals unique characteristics compared to other NADPH oxidases. *Cell Signal* **18:**69-82; 2006.
[68] Lee, Y. M.; Kim, B. J.; Chun, Y. S.; So, I.; Choi, H.; Kim, M. S.; Park, J. W. NOX4 as an oxygen sensor to regulate TASK-1 activity. *Cell Signal* **18:**499-507; 2006.
[69] Deliri, H.; McNamara, C. A. Nox 4 regulation of vascular smooth muscle cell differentiation marker gene expression. *Arterioscler Thromb Vasc Biol* **27:**12-14; 2007.
[70] Schroder, K.; Wandzioch, K.; Helmcke, I.; Brandes, R. P. Nox4 acts as a switch between differentiation and proliferation in preadipocytes. *Arterioscler Thromb Vasc Biol* **29:**239-245; 2009.
[71] Ismail, S.; Sturrock, A.; Wu, P.; Cahill, B.; Norman, K.; Huecksteadt, T.; Sanders, K.; Kennedy, T.; Hoidal, J. NOX4 mediates hypoxia-induced proliferation of human pulmonary artery smooth muscle cells: the role of autocrine production of transforming growth factor-{beta}1 and insulin-like growth factor binding protein-3. *Am J Physiol Lung Cell Mol Physiol* **296:**L489-499; 2009.

[72] Basuroy, S.; Bhattacharya, S.; Leffler, C. W.; Parfenova, H. Nox4 NADPH oxidase mediates oxidative stress and apoptosis caused by TNF-alpha in cerebral vascular endothelial cells. *Am J Physiol Cell Physiol* **296:**C422-432; 2009.
[73] Carmona-Cuenca, I.; Roncero, C.; Sancho, P.; Caja, L.; Fausto, N.; Fernandez, M.; Fabregat, I. Upregulation of the NADPH oxidase NOX4 by TGF-beta in hepatocytes is required for its pro-apoptotic activity. *J Hepatol* **49:**965-976; 2008.
[74] Hu, T.; Ramachandrarao, S. P.; Siva, S.; Valancius, C.; Zhu, Y.; Mahadev, K.; Toh, I.; Goldstein, B. J.; Woolkalis, M.; Sharma, K. Reactive oxygen species production via NADPH oxidase mediates TGF-beta-induced cytoskeletal alterations in endothelial cells. *Am J Physiol Renal Physiol* **289:**F816-825; 2005.
[75] Block, K.; Eid, A.; Griendling, K. K.; Lee, D. Y.; Wittrant, Y.; Gorin, Y. Nox4 NAD(P)H oxidase mediates Src-dependent tyrosine phosphorylation of PDK-1 in response to angiotensin II: role in mesangial cell hypertrophy and fibronectin expression. *J Biol Chem* **283:**24061-24076; 2008.
[76] Gozin, A.; Franzini, E.; Andrieu, V.; Da Costa, L.; Rollet-Labelle, E.; Pasquier, C. Reactive oxygen species activate focal adhesion kinase, paxillin and p130cas tyrosine phosphorylation in endothelial cells. *Free Radic Biol Med* **25:**1021-1032; 1998.
[77] DeLeo, F. R.; Burritt, J. B.; Yu, L.; Jesaitis, A. J.; Dinauer, M. C.; Nauseef, W. M. Processing and maturation of flavocytochrome b558 include incorporation of heme as a prerequisite for heterodimer assembly. *J Biol Chem* **275:**13986-13993; 2000.
[78] Zhu, Y.; Marchal, C. C.; Casbon, A. J.; Stull, N.; von Lohneysen, K.; Knaus, U. G.; Jesaitis, A. J.; McCormick, S.; Nauseef, W. M.; Dinauer, M. C. Deletion mutagenesis of p22phox subunit of flavocytochrome b558: identification of regions critical for gp91phox maturation and NADPH oxidase activity. *J Biol Chem* **281:**30336-30346; 2006.
[79] Dahan, I.; Issaeva, I.; Gorzalczany, Y.; Sigal, N.; Hirshberg, M.; Pick, E. Mapping of functional domains in the p22(phox) subunit of flavocytochrome b(559) participating in the assembly of the NADPH oxidase complex by "peptide walking". *J Biol Chem* **277:**8421-8432; 2002.
[80] Leto, T. L.; Adams, A. G.; de Mendez, I. Assembly of the phagocyte NADPH oxidase: binding of Src homology 3 domains to proline-rich targets. *Proc Natl Acad Sci U S A* **91:**10650-10654; 1994.
[81] Yu, L.; Quinn, M. T.; Cross, A. R.; Dinauer, M. C. Gp91(phox) is the heme binding subunit of the superoxide-generating NADPH oxidase. *Proc Natl Acad Sci U S A* **95:**7993-7998; 1998.
[82] Kawahara, T.; Ritsick, D.; Cheng, G.; Lambeth, J. D. Point mutations in the proline-rich region of p22phox are dominant inhibitors of Nox1- and Nox2-dependent reactive oxygen generation. *J Biol Chem* **280:**31859-31869; 2005.
[83] Bey, E. A.; Xu, B.; Bhattacharjee, A.; Oldfield, C. M.; Zhao, X.; Li, Q.; Subbulakshmi, V.; Feldman, G. M.; Wientjes, F. B.; Cathcart, M. K. Protein kinase C delta is required for p47phox phosphorylation and translocation in activated human monocytes. *J Immunol* **173:**5730-5738; 2004.
[84] Huang, J.; Kleinberg, M. E. Activation of the phagocyte NADPH oxidase protein p47(phox). Phosphorylation controls SH3 domain-dependent binding to p22(phox). *J Biol Chem* **274:**19731-19737; 1999.

[85] Takeya, R.; Ueno, N.; Kami, K.; Taura, M.; Kohjima, M.; Izaki, T.; Nunoi, H.; Sumimoto, H. Novel human homologues of p47phox and p67phox participate in activation of superoxide-producing NADPH oxidases. *J Biol Chem* **278:**25234-25246; 2003.
[86] Lapouge, K.; Smith, S. J.; Walker, P. A.; Gamblin, S. J.; Smerdon, S. J.; Rittinger, K. Structure of the TPR domain of p67phox in complex with Rac.GTP. *Mol Cell* **6:**899-907; 2000.
[87] Rinckel, L. A.; Faris, S. L.; Hitt, N. D.; Kleinberg, M. E. Rac1 disrupts p67phox/p40phox binding: a novel role for Rac in NADPH oxidase activation. *Biochem Biophys Res Commun* **263:**118-122; 1999.
[88] de Mendez, I.; Adams, A. G.; Sokolic, R. A.; Malech, H. L.; Leto, T. L. Multiple SH3 domain interactions regulate NADPH oxidase assembly in whole cells. *EMBO J* **15:**1211-1220; 1996.
[89] de Mendez, I.; Homayounpour, N.; Leto, T. L. Specificity of p47phox SH3 domain interactions in NADPH oxidase assembly and activation. *Mol Cell Biol* **17:**2177-2185; 1997.
[90] Han, C. H.; Freeman, J. L.; Lee, T.; Motalebi, S. A.; Lambeth, J. D. Regulation of the neutrophil respiratory burst oxidase. Identification of an activation domain in p67(phox). *J Biol Chem* **273:**16663-16668; 1998.
[91] Wientjes, F. B.; Panayotou, G.; Reeves, E.; Segal, A. W. Interactions between cytosolic components of the NADPH oxidase: p40phox interacts with both p67phox and p47phox. *Biochem J* **317 (Pt 3):**919-924; 1996.
[92] Bouin, A. P.; Grandvaux, N.; Vignais, P. V.; Fuchs, A. p40(phox) is phosphorylated on threonine 154 and serine 315 during activation of the phagocyte NADPH oxidase. Implication of a protein kinase c-type kinase in the phosphorylation process. *J Biol Chem* **273:**30097-30103; 1998.
[93] Heyworth, P. G.; Knaus, U. G.; Settleman, J.; Curnutte, J. T.; Bokoch, G. M. Regulation of NADPH oxidase activity by Rac GTPase activating protein(s). *Mol Biol Cell* **4:**1217-1223; 1993.
[94] Diekmann, D.; Abo, A.; Johnston, C.; Segal, A. W.; Hall, A. Interaction of Rac with p67phox and regulation of phagocytic NADPH oxidase activity. *Science* **265:**531-533; 1994.
[95] Miyano, K.; Ueno, N.; Takeya, R.; Sumimoto, H. Direct involvement of the small GTPase Rac in activation of the superoxide-producing NADPH oxidase Nox1. *J Biol Chem* **281:**21857-21868; 2006.
[96] Tsunawaki, S.; Kagara, S.; Yoshikawa, K.; Yoshida, L. S.; Kuratsuji, T.; Namiki, H. Involvement of p40phox in activation of phagocyte NADPH oxidase through association of its carboxyl-terminal, but not its amino-terminal, with p67phox. *J Exp Med* **184:**893-902; 1996.
[97] Valko, M.; Rhodes, C. J.; Moncol, J.; Izakovic, M.; Mazur, M. Free radicals, metals and antioxidants in oxidative stress-induced cancer. *Chem Biol Interact* **160:**1-40; 2006.
[98] Novo, E.; Parola, M. Redox mechanisms in hepatic chronic wound healing and fibrogenesis. *Fibrogenesis Tissue Repair* **1:**5; 2008.

[99] Valko, M.; Leibfritz, D.; Moncol, J.; Cronin, M. T.; Mazur, M.; Telser, J. Free radicals and antioxidants in normal physiological functions and human disease. *Int J Biochem Cell Biol* **39:**44-84; 2007.
[100] Droge, W. Free radicals in the physiological control of cell function. *Physiol Rev* **82:**47-95; 2002.
[101] Nordberg, J.; Arner, E. S. Reactive oxygen species, antioxidants, and the mammalian thioredoxin system. *Free Radic Biol Med* **31:**1287-1312; 2001.
[102] Thannickal, V. J.; Fanburg, B. L. Reactive oxygen species in cell signaling. *Am J Physiol Lung Cell Mol Physiol* **279:**L1005-1028; 2000.
[103] Turrens, J. F. Mitochondrial formation of reactive oxygen species. *J Physiol* **552:**335-344; 2003.
[104] Jankov, R. P.; Kantores, C.; Pan, J.; Belik, J. Contribution of xanthine oxidase-derived superoxide to chronic hypoxic pulmonary hypertension in neonatal rats. *Am J Physiol Lung Cell Mol Physiol* **294:**L233-245; 2008.
[105] Meunier, B.; de Visser, S. P.; Shaik, S. Mechanism of oxidation reactions catalyzed by cytochrome p450 enzymes. *Chem Rev* **104:**3947-3980; 2004.
[106] Zuo, L.; Christofi, F. L.; Wright, V. P.; Bao, S.; Clanton, T. L. Lipoxygenase-dependent superoxide release in skeletal muscle. *J Appl Physiol* **97:**661-668; 2004.
[107] Tu, B. P.; Weissman, J. S. Oxidative protein folding in eukaryotes: mechanisms and consequences. *J Cell Biol* **164:**341-346; 2004.
[108] Chu, R.; Lin, Y.; Reddy, K. C.; Pan, J.; Rao, M. S.; Reddy, J. K.; Yeldandi, A. V. Transformation of epithelial cells stably transfected with H2O2-generating peroxisomal urate oxidase. *Cancer Res* **56:**4846-4852; 1996.
[109] Ruoppolo, M.; Lundstrom-Ljung, J.; Talamo, F.; Pucci, P.; Marino, G. Effect of glutaredoxin and protein disulfide isomerase on the glutathione-dependent folding of ribonuclease A. *Biochemistry* **36:**12259-12267; 1997.
[110] Xie, Y.; Kole, S.; Precht, P.; Pazin, M. J.; Bernier, M. S-glutathionylation impairs signal transducer and activator of transcription 3 activation and signaling. *Endocrinology* **150:**1122-1131; 2009.
[111] Klatt, P.; Molina, E. P.; Lamas, S. Nitric oxide inhibits c-Jun DNA binding by specifically targeted S-glutathionylation. *J Biol Chem* **274:**15857-15864; 1999.
[112] Reynaert, N. L.; van der Vliet, A.; Guala, A. S.; McGovern, T.; Hristova, M.; Pantano, C.; Heintz, N. H.; Heim, J.; Ho, Y. S.; Matthews, D. E.; Wouters, E. F.; Janssen-Heininger, Y. M. Dynamic redox control of NF-kappaB through glutaredoxin-regulated S-glutathionylation of inhibitory kappaB kinase beta. *Proc Natl Acad Sci U S A* **103:**13086-13091; 2006.
[113] Saitoh, M.; Nishitoh, H.; Fujii, M.; Takeda, K.; Tobiume, K.; Sawada, Y.; Kawabata, M.; Miyazono, K.; Ichijo, H. Mammalian thioredoxin is a direct inhibitor of apoptosis signal-regulating kinase (ASK) 1. *EMBO J* **17:**2596-2606; 1998.
[114] Malik, G.; Gorbounov, N.; Das, S.; Gurusamy, N.; Otani, H.; Maulik, N.; Goswami, S.; Das, D. K. Ischemic preconditioning triggers nuclear translocation of thioredoxin and its interaction with Ref-1 potentiating a survival signal through the PI-3-kinase-Akt pathway. *Antioxid Redox Signal* **8:**2101-2109; 2006.
[115] Gurusamy, N.; Malik, G.; Gorbunov, N. V.; Das, D. K. Redox activation of Ref-1 potentiates cell survival following myocardial ischemia reperfusion injury. *Free Radic Biol Med* **43:**397-407; 2007.

[116] Welsh, S. J.; Bellamy, W. T.; Briehl, M. M.; Powis, G. The redox protein thioredoxin-1 (Trx-1) increases hypoxia-inducible factor 1alpha protein expression: Trx-1 overexpression results in increased vascular endothelial growth factor production and enhanced tumor angiogenesis. *Cancer Res* **62:**5089-5095; 2002.
[117] Hayashi, T.; Ueno, Y.; Okamoto, T. Oxidoreductive regulation of nuclear factor kappa B. Involvement of a cellular reducing catalyst thioredoxin. *J Biol Chem* **268:**11380-11388; 1993.
[118] Hirota, K.; Matsui, M.; Iwata, S.; Nishiyama, A.; Mori, K.; Yodoi, J. AP-1 transcriptional activity is regulated by a direct association between thioredoxin and Ref-1. *Proc Natl Acad Sci U S A* **94:**3633-3638; 1997.
[119] Karimpour, S.; Lou, J.; Lin, L. L.; Rene, L. M.; Lagunas, L.; Ma, X.; Karra, S.; Bradbury, C. M.; Markovina, S.; Goswami, P. C.; Spitz, D. R.; Hirota, K.; Kalvakolanu, D. V.; Yodoi, J.; Gius, D. Thioredoxin reductase regulates AP-1 activity as well as thioredoxin nuclear localization via active cysteines in response to ionizing radiation. *Oncogene* **21:**6317-6327; 2002.
[120] Xie, S.; Wang, Q.; Wu, H.; Cogswell, J.; Lu, L.; Jhanwar-Uniyal, M.; Dai, W. Reactive oxygen species-induced phosphorylation of p53 on serine 20 is mediated in part by polo-like kinase-3. *J Biol Chem* **276:**36194-36199; 2001.
[121] Polyak, K.; Xia, Y.; Zweier, J. L.; Kinzler, K. W.; Vogelstein, B. A model for p53-induced apoptosis. *Nature* **389:**300-305; 1997.
[122] Macip, S.; Igarashi, M.; Berggren, P.; Yu, J.; Lee, S. W.; Aaronson, S. A. Influence of induced reactive oxygen species in p53-mediated cell fate decisions. *Mol Cell Biol* **23:**8576-8585; 2003.
[123] Huang, L. E.; Arany, Z.; Livingston, D. M.; Bunn, H. F. Activation of hypoxia-inducible transcription factor depends primarily upon redox-sensitive stabilization of its alpha subunit. *J Biol Chem* **271:**32253-32259; 1996.
[124] Matsuzawa, A.; Saegusa, K.; Noguchi, T.; Sadamitsu, C.; Nishitoh, H.; Nagai, S.; Koyasu, S.; Matsumoto, K.; Takeda, K.; Ichijo, H. ROS-dependent activation of the TRAF6-ASK1-p38 pathway is selectively required for TLR4-mediated innate immunity. *Nat Immunol* **6:**587-592; 2005.
[125] Smith, D. P.; Ciccotosto, G. D.; Tew, D. J.; Fodero-Tavoletti, M. T.; Johanssen, T.; Masters, C. L.; Barnham, K. J.; Cappai, R. Concentration dependent Cu2+ induced aggregation and dityrosine formation of the Alzheimer's disease amyloid-beta peptide. *Biochemistry* **46:**2881-2891; 2007.
[126] Iwai, K.; Drake, S. K.; Wehr, N. B.; Weissman, A. M.; LaVaute, T.; Minato, N.; Klausner, R. D.; Levine, R. L.; Rouault, T. A. Iron-dependent oxidation, ubiquitination, and degradation of iron regulatory protein 2: implications for degradation of oxidized proteins. *Proc Natl Acad Sci U S A* **95:**4924-4928; 1998.
[127] Hanze, J.; Weissmann, N.; Grimminger, F.; Seeger, W.; Rose, F. Cellular and molecular mechanisms of hypoxia-inducible factor driven vascular remodeling. *Thromb Haemost* **97:**774-787; 2007.
[128] Kaelin, W. G., Jr.; Ratcliffe, P. J. Oxygen sensing by metazoans: the central role of the HIF hydroxylase pathway. *Mol Cell* **30:**393-402; 2008.
[129] Semenza, G. L.; Koury, S. T.; Nejfelt, M. K.; Gearhart, J. D.; Antonarakis, S. E. Cell-type-specific and hypoxia-inducible expression of the human erythropoietin gene in transgenic mice. *Proc Natl Acad Sci U S A* **88:**8725-8729; 1991.

[130] Semenza, G. L.; Nejfelt, M. K.; Chi, S. M.; Antonarakis, S. E. Hypoxia-inducible nuclear factors bind to an enhancer element located 3' to the human erythropoietin gene. *Proc Natl Acad Sci U S A* **88:**5680-5684; 1991.
[131] Wang, G. L.; Semenza, G. L. Characterization of hypoxia-inducible factor 1 and regulation of DNA binding activity by hypoxia. *J Biol Chem* **268:**21513-21518; 1993.
[132] Wang, G. L.; Semenza, G. L. General involvement of hypoxia-inducible factor 1 in transcriptional response to hypoxia. *Proc Natl Acad Sci U S A* **90:**4304-4308; 1993.
[133] Wenger, R. H.; Stiehl, D. P.; Camenisch, G. Integration of oxygen signaling at the consensus HRE. *Sci STKE* **2005:**re12; 2005.
[134] Wang, G. L.; Jiang, B. H.; Rue, E. A.; Semenza, G. L. Hypoxia-inducible factor 1 is a basic-helix-loop-helix-PAS heterodimer regulated by cellular O2 tension. *Proc Natl Acad Sci U S A* **92:**5510-5514; 1995.
[135] Wang, G. L.; Semenza, G. L. Purification and characterization of hypoxia-inducible factor 1. *J Biol Chem* **270:**1230-1237; 1995.
[136] Ema, M.; Taya, S.; Yokotani, N.; Sogawa, K.; Matsuda, Y.; Fujii-Kuriyama, Y. A novel bHLH-PAS factor with close sequence similarity to hypoxia-inducible factor 1alpha regulates the VEGF expression and is potentially involved in lung and vascular development. *Proc Natl Acad Sci U S A* **94:**4273-4278; 1997.
[137] Gu, Y. Z.; Moran, S. M.; Hogenesch, J. B.; Wartman, L.; Bradfield, C. A. Molecular characterization and chromosomal localization of a third alpha-class hypoxia inducible factor subunit, HIF3alpha. *Gene Expr* **7:**205-213; 1998.
[138] Hirose, K.; Morita, M.; Ema, M.; Mimura, J.; Hamada, H.; Fujii, H.; Saijo, Y.; Gotoh, O.; Sogawa, K.; Fujii-Kuriyama, Y. cDNA cloning and tissue-specific expression of a novel basic helix-loop-helix/PAS factor (Arnt2) with close sequence similarity to the aryl hydrocarbon receptor nuclear translocator (Arnt). *Mol Cell Biol* **16:**1706-1713; 1996.
[139] Takahata, S.; Sogawa, K.; Kobayashi, A.; Ema, M.; Mimura, J.; Ozaki, N.; Fujii-Kuriyama, Y. Transcriptionally active heterodimer formation of an Arnt-like PAS protein, Arnt3, with HIF-1a, HLF, and clock. *Biochem Biophys Res Commun* **248:**789-794; 1998.
[140] Wenger, R. H. Cellular adaptation to hypoxia: O2-sensing protein hydroxylases, hypoxia-inducible transcription factors, and O2-regulated gene expression. *Faseb J* **16:**1151-1162; 2002.
[141] Epstein, A. C.; Gleadle, J. M.; McNeill, L. A.; Hewitson, K. S.; O'Rourke, J.; Mole, D. R.; Mukherji, M.; Metzen, E.; Wilson, M. I.; Dhanda, A.; Tian, Y. M.; Masson, N.; Hamilton, D. L.; Jaakkola, P.; Barstead, R.; Hodgkin, J.; Maxwell, P. H.; Pugh, C. W.; Schofield, C. J.; Ratcliffe, P. J. C. elegans EGL-9 and mammalian homologs define a family of dioxygenases that regulate HIF by prolyl hydroxylation. *Cell* **107:**43-54; 2001.
[142] Huang, J.; Zhao, Q.; Mooney, S. M.; Lee, F. S. Sequence determinants in hypoxia-inducible factor-1alpha for hydroxylation by the prolyl hydroxylases PHD1, PHD2, and PHD3. *J Biol Chem* **277:**39792-39800; 2002.
[143] Maxwell, P. H.; Wiesener, M. S.; Chang, G. W.; Clifford, S. C.; Vaux, E. C.; Cockman, M. E.; Wykoff, C. C.; Pugh, C. W.; Maher, E. R.; Ratcliffe, P. J. The tumour suppressor protein VHL targets hypoxia-inducible factors for oxygen-dependent proteolysis. *Nature* **399:**271-275; 1999.

[144] Paltoglou, S.; Roberts, B. J. HIF-1alpha and EPAS ubiquitination mediated by the VHL tumour suppressor involves flexibility in the ubiquitination mechanism, similar to other RING E3 ligases. *Oncogene*; 2006.
[145] Jewell, U. R.; Kvietikova, I.; Scheid, A.; Bauer, C.; Wenger, R. H.; Gassmann, M. Induction of HIF-1alpha in response to hypoxia is instantaneous. *Faseb J* **15:**1312-1314; 2001.
[146] Berra, E.; Benizri, E.; Ginouves, A.; Volmat, V.; Roux, D.; Pouyssegur, J. HIF prolyl-hydroxylase 2 is the key oxygen sensor setting low steady-state levels of HIF-1alpha in normoxia. *Embo J* **22:**4082-4090; 2003.
[147] Lando, D.; Peet, D. J.; Gorman, J. J.; Whelan, D. A.; Whitelaw, M. L.; Bruick, R. K. FIH-1 is an asparaginyl hydroxylase enzyme that regulates the transcriptional activity of hypoxia-inducible factor. *Genes Dev* **16:**1466-1471; 2002.
[148] Hitchon, C. A.; El-Gabalawy, H. S. Oxidation in rheumatoid arthritis. *Arthritis Res Ther* **6:**265-278; 2004.
[149] Kietzmann, T.; Gorlach, A. Reactive oxygen species in the control of hypoxia-inducible factor-mediated gene expression. *Semin Cell Dev Biol* **16:**474-486; 2005.
[150] Chandel, N. S.; Maltepe, E.; Goldwasser, E.; Mathieu, C. E.; Simon, M. C.; Schumacker, P. T. Mitochondrial reactive oxygen species trigger hypoxia-induced transcription. *Proc Natl Acad Sci U S A* **95:**11715-11720; 1998.
[151] Chandel, N. S.; McClintock, D. S.; Feliciano, C. E.; Wood, T. M.; Melendez, J. A.; Rodriguez, A. M.; Schumacker, P. T. Reactive oxygen species generated at mitochondrial complex III stabilize hypoxia-inducible factor-1alpha during hypoxia: a mechanism of O2 sensing. *J Biol Chem* **275:**25130-25138; 2000.
[152] Emerling, B. M.; Platanias, L. C.; Black, E.; Nebreda, A. R.; Davis, R. J.; Chandel, N. S. Mitochondrial reactive oxygen species activation of p38 mitogen-activated protein kinase is required for hypoxia signaling. *Mol Cell Biol* **25:**4853-4862; 2005.
[153] Gerald, D.; Berra, E.; Frapart, Y. M.; Chan, D. A.; Giaccia, A. J.; Mansuy, D.; Pouyssegur, J.; Yaniv, M.; Mechta-Grigoriou, F. JunD reduces tumor angiogenesis by protecting cells from oxidative stress. *Cell* **118:**781-794; 2004.
[154] Liu, Q.; Berchner-Pfannschmidt, U.; Moller, U.; Brecht, M.; Wotzlaw, C.; Acker, H.; Jungermann, K.; Kietzmann, T. A Fenton reaction at the endoplasmic reticulum is involved in the redox control of hypoxia-inducible gene expression. *Proc Natl Acad Sci U S A* **101:**4302-4307; 2004.
[155] Goyal, P.; Weissmann, N.; Grimminger, F.; Hegel, C.; Bader, L.; Rose, F.; Fink, L.; Ghofrani, H. A.; Schermuly, R. T.; Schmidt, H. H.; Seeger, W.; Hanze, J. Upregulation of NAD(P)H oxidase 1 in hypoxia activates hypoxia-inducible factor 1 via increase in reactive oxygen species. *Free Radic Biol Med* **36:**1279-1288; 2004.
[156] Gorlach, A.; Berchner-Pfannschmidt, U.; Wotzlaw, C.; Cool, R. H.; Fandrey, J.; Acker, H.; Jungermann, K.; Kietzmann, T. Reactive oxygen species modulate HIF-1 mediated PAI-1 expression: involvement of the GTPase Rac1. *Thromb Haemost* **89:**926-935; 2003.
[157] Hirota, K.; Semenza, G. L. Rac1 activity is required for the activation of hypoxia-inducible factor 1. *J Biol Chem* **276:**21166-21172; 2001.

[158] Maranchie, J. K.; Zhan, Y. Nox4 is critical for hypoxia-inducible factor 2-alpha transcriptional activity in von Hippel-Lindau-deficient renal cell carcinoma. *Cancer Res* **65:**9190-9193; 2005.
[159] Richard, D. E.; Berra, E.; Pouyssegur, J. Nonhypoxic pathway mediates the induction of hypoxia-inducible factor 1alpha in vascular smooth muscle cells. *J Biol Chem* **275:**26765-26771; 2000.
[160] Page, E. L.; Robitaille, G. A.; Pouyssegur, J.; Richard, D. E. Induction of hypoxia-inducible factor-1alpha by transcriptional and translational mechanisms. *J Biol Chem* **277:**48403-48409; 2002.
[161] Ema, M.; Hirota, K.; Mimura, J.; Abe, H.; Yodoi, J.; Sogawa, K.; Poellinger, L.; Fujii-Kuriyama, Y. Molecular mechanisms of transcription activation by HLF and HIF1alpha in response to hypoxia: their stabilization and redox signal-induced interaction with CBP/p300. *Embo J* **18:**1905-1914; 1999.
[162] Kim, W. J.; Cho, H.; Lee, S. W.; Kim, Y. J.; Kim, K. W. Antisense-thioredoxin inhibits angiogenesis via pVHL-mediated hypoxia-inducible factor-1alpha degradation. *Int J Oncol* **26:**1049-1052; 2005.
[163] Kobayashi, M.; Yamamoto, M. Nrf2-Keap1 regulation of cellular defense mechanisms against electrophiles and reactive oxygen species. *Adv Enzyme Regul* **46:**113-140; 2006.
[164] Osburn, W. O.; Kensler, T. W. Nrf2 signaling: an adaptive response pathway for protection against environmental toxic insults. *Mutat Res* **659:**31-39; 2008.
[165] Itoh, K.; Wakabayashi, N.; Katoh, Y.; Ishii, T.; Igarashi, K.; Engel, J. D.; Yamamoto, M. Keap1 represses nuclear activation of antioxidant responsive elements by Nrf2 through binding to the amino-terminal Neh2 domain. *Genes Dev* **13:**76-86; 1999.
[166] Kobayashi, A.; Kang, M. I.; Watai, Y.; Tong, K. I.; Shibata, T.; Uchida, K.; Yamamoto, M. Oxidative and electrophilic stresses activate Nrf2 through inhibition of ubiquitination activity of Keap1. *Mol Cell Biol* **26:**221-229; 2006.
[167] McMahon, M.; Thomas, N.; Itoh, K.; Yamamoto, M.; Hayes, J. D. Dimerization of substrate adaptors can facilitate cullin-mediated ubiquitylation of proteins by a "tethering" mechanism: a two-site interaction model for the Nrf2-Keap1 complex. *J Biol Chem* **281:**24756-24768; 2006.
[168] Eggler, A. L.; Small, E.; Hannink, M.; Mesecar, A. D. Cul3-mediated Nrf2 ubiquitination and antioxidant response element (ARE) activation are dependent on the partial molar volume at position 151 of Keap1. *Biochem J* **422:**171-180; 2009.
[169] Kang, M. I.; Kobayashi, A.; Wakabayashi, N.; Kim, S. G.; Yamamoto, M. Scaffolding of Keap1 to the actin cytoskeleton controls the function of Nrf2 as key regulator of cytoprotective phase 2 genes. *Proc Natl Acad Sci U S A* **101:**2046-2051; 2004.
[170] McMahon, M.; Thomas, N.; Itoh, K.; Yamamoto, M.; Hayes, J. D. Redox-regulated turnover of Nrf2 is determined by at least two separate protein domains, the redox-sensitive Neh2 degron and the redox-insensitive Neh6 degron. *J Biol Chem* **279:**31556-31567; 2004.
[171] Huang, H. C.; Nguyen, T.; Pickett, C. B. Phosphorylation of Nrf2 at Ser-40 by protein kinase C regulates antioxidant response element-mediated transcription. *J Biol Chem* **277:**42769-42774; 2002.

[172] Huang, H. C.; Nguyen, T.; Pickett, C. B. Regulation of the antioxidant response element by protein kinase C-mediated phosphorylation of NF-E2-related factor 2. *Proc Natl Acad Sci U S A* **97:**12475-12480; 2000.
[173] Li, W.; Jain, M. R.; Chen, C.; Yue, X.; Hebbar, V.; Zhou, R.; Kong, A. N. Nrf2 Possesses a redox-insensitive nuclear export signal overlapping with the leucine zipper motif. *J Biol Chem* **280:**28430-28438; 2005.
[174] Motohashi, H.; Katsuoka, F.; Engel, J. D.; Yamamoto, M. Small Maf proteins serve as transcriptional cofactors for keratinocyte differentiation in the Keap1-Nrf2 regulatory pathway. *Proc Natl Acad Sci U S A* **101:**6379-6384; 2004.
[175] Kimura, M.; Yamamoto, T.; Zhang, J.; Itoh, K.; Kyo, M.; Kamiya, T.; Aburatani, H.; Katsuoka, F.; Kurokawa, H.; Tanaka, T.; Motohashi, H.; Yamamoto, M. Molecular basis distinguishing the DNA binding profile of Nrf2-Maf heterodimer from that of Maf homodimer. *J Biol Chem* **282:**33681-33690; 2007.
[176] Katsuoka, F.; Motohashi, H.; Ishii, T.; Aburatani, H.; Engel, J. D.; Yamamoto, M. Genetic evidence that small maf proteins are essential for the activation of antioxidant response element-dependent genes. *Mol Cell Biol* **25:**8044-8051; 2005.
[177] Venugopal, R.; Jaiswal, A. K. Nrf2 and Nrf1 in association with Jun proteins regulate antioxidant response element-mediated expression and coordinated induction of genes encoding detoxifying enzymes. *Oncogene* **17:**3145-3156; 1998.
[178] Zhang, Y.; Gordon, G. B. A strategy for cancer prevention: stimulation of the Nrf2-ARE signaling pathway. *Mol Cancer Ther* **3:**885-893; 2004.
[179] Pearson, K. J.; Lewis, K. N.; Price, N. L.; Chang, J. W.; Perez, E.; Cascajo, M. V.; Tamashiro, K. L.; Poosala, S.; Csiszar, A.; Ungvari, Z.; Kensler, T. W.; Yamamoto, M.; Egan, J. M.; Longo, D. L.; Ingram, D. K.; Navas, P.; de Cabo, R. Nrf2 mediates cancer protection but not prolongevity induced by caloric restriction. *Proc Natl Acad Sci U S A* **105:**2325-2330; 2008.
[180] Ramos-Gomez, M.; Dolan, P. M.; Itoh, K.; Yamamoto, M.; Kensler, T. W. Interactive effects of nrf2 genotype and oltipraz on benzo[a]pyrene-DNA adducts and tumor yield in mice. *Carcinogenesis* **24:**461-467; 2003.
[181] Fahey, J. W.; Haristoy, X.; Dolan, P. M.; Kensler, T. W.; Scholtus, I.; Stephenson, K. K.; Talalay, P.; Lozniewski, A. Sulforaphane inhibits extracellular, intracellular, and antibiotic-resistant strains of Helicobacter pylori and prevents benzo[a]pyrene-induced stomach tumors. *Proc Natl Acad Sci U S A* **99:**7610-7615; 2002.
[182] Wang, X. J.; Sun, Z.; Villeneuve, N. F.; Zhang, S.; Zhao, F.; Li, Y.; Chen, W.; Yi, X.; Zheng, W.; Wondrak, G. T.; Wong, P. K.; Zhang, D. D. Nrf2 enhances resistance of cancer cells to chemotherapeutic drugs, the dark side of Nrf2. *Carcinogenesis* **29:**1235-1243; 2008.
[183] Shibata, T.; Ohta, T.; Tong, K. I.; Kokubu, A.; Odogawa, R.; Tsuta, K.; Asamura, H.; Yamamoto, M.; Hirohashi, S. Cancer related mutations in NRF2 impair its recognition by Keap1-Cul3 E3 ligase and promote malignancy. *Proc Natl Acad Sci U S A* **105:**13568-13573; 2008.
[184] Ohta, T.; Iijima, K.; Miyamoto, M.; Nakahara, I.; Tanaka, H.; Ohtsuji, M.; Suzuki, T.; Kobayashi, A.; Yokota, J.; Sakiyama, T.; Shibata, T.; Yamamoto, M.; Hirohashi, S. Loss of Keap1 function activates Nrf2 and provides advantages for lung cancer cell growth. *Cancer Res* **68:**1303-1309; 2008.

[185] Singh, A.; Misra, V.; Thimmulappa, R. K.; Lee, H.; Ames, S.; Hoque, M. O.; Herman, J. G.; Baylin, S. B.; Sidransky, D.; Gabrielson, E.; Brock, M. V.; Biswal, S. Dysfunctional KEAP1-NRF2 interaction in non-small-cell lung cancer. *PLoS Med* **3:**e420; 2006.
[186] Tanito, M.; Agbaga, M. P.; Anderson, R. E. Upregulation of thioredoxin system via Nrf2-antioxidant responsive element pathway in adaptive-retinal neuroprotection in vivo and in vitro. *Free Radic Biol Med* **42:**1838-1850; 2007.
[187] Kim, Y. C.; Masutani, H.; Yamaguchi, Y.; Itoh, K.; Yamamoto, M.; Yodoi, J. Hemin-induced activation of the thioredoxin gene by Nrf2. A differential regulation of the antioxidant responsive element by a switch of its binding factors. *J Biol Chem* **276:**18399-18406; 2001.
[188] Qi, Y.; Grishin, N. V. Structural classification of thioredoxin-like fold proteins. *Proteins* **58:**376-388; 2005.
[189] Arner, E. S.; Holmgren, A. Physiological functions of thioredoxin and thioredoxin reductase. *Eur J Biochem* **267:**6102-6109; 2000.
[190] Spyrou, G.; Enmark, E.; Miranda-Vizuete, A.; Gustafsson, J. Cloning and expression of a novel mammalian thioredoxin. *J Biol Chem* **272:**2936-2941; 1997.
[191] Holmgren, A. Bovine thioredoxin system. Purification of thioredoxin reductase from calf liver and thymus and studies of its function in disulfide reduction. *J Biol Chem* **252:**4600-4606; 1977.
[192] Tamura, T.; Stadtman, T. C. A new selenoprotein from human lung adenocarcinoma cells: purification, properties, and thioredoxin reductase activity. *Proc Natl Acad Sci U S A* **93:**1006-1011; 1996.
[193] Williams, C. H., Jr. Mechanism and structure of thioredoxin reductase from Escherichia coli. *FASEB J* **9:**1267-1276; 1995.
[194] Holmgren, A. Thioredoxin and glutaredoxin systems. *J Biol Chem* **264:**13963-13966; 1989.
[195] Lundstrom, J.; Holmgren, A. Protein disulfide-isomerase is a substrate for thioredoxin reductase and has thioredoxin-like activity. *J Biol Chem* **265:**9114-9120; 1990.
[196] Zhou, J.; Damdimopoulos, A. E.; Spyrou, G.; Brune, B. Thioredoxin 1 and thioredoxin 2 have opposed regulatory functions on hypoxia-inducible factor-1alpha. *J Biol Chem* **282:**7482-7490; 2007.
[197] Vaux, E. C.; Wood, S. M.; Cockman, M. E.; Nicholls, L. G.; Yeates, K. M.; Pugh, C. W.; Maxwell, P. H.; Ratcliffe, P. J. Selection of mutant CHO cells with constitutive activation of the HIF system and inactivation of the von Hippel-Lindau tumor suppressor. *J Biol Chem* **276:**44323-44330; 2001.
[198] Dhakshinamoorthy, S.; Jaiswal, A. K. Functional characterization and role of INrf2 in antioxidant response element-mediated expression and antioxidant induction of NAD(P)H:quinone oxidoreductase1 gene. *Oncogene* **20:**3906-3917; 2001.
[199] Baniulis, D.; Nakano, Y.; Nauseef, W. M.; Banfi, B.; Cheng, G.; Lambeth, D. J.; Burritt, J. B.; Taylor, R. M.; Jesaitis, A. J. Evaluation of two anti-gp91phox antibodies as immunoprobes for Nox family proteins: mAb 54.1 recognizes recombinant full-length Nox2, Nox3 and the C-terminal domains of Nox1-4 and cross-reacts with GRP 58. *Biochim Biophys Acta* **1752:**186-196; 2005.

[200] O'Brien, W. J.; Krema, C.; Heimann, T.; Zhao, H. Expression of NADPH oxidase in rabbit corneal epithelial and stromal cells in culture. *Invest Ophthalmol Vis Sci* **47:**853-863; 2006.
[201] Fang, Q.; Sun, H.; Arrick, D. M.; Mayhan, W. G. Inhibition of NADPH oxidase improves impaired reactivity of pial arterioles during chronic exposure to nicotine. *J Appl Physiol* **100:**631-636; 2006.
[202] Kim, Y. J.; Ahn, J. Y.; Liang, P.; Ip, C.; Zhang, Y.; Park, Y. M. Human prx1 gene is a target of Nrf2 and is up-regulated by hypoxia/reoxygenation: implication to tumor biology. *Cancer Res* **67:**546-554; 2007.
[203] Leonard, M. O.; Kieran, N. E.; Howell, K.; Burne, M. J.; Varadarajan, R.; Dhakshinamoorthy, S.; Porter, A. G.; O'Farrelly, C.; Rabb, H.; Taylor, C. T. Reoxygenation-specific activation of the antioxidant transcription factor Nrf2 mediates cytoprotective gene expression in ischemia-reperfusion injury. *FASEB J* **20:**2624-2626; 2006.
[204] Richard, D. E.; Berra, E.; Gothie, E.; Roux, D.; Pouyssegur, J. p42/p44 mitogen-activated protein kinases phosphorylate hypoxia-inducible factor 1alpha (HIF-1alpha) and enhance the transcriptional activity of HIF-1. *J Biol Chem* **274:**32631-32637; 1999.
[205] Kang, K. W.; Lee, S. J.; Park, J. W.; Kim, S. G. Phosphatidylinositol 3-kinase regulates nuclear translocation of NF-E2-related factor 2 through actin rearrangement in response to oxidative stress. *Mol Pharmacol* **62:**1001-1010; 2002.
[206] Wingler, K.; Wunsch, S.; Kreutz, R.; Rothermund, L.; Paul, M.; Schmidt, H. H. Upregulation of the vascular NAD(P)H-oxidase isoforms Nox1 and Nox4 by the renin-angiotensin system in vitro and in vivo. *Free Radic Biol Med* **31:**1456-1464; 2001.
[207] Kawahara, T.; Kuwano, Y.; Teshima-Kondo, S.; Takeya, R.; Sumimoto, H.; Kishi, K.; Tsunawaki, S.; Hirayama, T.; Rokutan, K. Role of nicotinamide adenine dinucleotide phosphate oxidase 1 in oxidative burst response to Toll-like receptor 5 signaling in large intestinal epithelial cells. *J Immunol* **172:**3051-3058; 2004.
[208] Pleskova, M.; Beck, K. F.; Behrens, M. H.; Huwiler, A.; Fichtlscherer, B.; Wingerter, O.; Brandes, R. P.; Mulsch, A.; Pfeilschifter, J. Nitric oxide down-regulates the expression of the catalytic NADPH oxidase subunit Nox1 in rat renal mesangial cells. *FASEB J* **20:**139-141; 2006.
[209] Kobayashi, S.; Nojima, Y.; Shibuya, M.; Maru, Y. Nox1 regulates apoptosis and potentially stimulates branching morphogenesis in sinusoidal endothelial cells. *Exp Cell Res* **300:**455-462; 2004.
[210] Li, J. M.; Shah, A. M. Intracellular localization and preassembly of the NADPH oxidase complex in cultured endothelial cells. *J Biol Chem* **277:**19952-19960; 2002.
[211] Zhen, L.; Yu, L.; Dinauer, M. C. Probing the role of the carboxyl terminus of the gp91phox subunit of neutrophil flavocytochrome b558 using site-directed mutagenesis. *J Biol Chem* **273:**6575-6581; 1998.
[212] Pessach, I.; Shmelzer, Z.; Leto, T. L.; Dinauer, M. C.; Levy, R. The C-terminal flavin domain of gp91phox bound to plasma membranes of granulocyte-like X-CGD PLB-985 cells is sufficient to anchor cytosolic oxidase components and support NADPH oxidase-associated diaphorase activity independent of cytosolic phospholipase A2 regulation. *J Leukoc Biol* **80:**630-639; 2006.

[213] Rath, A.; Glibowicka, M.; Nadeau, V. G.; Chen, G.; Deber, C. M. Detergent binding explains anomalous SDS-PAGE migration of membrane proteins. *Proc Natl Acad Sci U S A* **106:**1760-1765; 2009.
[214] Yoshida, L. S.; Saruta, F.; Yoshikawa, K.; Tatsuzawa, O.; Tsunawaki, S. Mutation at histidine 338 of gp91(phox) depletes FAD and affects expression of cytochrome b558 of the human NADPH oxidase. *J Biol Chem* **273:**27879-27886; 1998.
[215] Paclet, M. H.; Henderson, L. M.; Campion, Y.; Morel, F.; Dagher, M. C. Localization of Nox2 N-terminus using polyclonal antipeptide antibodies. *Biochem J* **382:**981-986; 2004.
[216] Menshikov, M.; Plekhanova, O.; Cai, H.; Chalupsky, K.; Parfyonova, Y.; Bashtrikov, P.; Tkachuk, V.; Berk, B. C. Urokinase plasminogen activator stimulates vascular smooth muscle cell proliferation via redox-dependent pathways. *Arterioscler Thromb Vasc Biol* **26:**801-807; 2006.
[217] Ateghang, B.; Wartenberg, M.; Gassmann, M.; Sauer, H. Regulation of cardiotrophin-1 expression in mouse embryonic stem cells by HIF-1alpha and intracellular reactive oxygen species. *J Cell Sci* **119:**1043-1052; 2006.
[218] Valencia, A.; Kochevar, I. E. Nox1-based NADPH oxidase is the major source of UVA-induced reactive oxygen species in human keratinocytes. *J Invest Dermatol* **128:**214-222; 2008.
[219] Ambasta, R. K.; Schreiber, J. G.; Janiszewski, M.; Busse, R.; Brandes, R. P. Noxa1 is a central component of the smooth muscle NADPH oxidase in mice. *Free Radic Biol Med* **41:**193-201; 2006.
[220] Burritt, J. B.; Quinn, M. T.; Jutila, M. A.; Bond, C. W.; Jesaitis, A. J. Topological mapping of neutrophil cytochrome b epitopes with phage-display libraries. *J Biol Chem* **270:**16974-16980; 1995.
[221] Davis, A. R.; Mascolo, P. L.; Bunger, P. L.; Sipes, K. M.; Quinn, M. T. Cloning and sequencing of the bovine flavocytochrome b subunit proteins, gp91-phox and p22-phox: comparison with other known flavocytochrome b sequences. *J Leukoc Biol* **64:**114-123; 1998.
[222] Burritt, J. B.; DeLeo, F. R.; McDonald, C. L.; Prigge, J. R.; Dinauer, M. C.; Nakamura, M.; Nauseef, W. M.; Jesaitis, A. J. Phage display epitope mapping of human neutrophil flavocytochrome b558. Identification of two juxtaposed extracellular domains. *J Biol Chem* **276:**2053-2061; 2001.
[223] Vilhardt, F.; van Deurs, B. The phagocyte NADPH oxidase depends on cholesterol-enriched membrane microdomains for assembly. *EMBO J* **23:**739-748; 2004.
[224] Lener, B.; Koziel, R.; Pircher, H.; Hutter, E.; Greussing, R.; Herndler-Brandstetter, D.; Hermann, M.; Unterluggauer, H.; Jansen-Durr, P. The NADPH oxidase Nox4 restricts the replicative lifespan of human endothelial cells. *Biochem J* **423:**363-374; 2009.
[225] Nakano, Y.; Banfi, B.; Jesaitis, A. J.; Dinauer, M. C.; Allen, L. A.; Nauseef, W. M. Critical roles for p22phox in the structural maturation and subcellular targeting of Nox3. *Biochem J* **403:**97-108; 2007.
[226] Ueyama, T.; Lekstrom, K.; Tsujibe, S.; Saito, N.; Leto, T. L. Subcellular localization and function of alternatively spliced Noxo1 isoforms. *Free Radic Biol Med* **42:**180-190; 2007.

[227] Adessi, C.; Miege, C.; Albrieux, C.; Rabilloud, T. Two-dimensional electrophoresis of membrane proteins: a current challenge for immobilized pH gradients. *Electrophoresis* **18:**127-135; 1997.
[228] Dupuy, C.; Ohayon, R.; Valent, A.; Noel-Hudson, M. S.; Deme, D.; Virion, A. Purification of a novel flavoprotein involved in the thyroid NADPH oxidase. Cloning of the porcine and human cdnas. *J Biol Chem* **274:**37265-37269; 1999.
[229] Taylor, R. M.; Burritt, J. B.; Foubert, T. R.; Snodgrass, M. A.; Stone, K. C.; Baniulis, D.; Gripentrog, J. M.; Lord, C.; Jesaitis, A. J. Single-step immunoaffinity purification and characterization of dodecylmaltoside-solubilized human neutrophil flavocytochrome b. *Biochim Biophys Acta* **1612:**65-75; 2003.
[230] Taylor, R. M.; Baniulis, D.; Burritt, J. B.; Gripentrog, J. M.; Lord, C. I.; Riesselman, M. H.; Maaty, W. S.; Bothner, B. P.; Angel, T. E.; Dratz, E. A.; Linton, G. F.; Malech, H. L.; Jesaitis, A. J. Analysis of human phagocyte flavocytochrome b(558) by mass spectrometry. *J Biol Chem* **281:**37045-37056; 2006.
[231] Dikalov, S. I.; Dikalova, A. E.; Bikineyeva, A. T.; Schmidt, H. H.; Harrison, D. G.; Griendling, K. K. Distinct roles of Nox1 and Nox4 in basal and angiotensin II-stimulated superoxide and hydrogen peroxide production. *Free Radic Biol Med* **45:**1340-1351; 2008.
[232] Go, Y. M.; Gipp, J. J.; Mulcahy, R. T.; Jones, D. P. H2O2-dependent activation of GCLC-ARE4 reporter occurs by mitogen-activated protein kinase pathways without oxidation of cellular glutathione or thioredoxin-1. *J Biol Chem* **279:**5837-5845; 2004.
[233] Lim, S. D.; Sun, C.; Lambeth, J. D.; Marshall, F.; Amin, M.; Chung, L.; Petros, J. A.; Arnold, R. S. Increased Nox1 and hydrogen peroxide in prostate cancer. *Prostate* **62:**200-207; 2005.
[234] Chaplin, D. J.; Hill, S. A. Temporal heterogeneity in microregional erythrocyte flux in experimental solid tumours. *Br J Cancer* **71:**1210-1213; 1995.
[235] Dewhirst, M. W.; Braun, R. D.; Lanzen, J. L. Temporal changes in PO2 of R3230AC tumors in Fischer-344 rats. *Int J Radiat Oncol Biol Phys* **42:**723-726; 1998.
[236] Dennis, K. E.; Aschner, J. L.; Milatovic, D.; Schmidt, J. W.; Aschner, M.; Kaplowitz, M. R.; Zhang, Y.; Fike, C. D. NADPH oxidases and reactive oxygen species at different stages of chronic hypoxia-induced pulmonary hypertension in newborn piglets. *Am J Physiol Lung Cell Mol Physiol* **297:**L596-607; 2009.
[237] Rathore, R.; Zheng, Y. M.; Niu, C. F.; Liu, Q. H.; Korde, A.; Ho, Y. S.; Wang, Y. X. Hypoxia activates NADPH oxidase to increase [ROS]i and [Ca2+]i through the mitochondrial ROS-PKCepsilon signaling axis in pulmonary artery smooth muscle cells. *Free Radic Biol Med* **45:**1223-1231; 2008.
[238] Semenza, G. L. Targeting HIF-1 for cancer therapy. *Nat Rev Cancer* **3:**721-732; 2003.
[239] Vaupel, P.; Kallinowski, F.; Okunieff, P. Blood flow, oxygen and nutrient supply, and metabolic microenvironment of human tumors: a review. *Cancer Res* **49:**6449-6465; 1989.
[240] Dewhirst, M. W. Mechanisms underlying hypoxia development in tumors. *Adv Exp Med Biol* **510:**51-56; 2003.
[241] Cardenas-Navia, L. I.; Mace, D.; Richardson, R. A.; Wilson, D. F.; Shan, S.; Dewhirst, M. W. The pervasive presence of fluctuating oxygenation in tumors. *Cancer Res* **68:**5812-5819; 2008.

[242] Bennewith, K. L.; Durand, R. E. Quantifying transient hypoxia in human tumor xenografts by flow cytometry. *Cancer Res* **64:**6183-6189; 2004.
[243] Hill, S. A.; Pigott, K. H.; Saunders, M. I.; Powell, M. E.; Arnold, S.; Obeid, A.; Ward, G.; Leahy, M.; Hoskin, P. J.; Chaplin, D. J. Microregional blood flow in murine and human tumours assessed using laser Doppler microprobes. *Br J Cancer Suppl* **27:**S260-263; 1996.
[244] Pigott, K. H.; Hill, S. A.; Chaplin, D. J.; Saunders, M. I. Microregional fluctuations in perfusion within human tumours detected using laser Doppler flowmetry. *Radiother Oncol* **40:**45-50; 1996.
[245] Martinive, P.; Defresne, F.; Bouzin, C.; Saliez, J.; Lair, F.; Gregoire, V.; Michiels, C.; Dessy, C.; Feron, O. Preconditioning of the tumor vasculature and tumor cells by intermittent hypoxia: implications for anticancer therapies. *Cancer Res* **66:**11736-11744; 2006.
[246] Martinive, P.; Defresne, F.; Quaghebeur, E.; Daneau, G.; Crokart, N.; Gregoire, V.; Gallez, B.; Dessy, C.; Feron, O. Impact of cyclic hypoxia on HIF-1alpha regulation in endothelial cells--new insights for anti-tumor treatments. *FEBS J* **276:**509-518; 2009.
[247] Toffoli, S.; Feron, O.; Raes, M.; Michiels, C. Intermittent hypoxia changes HIF-1alpha phosphorylation pattern in endothelial cells: unravelling of a new PKA-dependent regulation of HIF-1alpha. *Biochim Biophys Acta* **1773:**1558-1571; 2007.
[248] Toffoli, S.; Roegiers, A.; Feron, O.; Van Steenbrugge, M.; Ninane, N.; Raes, M.; Michiels, C. Intermittent hypoxia is an angiogenic inducer for endothelial cells: role of HIF-1. *Angiogenesis* **12:**47-67; 2009.
[249] Csiki, I.; Yanagisawa, K.; Haruki, N.; Nadaf, S.; Morrow, J. D.; Johnson, D. H.; Carbone, D. P. Thioredoxin-1 modulates transcription of cyclooxygenase-2 via hypoxia-inducible factor-1alpha in non-small cell lung cancer. *Cancer Res* **66:**143-150; 2006.
[250] Semenza, G. L. Hydroxylation of HIF-1: oxygen sensing at the molecular level. *Physiology (Bethesda)* **19:**176-182; 2004.
[251] Mylonis, I.; Chachami, G.; Samiotaki, M.; Panayotou, G.; Paraskeva, E.; Kalousi, A.; Georgatsou, E.; Bonanou, S.; Simos, G. Identification of MAPK phosphorylation sites and their role in the localization and activity of hypoxia-inducible factor-1alpha. *J Biol Chem* **281:**33095-33106; 2006.
[252] Kim, J. S.; Diebold, B. A.; Babior, B. M.; Knaus, U. G.; Bokoch, G. M. Regulation of Nox1 activity via protein kinase A-mediated phosphorylation of NoxA1 and 14-3-3 binding. *J Biol Chem* **282:**34787-34800; 2007.
[253] Cheng, G.; Diebold, B. A.; Hughes, Y.; Lambeth, J. D. Nox1-dependent reactive oxygen generation is regulated by Rac1. *J Biol Chem* **281:**17718-17726; 2006.
[254] Chowdhury, I.; Mo, Y.; Gao, L.; Kazi, A.; Fisher, A. B.; Feinstein, S. I. Oxidant stress stimulates expression of the human peroxiredoxin 6 gene by a transcriptional mechanism involving an antioxidant response element. *Free Radic Biol Med* **46:**146-153; 2009.
[255] Ramos-Gomez, M.; Kwak, M. K.; Dolan, P. M.; Itoh, K.; Yamamoto, M.; Talalay, P.; Kensler, T. W. Sensitivity to carcinogenesis is increased and chemoprotective efficacy of enzyme inducers is lost in nrf2 transcription factor-deficient mice. *Proc Natl Acad Sci U S A* **98:**3410-3415; 2001.

Declaration

"I declare that I have completed this dissertation single-handedly without the unauthorized help of a second party and only with the assistance acknowledged therein. I have appropriately acknowledged and referenced all text passages that are derived literally from or are based on the content of published or unpublished work of others, and all information that relates to verbal communications. I have abided by the principles of good scientific conduct laid down in the charter of the Justus Liebig University of Giessen in carrying out the investigations described in the dissertation."

Place and Date

Signature

9. Appendix

9.1 Acknowledgments

I would like to express my gratitude to my supervisor **PD Dr. Jörg Hänze** as this work would not exist without his guidance. I thank him for seasoned guidance, healthy criticism, intensive theoretical discussions and enthusiastic support that were keynote for the success in this study.

I am also very grateful to **Prof. Dr. Werner Seeger** who gave me the opportunity to do my PhD study at the Faculty of Medicine of University Giessen and for enrolling me in graduate program Molecular Biology and Medicine of the Lung (MBML).

I want to express my warm and sincere gratitude to **Dr. Rory E. Morty** and **Dr. Oliver Eickelberg** for their guidance during the graduate program and suggestions in scientific discussions.

My special thanks should go to **Christiane Hild** and **Dr. Parag Goyal** for their excellent technical support and/or for teaching me methods from the "new world" of molecular biology.

Important thanks also belong to **Dr. Günter Lochnit** at the Departmant of proteomic for his material support and inspirative suggestion in the field of proteomic.

It was also a true pleasure for me to work with people that created friendly and inspirative atmosphere in our laboratory. I address my sincere acknowledgements and thanks to **Oana R. Gottschald, Shu Li, Diya Hasan and Puktie**.

I am indebted to my dear parents and family members for their understanding, encouragement and support through all these years.

Last thanks, I would like to express my girlfriend **Mišpulinka** for her love, sustained encouragement and accompany in all the way.

Der Lebenslauf wurde aus der elektronischen Version der Arbeit entfernt.

The curriculum vitae was removed from the electronic version of the paper.